Advanced Functional Materials

ADVANCED FUNCTIONAL MATERIALS
www.afm-journal.de

REVIEW

Engineering Polyacrylamide-Based Hydrogel Electrolytes for Zn-Ion Batteries: A Functional Modification Framework Bridging Mechanisms and Performance

Kaihan Xie[1] | Zhihao Li[1] | Jintao Feng[1] | Tianyu Zhang[2] | Hongfei Wang[1] | Yong Hu[2]

[1]Key Laboratory of Advanced Catalysis and Adsorption Materials, Zhejiang Key Laboratory of the Ministry of Education for Advanced Catalysis Materials, Department of Chemistry, Zhejiang Normal University, Jinhua, China | [2]Institute of Nanocatalysis and Energy Conversion, College of Chemistry and Materials Engineering, Zhejiang A&F University, Hangzhou, China

Correspondence: Hongfei Wang (whf0614@zjnu.edu.cn) | Yong Hu (yonghu@zafu.edu.cn)

Received: 16 April 2026 | **Revised:** 3 June 2026 | **Accepted:** 23 June 2026

Keywords: functional modification | ion transport | mechanical flexibility | PAM-based hydrogel | Zn anode

ABSTRACT

Aqueous Zn-ion batteries (ZIBs) are attractive for their safety and cost-effectiveness, but Zn anode instability and side reactions hinder their practical development. In this context, constructing polyacrylamide (PAM)-based hydrogel electrolytes has emerged as a compelling strategy to address these issues. Nonetheless, pristine PAM hydrogels are often constrained by limited ionic conductivity, inadequate mechanical strength, and suboptimal interfacial stability, motivating the exploration of diverse functional modification strategies. Herein, this review presents the first systematic overview of recent advances in the functional modification of PAM-based hydrogel electrolytes for ZIBs. We systematically elucidate the scientific mechanisms underlying key design approaches, including hydrogen-bond network modulation, multifunctional network construction, functional additive/filler incorporation, and functional group modification. These mechanisms are driven centrally by hydrogen bond competition, electrostatic repulsion, and coordination effects. The impact of these strategies on critical battery performance metrics, such as ion transport behavior, mechanical flexibility, and wide-temperature adaptability, is then comprehensively assessed. Subsequently, we offer a forward-looking perspective on remaining challenges and future directions. Collectively, this review consolidates advances in PAM-based hydrogel electrolytes, establishing a solid theoretical foundation and providing innovative insights for the rational design and fabrication of next-generation flexible ZIBs that synergistically integrate high performance, enhanced safety, and prolonged cycle life.

1 | Introduction

The relentless rise in global energy consumption, coupled with the escalating environmental concerns associated with fossil fuel depletion, has propelled sustainable and efficient energy storage technologies to the leading edge of scientific research [1–4]. Although clean energy sources like wind and solar hold great promise, their inherent intermittency calls for reliable energy storage systems to ensure grid stability [5–8]. Among diverse energy storage methods, Li-ion batteries (LIBs) have been extensively studied, yet their widespread adoption faces barriers from limited resources, safety issues, and ecological concerns [9–11]. Conventional organic electrolytes used in LIBs typically undergo exothermic decomposition and thermal runaway at temperatures as low as 120°C–150°C [12]. By contrast, aqueous electrolytes are inherently nonflammable and can operate safely at temperatures well above 200°C without any risk of combustion [13]. This intrinsic safety advantage originates from their water

-based composition, which completely eliminates the fire and explosion hazards associated with volatile organic solvents [14]. In this respect, aqueous Zn-ion batteries (ZIBs) have garnered considerable interest owing to the plentiful availability of Zn, intrinsic safety, and the environmentally benign nature of aqueous electrolytes, positioning them as promising candidates for smart grid systems and flexible electronic devices [15–18]. The crustal abundance of Zn, at approximately 70 ppm, exceeds that of Li (approximately 20 ppm) by more than threefold, rendering Zn a more sustainable and economically viable candidate for grid-scale energy storage applications [19]. Nevertheless, the application of ZIBs remains hindered by enduring technical obstacles, namely Zn dendrite formation [20, 21], parasitic side reactions [22, 23], and electrolyte leakage [24, 25]. These issues collectively compromise long-term cycling stability and impede real-world applicability [26, 27]. This challenge becomes particularly critical in flexible device configurations, where conventional separators such as glass fiber (GF) membranes show insufficient mechanical robustness and weak interfacial adhesion [28–30]. Under dynamic mechanical stresses, including repeated bending, folding, or stretching, these separators progressively undergo microscopic displacement and structural deterioration [31, 32]. GF membranes consist of rigid, non-entangled fibers that cannot accommodate dynamic strain [33]. Thus, even minor bending or shear induces relative sliding between the separator and electrodes. This microscopic displacement disrupts uniform interfacial contact, creating localized regions with reduced inter-electrode distance. These regions experience sharply increased local current density, intensifying the tip effect, where protruding Zn nuclei encounter amplified electric fields that accelerate dendrite growth [34]. As cycling continues, the displaced GF separator progressively degrades and loses its ability to block dendrite penetration. Such damage inevitably elevates the probability of internal short circuits, thereby severely undermining battery reliability and curtailing operational lifespan [35, 36].

To overcome these bottlenecks, replacing conventional separators and liquid electrolytes with hydrogel electrolytes has become an effective approach to the long-term cycling stability of ZIBs [37–39]. Hydrogel electrolytes contain an interconnected porous network that enables homogeneous ion migration, promotes homogeneous Zn deposition, and suppresses dendrite growth, thereby reducing the likelihood of internal short circuits and extending battery cycle life [40, 41]. In contrast to liquid electrolytes, hydrogels exhibit superior leakage resistance, mitigating associated safety hazards [42–44]. Moreover, the strong water–polymer interactions within hydrogels decrease free water activity [45], suppress hydrogen evolution reactions (HER) [46], and widen the electrochemical stability window [47]. The HER is thermodynamically favored on Zn anodes due to the low reduction potential of Zn^{2+}/Zn (−0.76 V vs. SHE) [48]. Under high overpotentials during charging, the cathodic polarization can drive proton reduction, generating H_2 gas and locally increasing the pH at the electrode surface [49]. The resulting pH rise promotes the formation of insulating by-products, such as Zn hydroxide sulfate ($Zn_4(OH)_6SO_4 \cdot xH_2O$), which passivate the anode surface, increase interfacial resistance, and exacerbate nonuniform Zn deposition. These parasitic reactions not only reduce Coulombic efficiency and consume active materials but also accelerate electrolyte decomposition and ultimately lead to premature cell failure [50]. Among various hydrogel matrices, polyacrylamide (PAM) is widely regarded as an ideal platform for constructing high-performance Zn battery electrolytes, owing to its abundant amide groups (—$CONH_2$) capable of forming hydrogen bonds, its straightforward synthesis, low cost, and its highly tunable three-dimensional (3D) network structure, which provides a versatile platform for subsequent functionalization and performance optimization [51, 52]. For comparison, other commonly used hydrogel matrices present distinct trade-offs. Poly(vinyl alcohol) (PVA)-based hydrogels offer good film-forming ability and mechanical strength but suffer from poor ionic conductivity due to their semicrystalline nature and limited functional group diversity [53]. Alginate-based hydrogels, derived from natural polysaccharides, exhibit excellent biocompatibility and abundant carboxyl groups for Zn^{2+} coordination. However, their mechanical robustness and long-term stability in aqueous electrolytes are often inadequate [54]. Cellulose-based hydrogels provide outstanding hydrophilicity and biodegradability but typically require chemical modification to achieve satisfactory ion transport properties and crosslinking density [39]. In contrast, PAM strikes a favorable balance: its amide groups enable strong hydrogen bonding with water molecules for water activity suppression, while its synthetic versatility allows precise control over crosslinking density, functionalization, and network architecture [55]. Moreover, PAM can be readily copolymerized with various functional monomers or combined with fillers and additives, offering a modular platform that other matrices often lack. These unique attributes collectively position PAM as a superior and versatile matrix for functional modification in advanced ZIBs [56].

Despite the progress already made, PAM-based hydrogel electrolytes still face several inherent limitations [57]. Mechanically, their strength is often insufficient to effectively resist Zn dendrite penetration [58]. From an ion transport perspective, the channels lack selectivity toward Zn^{2+} ions, leading to low Zn^{2+} transport efficiency and a high susceptibility to concentration polarization [59]. Moreover, the abundant free water within the network acts as active nucleation sites for HER and corrosion [60]. Finally, at sub-zero temperatures, this free water readily freezes, causing a drastic drop in ionic conductivity that can ultimately lead to battery failure [61]. It is precisely these challenges that underscore the unique value of PAM as an electrolyte matrix, as its highly tunable chemical structure and physical framework endow it with immense potential for modification [62]. This modifiability is not merely a matter of adding functional components; rather, it stems from its dual designability at both the molecular and network architecture levels [63]. At the molecular scale, the reactive functional groups on the PAM chains not only participate in constructing the crosslinked network but also serve as reactive sites [64, 65]. By tuning intermolecular forces, including hydrogen bonds and electrostatic interactions, they enable precise control over the state of water molecules [66, 67]. This implies that through chemical modification of the polymer chains, the internal microenvironment of the electrolyte can be fundamentally reshaped [68, 69]. At the network architecture level, the 3D network of PAM is not a rigid skeleton but a tunable confined space [70]. Its topological structure, crosslinking density, and pore size can all be adjusted through synthesis protocols, thereby altering the ion transport pathways and migration behavior [71].

In recent years, significant research has been directed toward the development of PAM-based hydrogel electrolytes for ZIBs [72]. Early studies focused on basic material development, demonstrating the feasibility of cross-linked PAM as a flexible and waterproof electrolyte [73, 74]. Subsequently, the introduction of multi-network architectures (e.g., double-network) and nano-reinforcing fillers markedly improved mechanical strength and fatigue resistance, effectively resisting dendrite puncture [75, 76]. To suppress HER and low-temperature failure, strategies such as introducing cryoprotective additives (e.g., glycerol and other small organic molecules) and strengthening polymer–water hydrogen bonding were developed [77]. These strategies transform free water into bound water and lower the freezing point, thereby enabling wide-temperature operation from sub-zero to elevated temperatures. To address poor ion selectivity, the chemical microenvironment of PAM networks was tailored by developing single-ion-conducting hydrogels or constructing specific ion channels, which significantly increased Zn^{2+} transference numbers (often exceeding 0.85) and mitigated concentration polarization [78–80]. More recently, advances have moved toward multi-parameter synergistic engineering and scenario-oriented application, aiming to balance ionic conductivity, mechanical robustness, electrochemical stability, and environmental adaptability, thereby extending the practical deployment of PAM-based hydrogels across diverse operating conditions [81, 82]. Figure 1 illustrates the evolutionary trajectory of PAM hydrogels in the field of ZIBs, charting their progression from initial material development through performance enhancement via multifunctional integration, exploration of microscopic mechanisms, and finally to multi-parameter synergistic design and all-scenario application.

When delving into its working mechanisms, one finds that the ability of PAM to address the aforementioned challenges through modification primarily lies in its capacity to systematically reconstruct the physicochemical environment within the electrolyte [83]. First, to counter dendrite penetration and insufficient mechanical strength, a reinforced design of the network structure can introduce energy dissipation mechanisms [84, 85]. This allows the hydrogel to effectively buffer stress concentrations under external forces, thereby enhancing its physical barrier against dendrite growth [86, 87]. Second, to address poor ion selectivity, tailoring the chemical environment within the network enables the introduction of specific interaction sites [88]. These sites can selectively coordinate or electrostatically interact with ions, thereby optimizing the desolvation process of hydrated Zn^{2+} ions and inhibiting the disordered migration of anions [89]. This fundamentally increases the Zn^{2+} transference number and mitigates concentration polarization [90]. Third, to tackle HER and low-temperature failure, the key lies in confining water molecules and modulating their activation energy [91]. Strengthening the polymer-water interactions enables the conversion of a large fraction of free water into bound water [92]. Due to its tight association with the polymer chains, bound water loses its ability to participate in side reactions [93]. Simultaneously, its altered physical state within the confined space results in a lower freezing point, enabling the battery system to maintain favorable kinetic performance even under low-temperature environments [94].

In this review, we systematically outline recent advances in functional modification strategies for PAM-based hydrogel electrolytes in ZIBs (Scheme 1). The article first elucidates the scientific mechanisms behind various design strategies, such as hydrogen bond network modulation, multifunctional network construction, functional additive introduction, and functional group modification. These strategies are driven by mechanisms including hydrogen bond competition, electrostatic repulsion, and coordination effects. Following this, we comprehensively assess how these strategies enhance key battery performance metrics, including ion transference number, ionic conductivity, mechanical flexibility, and environmental adaptability. Finally, the review presents a forward-looking perspective on future challenges and development directions in the field. This aims to provide a robust theoretical basis and offer innovative insights for the design and fabrication of next-generation flexible ZIBs with high performance, improved safety, and extended cycle life, thereby supporting the rational design of next-generation energy storage devices with inherent safety and mechanical robustness.

2 | Key Kinetic and Mechanical Parameters and Their Regulation Mechanisms in Hydrogel Systems

2.1 | Ionic Conductivity

Electrolytes can generally be classified into three types: liquid, quasi-solid, and solid [95]. Liquid and solid electrolytes each form single-phase systems: the former consist of aqueous solutions, whereas the latter encompass materials like polymers and ceramics [96]. Quasi-solid electrolytes, in contrast, consist of a biphasic structure resulting from the combination of an aqueous solution and a solid framework [97]. Liquid electrolytes generally exhibit the highest ionic conductivity, yet their vulnerability to leakage and weak interfacial stability make them less suitable for flexible device applications [98]. Solid electrolytes, while offering outstanding mechanical strength and the ability to suppress dendrite growth, often struggle to achieve high ionic conductivity [99]. Representing a typical quasi-solid system, hydrogel electrolytes successfully bridge the strengths of liquid and solid electrolytes [100]. Their hydrophilic polymer networks tether free water molecules via hydrogen bonding, effectively curbing water activity and mitigating parasitic reactions such as HER [101]. Concurrently, the liquid phase encapsulated within the 3D network sustains continuous ion conduction pathways, thereby maintaining high ionic conductivity. This architectural synergy allows hydrogel electrolytes to strike an essential balance between safety and ionic transport, positioning them as a highly promising platform for advanced ZIBs [102].

As a critical parameter for evaluating ion migration capability in hydrogel electrolytes, ionic conductivity (σ) directly governs the rate capability and power density of batteries. For hydrogel electrolytes, which fall between liquid and solid states, the ion conduction mechanism is considerably more intricate than that of purely liquid or purely solid phases [103]. The corresponding formula is given as follows:

$$\sigma = \frac{\mathrm{d}}{\mathrm{R} \times \mathrm{S}} \tag{1}$$

where d denotes the thickness of the hydrogel electrolyte between the two electrodes, S is the contact area between the electrolyte

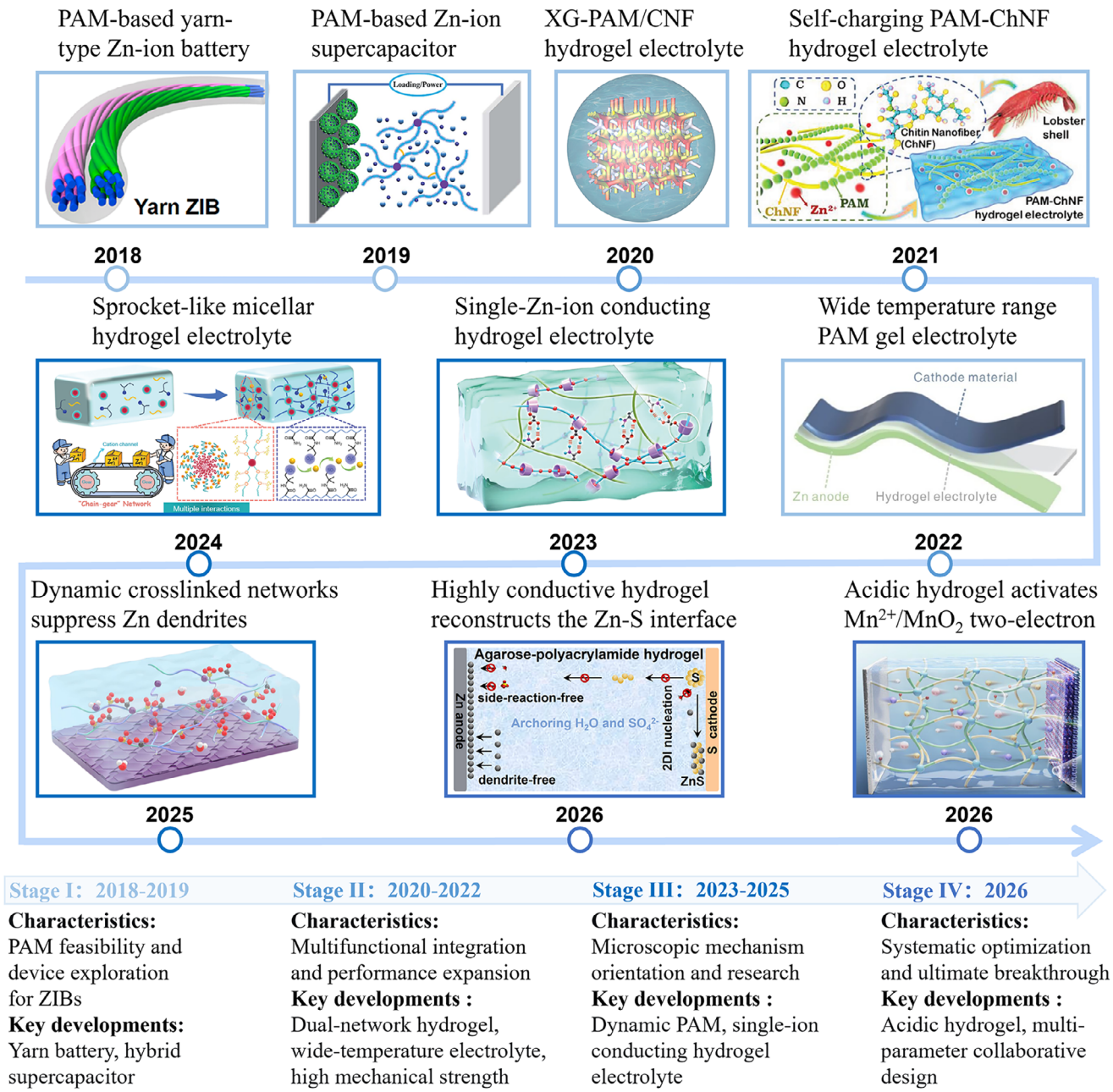

FIGURE 1 | Evolutionary trajectory of PAM-based hydrogel electrolytes in ZIBs. Reproduced with permission [73]. Copyright 2018, American Chemical Society. Reproduced with permission [74]. Copyright 2019, Royal Society of sChemistry. Reproduced with permission [75]. Copyright 2020, American Chemical Society. Reproduced with permission [76]. Copyright 2021, Wiley-VCH. Reproduced with permission [77]. Copyright 2022, Elsevier. Reproduced with permission [78]. Copyright 2023, Wiley-VCH. Reproduced with permission [79]. Copyright 2024, Wiley-VCH. Reproduced with permission [80]. Copyright 2025, Wiley-VCH. Reproduced with permission [81]. Copyright 2026, Wiley-VCH. Reproduced with permission [82]. Copyright 2026, Wiley-VCH.

and the electrodes, and R represents the bulk resistance of the hydrogel electrolyte. Within hydrogel electrolytes, ion migration predominantly takes place through the continuous liquid-phase pathways formed by free water confined in the polymer network [104]. Therefore, ionic conductivity is strongly dependent on factors such as water content, pore architecture, Zn salt concentration, and temperature [105]. For PAM-based hydrogels, the hydrophilic amide groups effectively immobilize a large quantity of water molecules, constructing continuous and abundant ion transport channels, which intrinsically endow them with relatively high ionic conductivity.

2.2 | Zn^{2+} Transference Number

Building on the discussion of ionic conductivity, another critical parameter governing ion transport in hydrogel electrolytes is the Zn^{2+} transference number ($t_{Zn^{2+}}$), which reflects the proportion

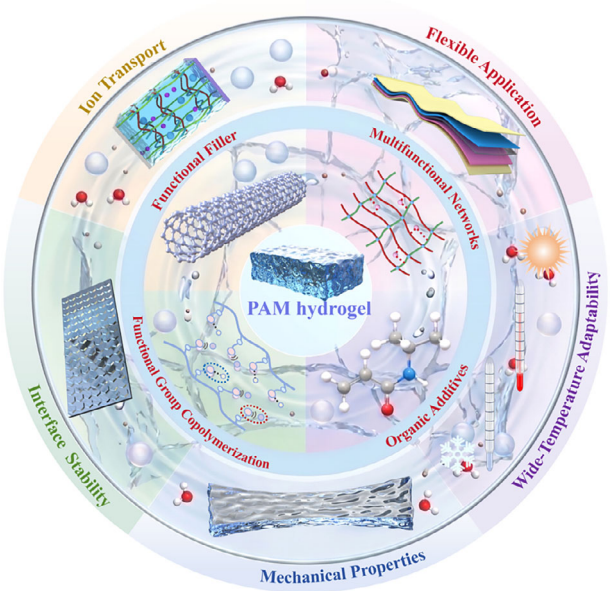

SCHEME 1 | Schematic illustration of functional modification strategies for PAM-based hydrogel electrolytes applied in ZIBs.

of total current carried by cations and serves as a key indicator of selective Zn^{2+} transport capability [106]. In ZIBs, uncontrolled anion migration exacerbates concentration polarization at the electrode interface, which can induce dendrite growth [107]. Therefore, increasing Zn^{2+} transference number is critical for attaining uniform Zn deposition and extending cycle life. This value is typically calculated using the Bruce-Vincent method:

$$t_{Zn^{2+}} = \frac{I_s(\Delta V - I_0 R_0)}{I_0(\Delta V - I_s R_s)} \tag{2}$$

where I_0 and I_s are the initial and steady-state currents, R_0 and R_s are the initial and steady-state interfacial resistances, and ΔV is the applied polarization voltage. Enhancing Zn^{2+} transference number primarily relies on two strategies: constructing polyanionic networks or introducing anion receptors to constrain the free migration of anions such as SO_4^{2-} and OTf^- [108]. A high Zn^{2+} transference number signifies that Zn^{2+} ions dominate ionic conduction, effectively mitigating concentration polarization and establishing kinetic conditions conducive to dendrite-free Zn deposition [109]. The realization of a high Zn^{2+} transference number is intimately tied to the chemical characteristics of functional groups in polymer-based hydrogels, which mediate distinct interactions with Zn^{2+} ions and their accompanying anions. In the case of PAM hydrogels, the polar $-CONH_2$ groups along the polymer chains function as key regulators [76]. The carbonyl oxygen serves as a hydrogen bond acceptor, anchoring anions such as ClO_4^-, whereas the amino group engages in Zn^{2+} coordination and solvation sheath modulation [110]. Through preferential binding with ClO_4^-, $-CONH_2$ groups generate localized anion-rich domains that weaken Zn^{2+}-anion electrostatic interactions. This promotes the dissociation of $[Zn(H_2O)_6]^{2+}$ ions and reduces the desolvation energy barrier. Consequently, Zn^{2+} transport is enhanced, concentration polarization is suppressed, and the transference number is elevated, thereby providing molecular-scale kinetic assurance for uniform Zn deposition. Recent non-PAM electrolyte systems provide valuable benchmarks for PAM-based hydrogels. A dual-modulation electrolyte disrupts interfacial hydrogen bonding and promotes an inorganic-rich solid electrolyte interphase (SEI) [111]. Meanwhile, a polyacrylonitrile-based electrolyte achieves a high Zn^{2+} transference number of 0.9 through differential adsorption on cyanide groups [112]. Additionally, a trace liquid crystal molecule self-assembles into an ordered interfacial layer, raising the transference number from 0.29 to 0.71 [113]. PAM-based hydrogels offer synthetic simplicity, low cost, and versatile functionalization, yet the ultrahigh transference numbers of non-PAM systems serve as future benchmarks. Three universal design principles, including hydrogen bond disruption, anion immobilization, and interfacial ordering, are fully applicable to PAM optimization.

2.3 | Activation Energy

Reaction activation energy serves as a critical kinetic parameter that dictates the electrochemical performance of ZIBs under different temperatures, as it directly reflects the temperature sensitivity of the electrode reaction rate and the energy barrier of the interfacial charge transfer process [114]. The Arrhenius equation commonly describes the quantitative dependence of activation energy on temperature, as shown in Equation (3), which reveals the fundamental principle that the rate constant varies exponentially with temperature:

$$k = Ae^{-\frac{E_a}{RT}} \tag{3}$$

where k is the rate constant, A is the pre-exponential factor, E_a represents the activation energy, R is the universal gas constant, and T is the absolute temperature. This equation elucidates the influence of temperature on the electrochemical reaction rate: as temperature decreases, the reaction rate constant decreases exponentially, leading to significant sluggishness in electrode reaction kinetics. Specifically, under low-temperature conditions, the viscosity of the electrolyte increases, the ion migration rate decreases, and the desolvation energy barriers of hydrated Zn^{2+} ions rise, collectively hindering the interfacial charge transfer process. At elevated temperatures, rapid water evaporation leads to a detrimental increase in Zn^{2+} concentration (inducing a salting-out effect) and disrupts the hydrogen-bond equilibrium within the hydrogel. This combined effect ultimately causes the collapse of its network and pore structure [24]. This not only blocks ion transport channels and increases migration resistance but may also induce microcracks, thereby compromising mechanical strength and structural integrity. The superposition of these physical structural damages and interfacial kinetic retardation exacerbates battery polarization and degrades rate performance, ultimately limiting the practical application of ZIBs over a wide temperature range [115]. Therefore, activation energy serves not only as a quantitative indicator for evaluating the difficulty of Zn^{2+} desolvation but also as a critical criterion for assessing the synergistic optimization of interfacial compatibility and reaction kinetics in hydrogel electrolytes.

At elevated temperatures, rapid water evaporation leads to a detrimental increase in Zn^{2+} concentration and disrupts the hydrogen-bond equilibrium within the hydrogel. Critically, during elec-

trochemical impedance spectroscopy (EIS) measurements at elevated temperatures, free water evaporation causes progressive network shrinkage and salt concentration fluctuations [24]. Therefore, the apparent E_a value derived from conventional Arrhenius fitting is invariably convoluted with the variable of water loss. This combined effect not only blocks ion transport channels and increases migration resistance but may also induce microcracks, thereby compromising mechanical strength and structural integrity. To address this issue, modification strategies such as introducing hydrophilic, high-boiling-point polyols (e.g., glycerol, 1,2-propanediol) or hygroscopic fillers have been shown to enhance water retention capability, ensuring both the accuracy of E_a evaluation and high-temperature kinetic stability [116]. The superposition of these physical structural damages and interfacial kinetic retardation exacerbates battery polarization and degrades rate performance, ultimately limiting the practical application of ZIBs over a wide temperature range.

2.4 | Mechanical Properties

For ZIBs intended for flexible electronic devices, the mechanical properties of PAM hydrogel electrolytes are critical in determining their ability to maintain structural integrity and interfacial stability under dynamic deformation [117]. These properties are primarily evaluated through the following parameters.

Tensile strength and elongation at break reflect a hydrogel's ability to withstand tensile failure [118]. While pristine PAM hydrogels generally exhibit modest mechanical performance, these parameters can be markedly enhanced by strategies including dual-network construction, nanofiller incorporation, and the introduction of additional physical crosslinking points [75]. Interfacial adhesion, often assessed by lap shear tests, serves as a key link between mechanical integrity and electrochemical functionality [119]. Robust adhesion ensures close electrolyte/electrode contact, minimizes interfacial resistance, and prevents delamination or slippage under mechanical deformation.

Flexibility characterizes a material or device's ability to withstand bending-induced failure. In layered flexible batteries, bending is the dominant form of mechanical deformation [120]. The maximum stress (F) generated during bending can be expressed as Equation (4):

$$F = E \times \frac{0.5 \times d}{r + 0.5 \times d} \tag{4}$$

where E is the Young's modulus of the material, d is the total thickness of the device, and r is the bending radius. This equation fundamentally reveals two primary strategies for enhancing flexibility: selecting materials with a low Young's modulus (e.g., soft hydrogels) and reducing the device thickness d. It also fundamentally explains why ultrathin, integrated hydrogel electrolytes have become a research focus in the field of flexible energy storage devices.

Fatigue resistance is a key indicator of the structural integrity and functional stability of hydrogel electrolytes under cyclic loading. Studies reveal that during battery assembly and cycling, hydrogel electrolytes experience two primary forms of deformation [121]. The first is irreversible compression from external pressure during assembly, where under a pressure of 50 kg·cm^{-2}, a glass fiber separator can be compressed from 1 mm to roughly 200 μm. The second is periodic reversible deformation arising from repeated Zn plating and stripping during charge/discharge cycles. Theoretical analysis indicates that each 1 mAh·cm^{-2} of Zn deposition adds approximately 5 μm to the thickness of the Zn anode. Consequently, under high-capacity cycling conditions (e.g., 10 mAh·cm^{-2}), the compressive strain on the hydrogel electrolyte can exceed 50%, presenting a substantial challenge to its fatigue resistance.

To quantify the damage accumulation process of hydrogels under cyclic compression, a bilinear damage rule (DLDR) derived from Miner's rule is introduced [122]. This model divides fatigue damage into two stages: crack initiation and crack propagation, which are described by the following equations:

$$\sum n_i/(a_i N_i) = 1 \tag{5}$$

$$\sum \frac{m_i}{(1-a_i)N_i} = 1 \tag{6}$$

where n_i and m_i represent the number of cycles in the fatigue crack formation and propagation stages, respectively. N_i is the number of cycles to failure, and a_i denotes the proportion of cycles corresponding to the crack initiation stage relative to the total cycles. For PAM hydrogels, cracks form rapidly during the initial loading stage, and damage accumulation is dominated by crack propagation, with both n and a approaching zero. By contrast, dual-network hydrogels effectively dissipate mechanical energy via slippage of physical entanglement points and network conformation rearrangement, leading to marked increases in n and m. This delays crack initiation and suppresses propagation, while a exhibits a finite positive value, thus significantly extending fatigue life. In summary, fatigue resistance, together with deposition uniformity, represents a critical design parameter for hydrogel electrolytes that governs the cycling stability of high-capacity Zn anodes [123].

3 | Functional Modification Strategies for PAM-Based Hydrogels

The rational design of functionalized PAM-based hydrogel electrolytes, achieved through diverse modification strategies, can establish a 3D porous network with tailored chemical microenvironments. This network modulates Zn^{2+} solvation structures, restricts free water activity, and promotes uniform ion flux at the interface between the electrode and the electrolyte. These intrinsic characteristics of the hydrogel matrix provide a viable route to enhance interfacial stability and extend electrode cycling longevity [124]. The primary objective of such functional hydrogel engineering is to control Zn deposition kinetics, concurrently inhibiting dendrite formation and unwanted side reactions. Functional modification offers the benefits of multifunctional synergy, yet certain fundamental and universal mechanisms remain unchanged. This chapter outlines four strategies for the optimization of functionally modified hydrogels. The working mech-

TABLE 1 | Comparison of the reported electrochemical performance of ZIBs employing different PAM-based hydrogel systems.

Nos.	Hydrogel system	Modifying strategy	Mechanism of action	Cycling in Zn//Zn cells	Refs.
1	MMT-PAM	Functional filler	MMT enhances mechanical strength, optimizes ion transport channels, and suppresses dendrites	300 h (0.5 mA cm^{-2}, 0.25 mAh cm^{-2})	[128]
2	CPAM	Functional filler	Carbon nanotube nanochannels enable ultrafast ion transport and induce desolvation	7000 h (1 mA cm^{-2}, 0.5 mAh cm^{-2})	[129]
3	PAM/CBZn	Functional filler	COFs enable rapid Zn^{2+} transport, while sulfonic acid groups regulate uniform deposition	1800 h (1 mA cm^{-2}, 1 mAh cm^{-2})	[130]
4	PAM@ZIF-8	Functional filler	ZIF-8 captures anions and water, guides Zn^{2+} hopping, and induces (002)-textured deposition	6500 h (1 mA cm^{-2}, 1 mAh cm^{-2})	[131]
5	PAM/trehalose	Construction of multifunctional networks	Trehalose improves mechanical properties and interfacial adhesion, regulates the solvation structure, and promotes (002)-oriented deposition	2400 h (1 mA cm^{-2}, 1 mAh cm^{-2})	[135]
6	FG/PAM	Construction of multifunctional networks	FG forms hydrogen bonds for mechanical strength, modulates Zn^{2+} flux with negative charges, and lowers water activity	2238 h (0.5 mA cm^{-2}, 0.5 mAh cm^{-2})	[136]
7	PAM/SA	Construction of multifunctional networks	SA carboxyls coordinate to promote Zn^{2+} desolvation; the dual-network enhances mechanics and deposition uniformity	3750 h (0.2 mA cm^{-2}, 0.2 mAh cm^{-2})	[138]
8	PCZ-gel	Construction of multifunctional networks	Zwitterions homogenize Zn^{2+} flux, while carboxyls coordinate Zn^{2+} to induce desolvation and favor (002) deposition	3000 h (0.5 mA cm^{-2}, 0.5 mAh cm^{-2})	[139]
9	PMC	Construction of multifunctional networks	Amide groups coordinate Zn^{2+} to lower the desolvation barrier and favor (002) deposition	5000 h (1 mA cm^{-2}, 1 mAh cm^{-2})	[140]
10	s-PPMHE	Construction of multifunctional networks	Coordinating ether oxygens lowers the Zn^{2+} electrostatic potential, which accelerates desolvation and ion migration	350 h (1 mA cm^{-2}, 1 mAh cm^{-2})	[141]
11	PAZPM	Construction of multifunctional networks	The hydrophobic surface reduces water activity to suppress dendrites, while the hydrophilic surface maintains high water activity to promote H^+ intercalation	3600 h (0.5 mA cm^{-2}, 0.25 mAh cm^{-2})	[142]
12	SUC/ZS/PAM	Organic molecular additives	Sucrose and PAM synergistically disrupt the water hydrogen bond network, tune Zn^{2+} solvation, lower water activity, and inhibit side reactions	6240 h (0.5 mA cm^{-2}, 0.5 mAh cm^{-2})	[143]

(Continues)

TABLE 1 | (Continued)

Nos.	Hydrogel system	Modifying strategy	Mechanism of action	Cycling in Zn//Zn cells	Refs.
13	PAM/T	Organic molecular additives	Trehalose displaces bound water to rebuild hydrogen bond networks, tunes Zn^{2+} solvation, and inhibits HER and corrosion	1200 h (1 mA cm^{-2}, 1 mAh cm^{-2})	[144]
14	β-SF/PAM	Organic molecular additives	The β-sheet structure forms a dense interfacial layer, where enriched polar groups regulate Zn^{2+} solvation and induce (002)-textured deposition	2500 h (1 mA cm^{-2}, 1 mAh cm^{-2})	[145]
15	PAGa	Organic molecular additives	Ga's polyhydroxy groups convert free water into bound water, improving interfacial adhesion and reducing interfacial resistance	5000 h (1 mA cm^{-2}, 1 mAh cm^{-2})	[146]
16	OR-PUU/PAM	Organic molecular additives	OR-PUU carbonyls serve as ion hopping sites for fast channels, while hierarchical H-bonds impart self-healing	2000 h (1 mA cm^{-2}, 1 mAh cm^{-2})	[147]
17	PAM-1,2-PG	Organic molecular additives	1,2-PG's terminal methyl groups break solvent chains, lower viscosity, reorganize hydrogen bond networks, and form organic-inorganic SEI	2160 h (10 mA cm^{-2}, 1 mAh cm^{-2})	[148]
18	PAM-Hbimcp-Zn	Organic molecular additives	Zn-Hbimcp dynamic coordination bonds dissipate energy to boost mechanics, tune Zn^{2+} solvation, and guide (002) deposition	500 h (1 mA cm^{-2}, 1 mAh cm^{-2})	[149]
19	PAPTMA	Functional group copolymerization	Cationic side chains repel to accelerate Zn^{2+} transport, suppress free water, and convert it to interfacial water	6060 h (1 mA cm^{-2}, 1 mAh cm^{-2})	[152]
20	PAME	**Functional group copolymerization**	$-BF_3^-$ converts free water to bound water, enhances electrostatic interactions for uniform deposition, and guides (002) orientation	1800 h (1 mA cm^{-2}, 1 mAh cm^{-2})	[153]
21	PASHE	Functional group copolymerization	Zwitterions enable distinct ion channels; sulfonate groups adsorb Zn^{2+}, enhancing desolvation and fast migration	400 h (2 mA cm^{-2}, 2 mAh cm^{-2})	[154]
22	PAP	Functional group copolymerization	PHEA's benzene ring immobilizes OTf^- via π-anion interactions, while oxygen groups restructure hydrogen bonds to limit water activity	6400 h (1 mA cm^{-2}, 1 mAh cm^{-2})	[155]
23	PAM-CS	Functional group copolymerization	The polar groups of CS (—OH, $-SO_3^-$, $-COO^-$) reduce water activity through hydrogen bonds and construct a dynamic network enabling fast migration	1200 h (1 mA cm^{-2}, 1 mAh cm^{-2})	[80]
24	PM-HE	Functional group copolymerization	The micellar "sprockets" support hierarchical pores, while ether bonds compete with sulfonic groups to promote ion decoupling and accelerate Zn^{2+} transport	1500 h (1 mA cm^{-2}, 1 mAh cm^{-2})	[79]

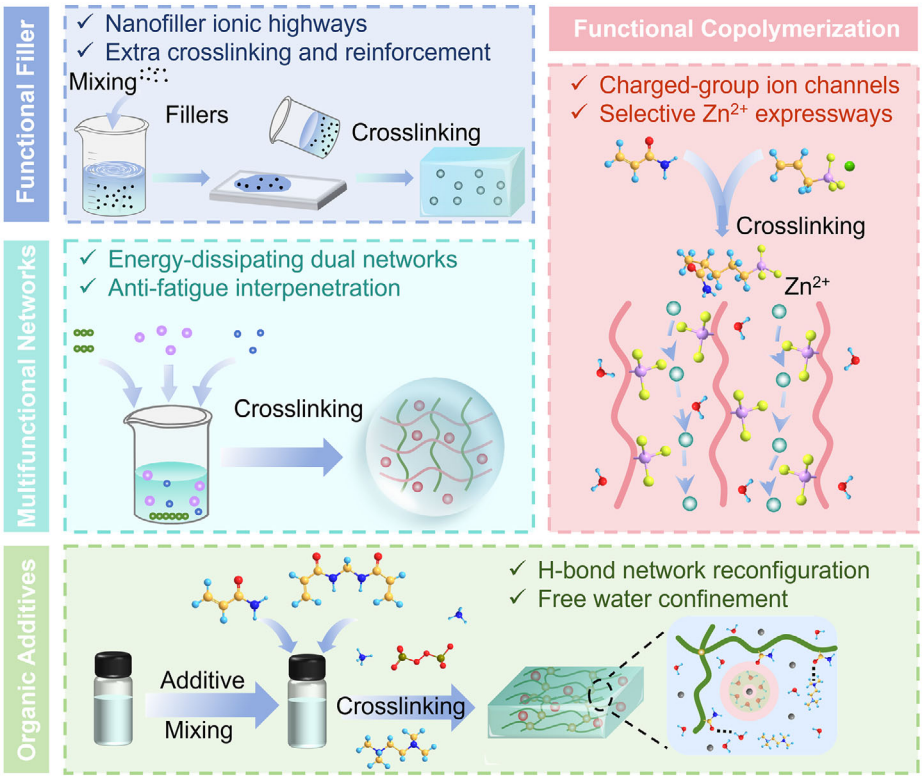

SCHEME 2 | Schematic illustration of the four functional modification strategies for PAM-based hydrogels.

anisms and corresponding electrochemical performance metrics of selected representative functionalized hydrogel electrolytes are summarized in Table 1. A schematic that systematically summarizes the four major functional modification strategies for PAM-based hydrogel electrolytes is presented in Scheme 2. These strategies include: (i) the introduction of functional fillers; (ii) the construction of multifunctional networks (e.g., dual-network and semi-interpenetrating structures); (iii) the utilization of organic additives; and (iv) polymerization with monomers bearing special functional groups. Collectively, these strategies operate through three core mechanisms: hydrogen bond competition, which reconstructs the water–polymer hydrogen-bond network to convert free water into bound water and lower the freezing point; electrostatic repulsion, which accelerates cation migration while immobilizing anions to enhance Zn^{2+} transport; and coordination effects, which modulate the Zn^{2+} solvation sheath to reduce desolvation energy barriers and guide uniform (002)-textured deposition. The interplay among these mechanisms determines the ultimate electrochemical and mechanical performance of the hydrogel electrolyte. In the following sections, each strategy is described in detail, with particular emphasis on the mechanistic origins of performance enhancement.

3.1 | Introduction of Functional Filler

Conventionally, hydrogel electrolytes face the dual bottlenecks of insufficient ionic conductivity and poor mechanical strength when applied in ZIBs, severely limiting their practical viability under high-rate and long-cycle operation [125]. Recent studies have demonstrated that introducing functional nanofillers is an effective strategy to alleviate these limitations [126]. These fillers not only serve as a reinforcing phase to form composite structures with the hydrogel matrix, thereby enhancing mechanical stability, but also synergistically optimize ion transport behavior through their inherent physicochemical properties. Specifically, functional fillers generally contain abundant polar moieties such as hydroxyl and carboxyl moieties. These active sites can coordinate or electrostatically interact with Zn^{2+} ions, thus reducing ion aggregation, increasing the concentration of freely mobile ions, and modulating the ion migration pathways within the gel [127]. In the context of PAM hydrogel electrolytes, the incorporation of functional fillers has emerged as a core modification strategy aimed at synergistically optimizing their mechanical properties, ion transport kinetics, and electrode/electrolyte interfacial stability. The multifunctionality of these fillers stems not only from their own physicochemical attributes, including ordered pore structures, large specific surface area, plentiful surface functional groups, and specific charge characteristics, but more critically, from their capacity for complex interactions with PAM, Zn salts, and water molecules [128]. These interactions remodel the internal microenvironment and interfacial behavior of the gel, facilitating rapid and uniform Zn^{2+} transport as well as dendrite-free deposition.

Inorganic layered silicate materials, such as montmorillonite (MMT), have also been employed as ideal fillers to reinforce PAM hydrogels, owing to their unique two-dimensional rigid layered architecture, plentiful surface hydroxyl groups, and excellent cation exchange capacity. For instance, Ji et al. utilized the rigid skeleton and hydrophilic groups of Na-MMT to prepare an MMT-PAM composite hydrogel electrolyte (Figure 2a) [128].

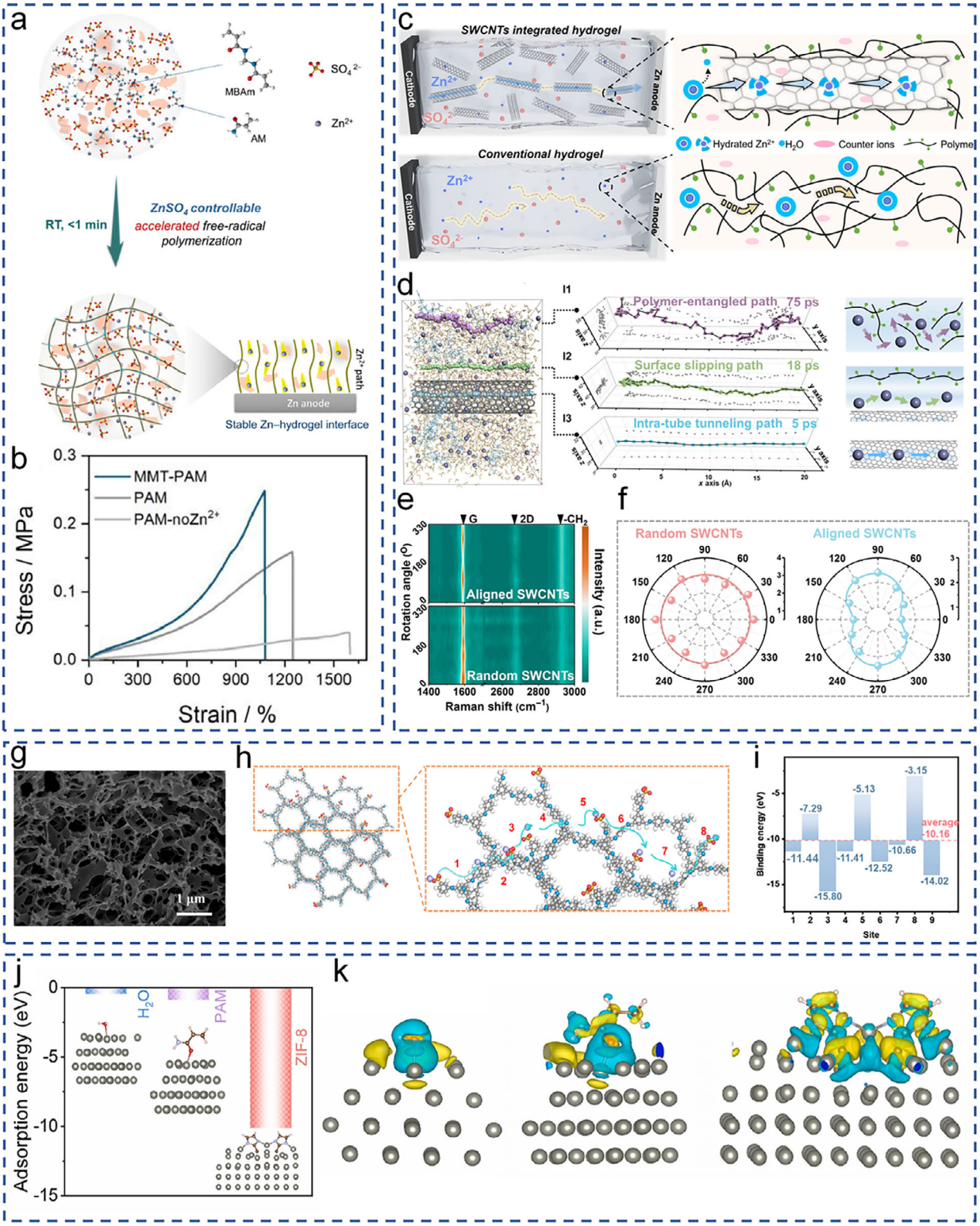

FIGURE 2 | (a) Schematic depicting the synthesis pathway of the MMT-PAM hydrogel via a controllable accelerated polymerization process. (b) Stress–strain tests of MMT-PAM. Reproduced with permission [128]. Copyright 2023, Elsevier. (c) Schematic depicting rapid ion migration via SWCNT channels in CPAM versus the convoluted ion pathway in conventional PAM. (d) Instantaneous depiction of Zn^{2+} migration pathways within the molecular framework of CPAM, the corresponding 3D plots, and schematic illustrations of the three transport mechanisms. (e) Raman contour plots of aligned SWCNTs and random SWCNTs in CPAM. (f) Polar plots of I_G/I_{-CH2} versus sample rotation angle for random SWCNTs and aligned SWCNTs integrated CPAM. Reproduced with permission [129]. Copyright 2025, American Association for the Advancement of Science (AAAS). (g) Scanning electron microscopy (SEM) images of PAM/CBZn. (h) Simulation of Zn^{2+} transport pathway and (i) the corresponding changes of binding energy. Reproduced with permission [130]. Copyright 2025, Wiley-VCH. (j) Adsorption energies of H_2O, AM, and ZIF-8 on Zn (002) plane. (k) Charge density difference of Zn slab with the adsorbed H_2O, AM, and ZIF-8. Reproduced with permission [131]. Copyright 2026, Elsevier.

Adding MMT greatly improves the mechanical performance of the hydrogel, yielding a tensile strength of 0.25 MPa (Figure 2b) and an elongation at break of 1075%. This improved mechanical robustness provides a physical barrier against Zn dendrite growth. Concurrently, the hydrogen-bond network formed between MMT and PAM chains optimizes ion transport pathways and further immobilizes free water molecules, lowering the freezing point of the electrolyte and thereby enhancing the low-temperature adaptability and interfacial stability of the battery. The overall performance of hydrogels is mainly enhanced by two-dimensional layered materials, which optimize the bulk ion-transport environment and boost mechanical properties. In contrast, one-dimensional nanomaterials offer an alternative strategy for constructing novel, ultrafast ion transport channels based on their unique geometric confinement effects and structural characteristics. Carbon nanotubes (CNTs), in particular, have opened new avenues for creating rapid ion transport pathways due to their distinctive one-dimensional hollow structure and ultrasmooth inner walls. For example, Lin et al. embedded single-walled carbon nanotubes (SWCNTs) into a PAM matrix via photoinitiated polymerization, constructing a CPAM hydrogel electrolyte [129]. The SWCNT inner cavities form low-friction nanofluidic channels that act as "ion highways" for Zn^{2+} ions (Figure 2c). Molecular dynamics (MD) simulations reveal three distinct ion transport modes (Figure 2d), namely a slow polymer winding path, a faster surface slip path along the nanotube exterior, and the fastest tunneling path through the nanotube interior, with the latter being nearly 15 times faster than transport in the bulk phase. Furthermore, through in situ dielectrophoresis, vertically aligned SWCNTs were incorporated into PAM to form ACPAM. Angle-resolved Raman spectroscopy shows that the G-band intensity variation is < 9% for random CPAM but reaches 40% for ACPAM (Figure 2e). Using the $-CH_2$ peak as an internal reference, polar plots reveal an anisotropic "gourd-shaped" distribution for ACPAM, with 56% of SWCNTs aligned within ± 30° of the vertical direction (Figure 2f). This architecture boosts the ionic conductivity to 36 mS cm^{-1}. Notably, randomly distributed CPAM still retains 85% of the conductivity of ACPAM, suggesting that it is the introduction of SWCNTs, not their precise alignment, that plays the dominant role in enhancing ion transport. With hydrophobic inner walls, the design of such physical nanochannels not only improves ionic conductivity but also induces partial desolvation of Zn^{2+} ions, widens the electrochemical stability window, and protects the polymer matrix from ion impact damage under high current densities.

Crystalline porous materials with intrinsic ordered pore structures, such as covalent organic frameworks (COFs) and metal–organic frameworks (MOFs), provide an ideal platform for constructing well-defined ion transport channels. For instance, a sulfonate-modified COF, denoted as COF-BSO_3Zn, was developed to improve the performance of PAM-based hydrogel electrolytes [130]. The addition of zincophilic $-SO_3^-$ groups into the hydrophobic COF skeleton markedly improves the dispersibility of the filler within the PAM matrix. The ordered micropores of COF-BSO_3Zn provide directional pathways for rapid Zn^{2+} transport, while the $-SO_3^-$ groups on its surface direct Zn^{2+} migration along specific channels through strong electrostatic interactions (Figure 2g). Simulations of the migration pathway reveal periodic and uniform fluctuations in binding energy (Figure 2h,i), a feature conducive to fast ion transport. In addition, the π-electrons of the benzene rings and the sulfonate ions within the framework effectively adsorb Zn^{2+} ions and modulate their solvation structure, yielding a high ionic conductivity of 64.43 mS·cm^{-1} and a Zn^{2+} transference number of 0.84. Analogous to COFs, MOFs have also been extensively investigated. For instance, ZIF-8 was introduced into a PAM matrix by leveraging the Lewis acid–base interactions between the Zn nodes of ZIF-8 and the carbonyl groups of PAM [131]. This approach not only enhances interfacial compatibility but also optimizes the binding energy for Zn^{2+} ions, enabling the framework to function as a hopping site for ion migration. Furthermore, the C═N groups within the ZIF-8 skeleton exhibit stronger adsorption affinity toward SO_4^{2-} anions and water molecules. This anchoring effect suppresses the disordered migration of anions and restricts the activity of free water, thereby stabilizing mass transport at the electrode/electrolyte interface. Density functional theory (DFT) calculations in Figure 2j reveal that the adsorption energy of ZIF-8 on the Zn (002) crystal plane (−10.11 eV) is substantially stronger than that of H_2O (−0.48 eV) and AM (−0.89 eV). Charge density difference analysis further confirms more pronounced electron accumulation at the ZIF-8/Zn interface (Figure 2k). The selective adsorption of ZIF-8 regulates the deposition kinetics of Zn^{2+} ions on the (002) plane, retarding its growth rate and thereby inducing a preferentially oriented (002) deposition morphology, which effectively suppresses dendrite growth.

Functional fillers synergistically enhance the overall performance of PAM-based hydrogel electrolytes through diverse mechanisms. Their common features are primarily reflected in two aspects. First, all types of fillers are dedicated to constructing ordered or rapid ion transport channels. Whether it is the optimized interlayer structure of MMT, the one-dimensional confined channels of SWCNTs, or the intrinsically ordered pores of COFs and MOFs, the core objective is to reduce the transport energy barrier for Zn^{2+} ions. Second, the incorporation of rigid fillers effectively strengthens the mechanical stability of the system, suppressing dendrite growth through stress dissipation or network protection mechanisms. The working mechanisms of different fillers exhibit distinct emphases in terms of spatial scale and mode of action. One category focuses on constructing static, well-defined ion conduction networks within the gel bulk phase, while the other leverages physical confinement effects to create novel ultrafast transport modes. These differentiated design concepts collectively enrich the landscape of functionalized PAM-based hydrogel electrolytes, enabling them to achieve a precise balance among ionic conductivity, interfacial stability, and mechanical strength according to the requirements of various application scenarios. This offers a diverse range of solutions for the development of high-performance and long-life ZIBs.

3.2 | Construction of Multifunctional Networks

In hydrogel electrolytes, 3D crosslinked networks work in conjunction with electrolyte salts to deliver mobile ions [132]. Currently, PAM is widely employed as the physical backbone for hydrogel electrolytes in ZIBs. Yet its performance, especially in terms of mechanical durability and electrochemical characteristics, continues to be less than ideal. Under complex stress conditions such as bending and stretching, the interfacial contact between the gel electrolyte and electrodes tends to

degrade, leading to a sharp increase in interfacial impedance, uneven distribution of ion flow, and ultimately, uncontrolled Zn dendrite growth and rapid battery performance degradation [133]. A multifunctional integrated network construction strategy has been proposed to overcome these bottlenecks. Moving beyond the pursuit of individual performance enhancements, this approach seeks to combine high mechanical strength, excellent interfacial adhesion, efficient and selective ion transport, and directed regulation of Zn deposition behavior into a single system via molecular and structural design. At the heart of this integrated network is the use of synergistic effects among different components, such as covalent and noncovalent crosslinking and electrostatic interactions, to build a stable and functionally rich 3D architecture. As a result, this integrated network strategy simultaneously addresses multiple challenges associated with Zn anodes, including dendrite growth, side reactions, and interfacial contact failure in flexible devices, thereby establishing a material foundation for high-performance and highly reliable ZIBs.

Inspired by the protective mechanisms of biomolecules in nature, introducing small molecules as network repair agents offers an innovative route for constructing multifunctional networks [134]. For example, trehalose, a natural disaccharide, has been incorporated into a PAM hydrogel to form a composite network [135]. The abundant hydroxyl groups of trehalose form strong hydrogen bonds with the —$CONH_2$ groups on PAM chains, effectively repairing defects within the PAM network, such as dangling chains and cyclic defects, while acting as molecular bridges to enhance network integrity. This noncovalent crosslinking mechanism not only strengthens network completeness but also introduces dynamic and reversible physical crosslinking points, endowing the hydrogel with superior self-healing and fatigue resistance. Furthermore, finite element simulation analysis reveals that the PAM/trehalose electrolyte, through selective adsorption of its polar functional groups onto the Zn surface, effectively equalizes the electric field distribution at the interface, promotes a uniform distribution of Zn^{2+} flux, and guides the initial nucleation and 3D diffusion of Zn nuclei toward a uniform morphology (Figure 3a). In contrast, a conventional 2 M $ZnSO_4$/PAM electrolyte is highly susceptible to dendrite initiation due to the tip effect. Additional simulations of the HER and Zn corrosion processes demonstrate that the PAM/trehalose electrolyte effectively suppresses both HER and corrosion during deposition (Figure 3b), confirming its excellent interfacial stability and capability to inhibit side reactions. Likewise, Cheng et al. proposed a network repair strategy using fish gelatin (FG)-modified PAM, which utilizes the rich hydroxyl groups and biopolymer structure of FG to improve the mechanical robustness and interfacial properties of the PAM hydrogel electrolyte [136]. The addition of FG promotes strong adsorption interactions with Zn atoms (Figure 3c), lowers the activity of water molecules, and enables directional ion transport along with uniform Zn deposition at the anode/electrolyte interface.

A dual-network architecture featuring energy dissipation has been created to concurrently improve the mechanical robustness of hydrogel electrolytes and inhibit the growth of Zn dendrites. This design reinforces structural integrity, mechanical endurance, and flexibility, all of which are essential to accommodate volume changes and stress variations induced by repeated Zn plating and stripping. Dual-network hydrogels typically consist of two interpenetrating polymer networks with distinct mechanical roles [137]. For instance, a dual-network hydrogel electrolyte has been designed using physically crosslinked sodium alginate (SA) and chemically crosslinked PAM to form a PAM/SA composite [138]. Through in situ ultraviolet (UV) polymerization, this system creates a tightly integrated interface on the surface of Zn fibers. Synergistic interactions among covalent crosslinking, hydrogen bonds, and ionic bonds, where Zn^{2+} ions serve as ionic crosslinkers, occur between the zincophilic groups (—COO^-) on SA chains and the PAM network. These interactions significantly enhance the toughness and energy dissipation capacity of the hydrogel. The PAM/SA hydrogel exhibits a hierarchical porous structure with uniform and interconnected pores, which outperforms the isolated pores of a single SA network, thereby providing efficient channels for ion migration. Furthermore, binding energy calculations indicate that the interaction energy between Zn^{2+} and PAM/SA (−76.2 kJ·mol^{-1}) is significantly lower than that between individual components (SA or PAM) and water molecules, suggesting that Zn^{2+} is more preferentially and strongly adsorbed onto the PAM/SA composite (Figure 3d). Molecular orbital analysis reveals that PAM/SA possesses a narrower HOMO–LUMO gap compared to H_2O and SA alone, indicating enhanced electron transfer capability, which further promotes the effective adsorption of PAM/SA onto the Zn electrode surface (Figure 3e). Beyond enhancing mechanical properties through multiple crosslinking, the design potential of dual-network structures also lies in the specific molecular engineering of their components to endow hydrogel electrolytes with superior ion transport properties. Zhang et al. developed an amphoteric cellulose-based dual-network hydrogel electrolyte (PCZ-gel) (Figure 3f), consisting of PAM, carboxyethyl-quaternized cellulose (CEQC), and $ZnSO_4$ [139]. The CEQC chains contain both anionic carboxyl groups (—COO^-) and cationic quaternary ammonium groups (—$N^+(CH_3)_3$), with the amphoteric groups providing separated migration channels that facilitate and regulate ion transport. The anionic groups guide Zn^{2+} migration through electrostatic interactions, while the cationic groups immobilize SO_4^{2-}, significantly improving ion transport performance.

Semi-interpenetrating network structures offer comparable advantages. In one approach, a hydrogel was synthesized by thermally initiating the polymerization of AM with ammonium persulfate (APS) in the presence of poly(ethylene glycol) diacrylate (PEGDA) and carboxymethyl cellulose (CMC), forming a semi-interpenetrating network denoted as PMC (Figure 3g) [140]. Fourier transform infrared (FTIR) spectroscopy confirms complete monomer polymerization and the formation of a free radical-initiated covalently crosslinked network. Additionally, the successful incorporation of Zn salts into the hydrogel system was beneficial for regulating Zn deposition behavior. Tensile tests verify that the semi-interpenetration of CMC enhances mechanical strength and reinforces the overall structure. A similar strategy led to the development of a semi-interpenetrating network hydrogel electrolyte (s-PPMHE) based on P(PEGMEA-AM)/PAM [141]. In this architecture, the linear polymer P(PEGMEA-AM) contains abundant C—O—C groups that coordinate with Zn^{2+} and reduce its electrostatic potential (ESP). This creates an efficient transport pathway, reminiscent of a highway, that substantially accelerates Zn^{2+} migration. Concurrently, hydrogen bonding between the

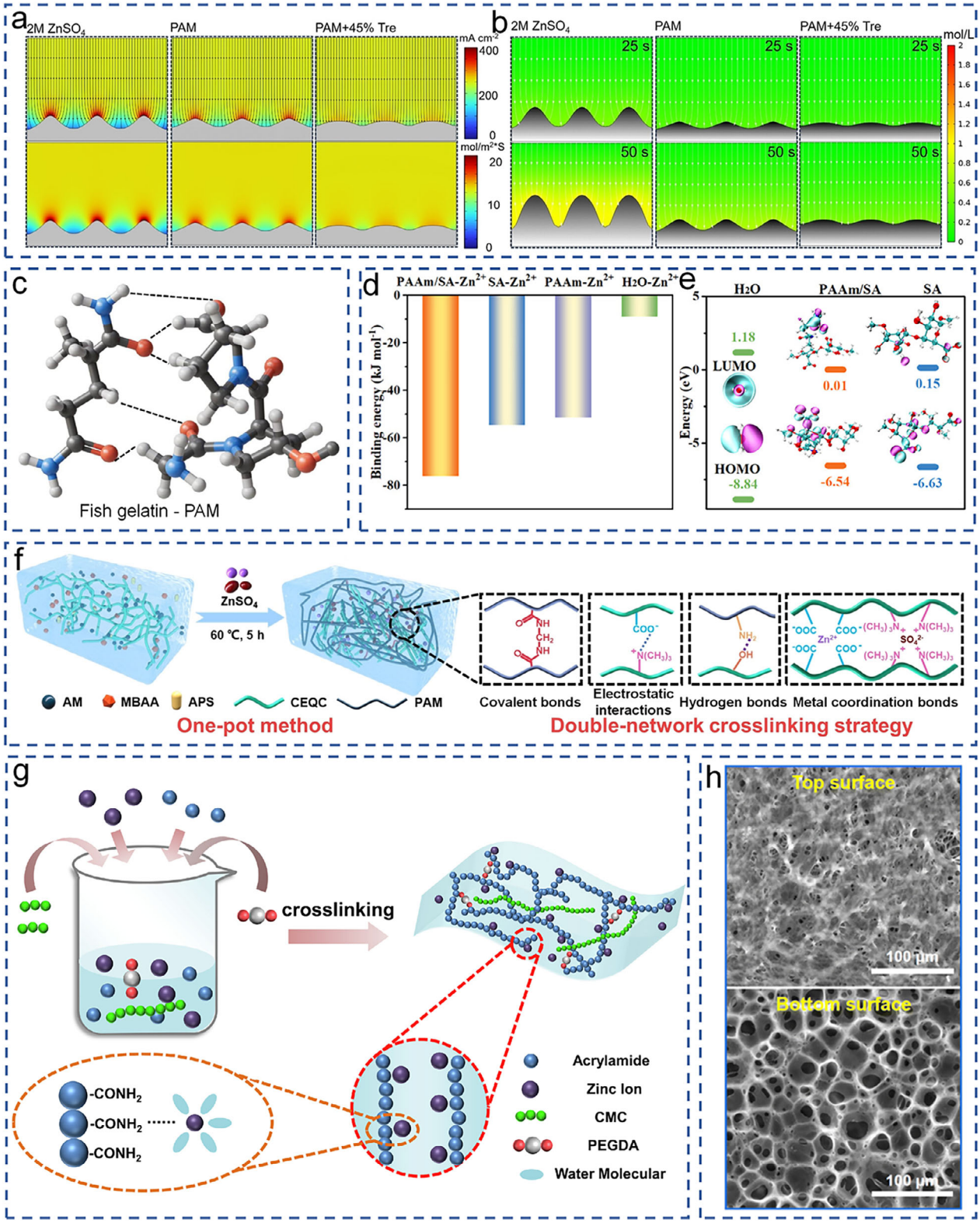

FIGURE 3 | COMSOL simulations of (a) electric field distributions and Zn^{2+} concentration field distributions, (b) Zn corrosion and HER during the Zn plating/stripping process in different electrolytes. Reproduced with permission [135]. Copyright 2024, Wiley-VCH. (c) Molecular interactions in the FG-modified PAM hydrogel electrolytes. Reproduced with permission [136]. Copyright 2025, Elsevier. (d) Binding energy of pairs of PAM/SA-Zn^{2+}, SA-Zn^{2+}, PAM-Zn^{2+}, H_2O-Zn^{2+}. (e) Molecular orbital energies of H_2O, PAAm/SA, and SA. Reproduced with permission [138]. Copyright 2025, Wiley-VCH. (f) Schematic depicting the fabrication process of PCZ-gel and the various internal interactions. Reproduced with permission [139]. Copyright 2023, Wiley-VCH. (g) Synthetic schematic diagram of PMC hydrogel electrolyte. Reproduced with permission [140]. Copyright 2022, Elsevier. (h) ESEM images of the top and bottom surfaces. Reproduced with permission [142]. Copyright 2024, Royal Society of Chemistry.

linear chains and the PAM network enhances the mechanical performance. Analyses of the radial distribution function and coordination number confirm that the ether oxygen atoms from the polymer chains enter the Zn^{2+} solvation shell, partially displace coordinated water molecules, and establish a stable Zn—O coordination environment with a bond length of approximately 2.65 Å. More intuitively, within s-PPMHE, Zn^{2+} is continuously shuttled along the oxygen atoms of the polymer chains, enabling efficient migration through dynamic segmental motion, thereby substantially improving ion transport performance.

In addition to semi-interpenetrating network architectures, hierarchical structuring of hydrogel networks offers an effective means to satisfy the contrasting water content demands at the anode and cathode in liquid electrolytes while enabling selective ion transport. A notable implementation involves an integrated Janus hydrogel with distinct hydrophilic properties on its two surfaces and a gradient pore structure within the bulk material [142]. Environmental scanning electron microscopy (ESEM) presents clear differences in surface morphology, with pore size increasing markedly from the top to the bottom (Figure 3h). The top surface shows a greater density of pores, though smaller in size than those on the bottom surface, resulting from entanglement of dense polymer chains with hydrophobic segments. When employed as an electrolyte, this Janus hydrogel endows ZIBs with superior capacity and excellent cycling stability.

The essence of multifunctional network strategies resides in the coordinated improvement of mechanical properties, interfacial stability, and ion transport efficiency. By combining structural concepts such as interpenetrating networks, energy-dissipating frameworks, and hierarchical architectures, these designs transcend the conventional trade-offs between strength, toughness, and electrochemical performance. In addition, bioinspired intelligent engineering introduces functionalities like dynamic interfacial regulation and spatially controlled ion conduction, enabling a more refined management of Zn deposition behavior. The result is a multi-pronged approach to inhibiting dendrite formation and unwanted side reactions, which translates into markedly enhanced cycle life and safety characteristics for ZIBs.

3.3 | Utilization of Organic Additives

Despite the ability of PAM-based hydrogel electrolytes to leverage their 3D network for guiding Zn^{2+} migration and promoting uniform Zn deposition, their capacity to regulate the solvation structure of hydrated Zn^{2+} ions remains inherently constrained [59]. The amide groups on PAM chains exhibit relatively weak coordination interactions with Zn^{2+} ions, insufficient to perturb the stable $[Zn(H_2O)_6]^{2+}$ solvation sheath. Consequently, a substantial number of water molecules remain coordinated with Zn^{2+} ions and participate in interfacial reactions, leading to HER, Zn corrosion, and eventual cell failure. These issues significantly limit the viability of pure PAM-based hydrogels for high-performance ZIBs. The introduction of electrolyte additives provides a targeted approach to address this limitation by modulating the solvation structure of hydrated Zn^{2+} ions. By introducing molecules bearing functional groups with high binding affinity toward Zn^{2+} ions, such as carbonyl, hydroxyl, or sulfonic moieties, the original solvation sheath can be reconfigured. These additive molecules competitively coordinate with Zn^{2+} ions, displacing water molecules and reducing the population of free water in the solvation environment. This reconfiguration not only mitigates side reactions but also alters the energetics of Zn^{2+} desolvation, influencing nucleation overpotential and deposition uniformity [143]. As such, solvation structure regulation via additive incorporation has become an indispensable strategy for elevating the electrochemical performance of PAM-based hydrogel electrolytes, working in concert with structural innovations to deliver robust and long-lasting ZIBs.

Electrolyte additives can be categorized into sacrificial and non-sacrificial types based on their reaction mechanisms. Non-sacrificial additives typically exist in molecular form within the solution and do not undergo any chemical changes during battery cycling. In contrast, sacrificial additives continuously decompose during Zn plating/stripping processes, leading to the formation of an excessive protective layer on the Zn anode surface, which is detrimental to long-term cycling stability. Among non-sacrificial additives, sugars constitute a representative category, with sucrose (SUC) standing out due to its high molecular polarity and strong solvation capability. A typical approach involves incorporating SUC into a PAM hydrogel, where its abundant hydroxyl groups coordinate strongly with Zn^{2+} ions, enabling effective regulation of the solvation structure [143]. ESP analysis in Figure 4a displays that SUC contains highly electronegative regions capable of acting as binding sites for Zn^{2+}. Upon replacing water molecules, SUC markedly reduces the ESP surrounding Zn^{2+}, thereby diminishing electrostatic repulsion and promoting ion transport. Binding energy calculations further show that the interaction energy between SUC and Zn^{2+} exceeds that between water and Zn^{2+} (Figure 4b), indicating a greater tendency for SUC to enter the solvation sheath and displace coordinated water. As a result, free water activity is significantly reduced, HER and corrosion-related side reactions are suppressed, and the cycling stability along with interfacial compatibility of the Zn anode is substantially improved. Additionally, other sugar molecules may similarly regulate interfacial chemistry via coordination interactions and could impart extra functional properties. Trehalose has also been utilized as an additive in PAM-based hydrogels (PAM/T), leveraging its high electronegativity to preferentially coordinate with Zn^{2+} and partially replace coordinated water molecules [144]. Molecular orbital analysis reveals that the higher HOMO energy level and lower LUMO energy level of trehalose enhance its electron-donating capacity, promoting the formation of a protective adsorption layer on the Zn surface and enabling uniform Zn deposition. Beyond interfacial regulation, trehalose reinforces the mechanical properties and water retention capability of the hydrogel, ensuring reliable performance in flexible battery configurations. Finite element simulations further confirm that trehalose incorporation facilitates a more uniform interfacial electric field, regulates Zn^{2+} transport, and prevents tip effect-induced nonuniform deposition (Figure 4c).

In addition to small organic molecules, biomacromolecules have attracted attention as natural composite additive precursors due to their abundant functional groups and unique conformational transition capabilities. For instance, Shen et al. introduced silk fibroin into a PAM hydrogel after inducing its conformational transition from random coil/α-helix to β-sheet via ethanol

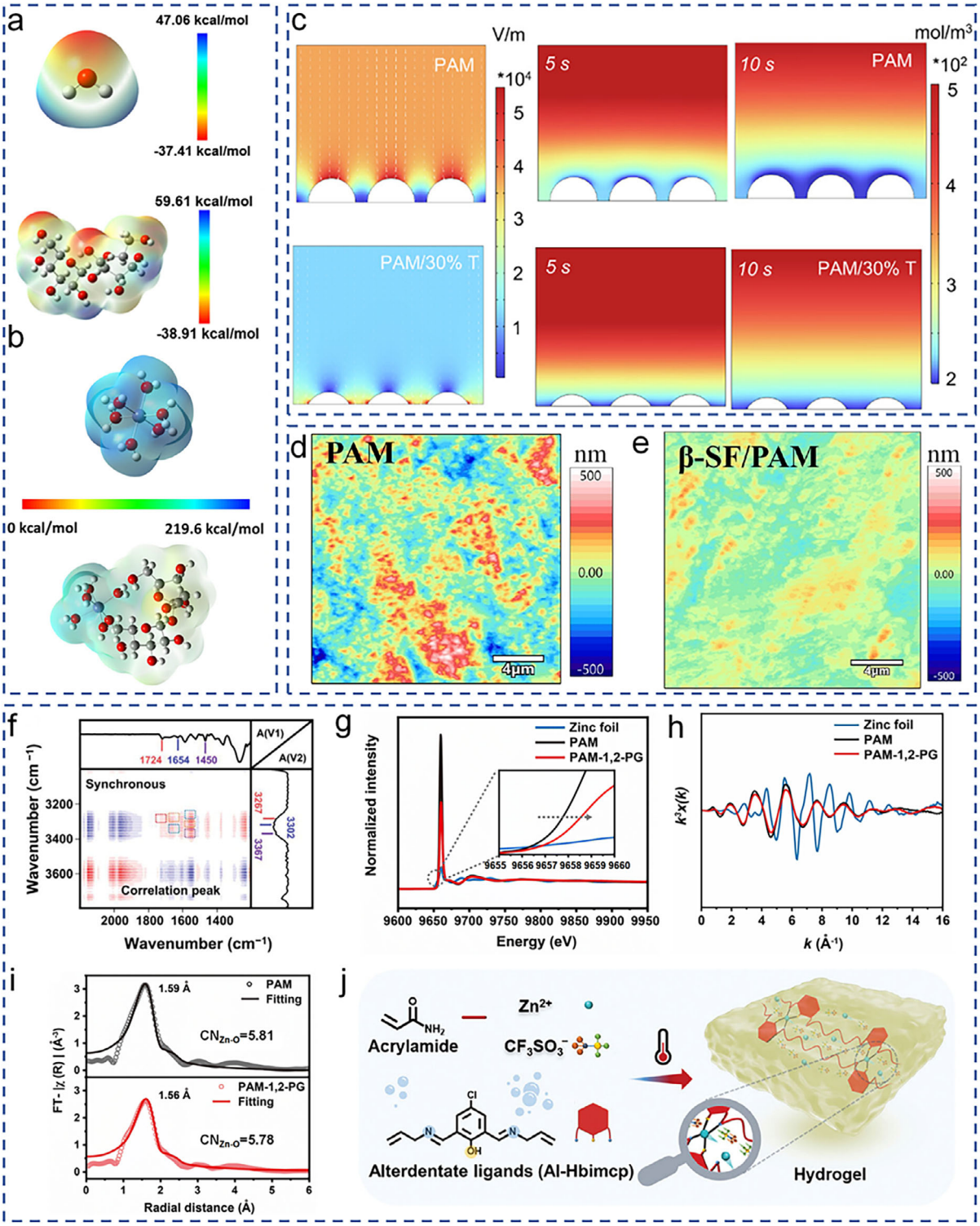

FIGURE 4 | (a) ESP of an H_2O molecule and a SUC molecule. (b) ESP of the original Zn^{2+}-$6H_2O$ and SUC-Zn^{2+}-$5H_2O$ solvation structures. Reproduced with permission [143]. Copyright 2025, American Chemical Society. (c) Numerical simulations of electric field distribution and equilibrium Zn^{2+} concentration profiles. Reproduced with permission [144]. Copyright 2025, American Chemical Society. AFM plan views of Zn anodes cycled in (d) PAM and (e) *β*-SF/PAM electrolytes, respectively. Reproduced with permission [145]. Copyright 2025, Elsevier. (f) Synchronous two-dimensional correlation FTIR spectrum of the OR-PUU molecule. Reproduced with permission [147]. Copyright 2024, Wiley-VCH. (g) Normalized Zn K-edge x-ray absorption near-edge structure (XANES) spectra and enlarged Zn K-edge XANES spectra of metal Zn, PAM, and PAM-1,2-PG hydrogel electrolytes. (h) k^3-weighted Fourier transform of Zn K-edge extended x-ray absorption fine structure (EXAFS) spectra in the k-space of the Zn foil, PAM, and PAM-1,2-PG hydrogel electrolytes. (i) The fitting of EXAFS spectra in R-space for PAM and PAM-1,2-PG hydrogel electrolytes. Reproduced with permission [148]. Copyright 2025, Royal Society of Chemistry. (j) The schematic illustration of the PAM-Hbimcp-Zn hydrogel. Reproduced with permission [149]. Copyright 2024, Wiley-VCH.

treatment [145]. The resulting β-sheet structures can self-assemble into a dense, polar-group-rich bio-inspired interfacial layer on the Zn anode surface. This layer effectively reconstructs the Zn^{2+} solvation structure and accelerates the desolvation process, achieving a high ionic conductivity of 32.4 mS cm^{-1} and a Zn^{2+} transference number of 0.80. Atomic force microscopy (AFM) measurements show that the Zn deposited in the β-SF/PAM system exhibits significantly lower surface roughness compared to that in pure PAM, confirming its superior dendrite-suppressing capability (Figure 4d,e). DFT calculations further reveal a strong adsorption energy of −2.069 eV for β-SF on the Zn (002) crystal plane, indicating preferential adsorption and favorable uniform Zn deposition. Beyond constructing ordered interfaces through conformational transitions, the inherent abundance of functional groups in biomacromolecules also provides a natural advantage for building robust interfaces and modulating the electrolyte microenvironment. Another illustrative system involves the use of gum arabic (Ga) as a biomass additive in PAM to form a hydrogel electrolyte (PAGa) with pronounced interfacial interactions [146]. Owing to its natural polysaccharide structure, Ga provides abundant hydroxyl and carbonyl groups that engage in extensive intermolecular hydrogen bonding, effectively converting free water into bound water and thereby reducing HER. According to DFT calculations, PAGa exhibits a lower binding energy with water and a more negative adsorption energy on the Zn (002) plane, signifying stronger interfacial affinity that directs uniform Zn deposition and enhances long-term cycling reversibility.

Polymer-based additives, leveraging their long-chain architecture and abundant polar functional groups, can form dynamic cross-linked structures with the PAM matrix, thereby enabling the construction of ion transport pathways and the modulation of solvation structures. For instance, Zhu et al. designed an oxygen-rich poly(urea-urethane) (OR-PUU) long-chain polymer and incorporated it into a PAM hydrogel to fabricate an OR-PUU/PAM composite electrolyte [147]. The OR-PUU molecular chains are abundant in functional groups such as carbonyl (C═O), thiocarbonyl (C═S), and amino (—NH_2) moieties, which can form multiple types of hydrogen bonds with PAM segments and among themselves. Two-dimensional correlation FTIR spectroscopy in Figure 4f confirms the synchronous correlation among six types of hydrogen-bond vibrational modes, demonstrating the excellent synergistic reconstruction capability of these bonds. This dynamic hydrogen-bond network significantly enhances the mechanical strength and toughness of the hydrogel while imparting outstanding self-healing properties, enabling rapid recovery after damage. Simultaneously, through synergistic interplay with ion migration pathways, it optimizes mass transport, facilitating uniform ion deposition. Charge density analysis further reveals that OR-PUU induces charge redistribution at the Zn interface, generating a built-in electric field that effectively promotes interfacial Zn^{2+} migration and stable deposition. Simple organic molecules have also proven effective in tuning the internal hydrogen-bonding and solvation environment of hydrogels. Small-molecule alcohols featuring hydroxyl groups function as effective co-solvents by forming alternative hydrogen bonds with water molecules, thereby restructuring solvation environments and promoting stable electrode–electrolyte interfaces. A representative system utilizes 1,2-propylene glycol as a co-solvent within a PAM hydrogel [148]. The presence of hydroxyl and terminal methyl groups in this co-solvent enables modulation of the hydrogen-bond network, suppressing water activity and preventing the formation of continuous water chain structures. Quantitative Raman spectroscopy analysis of the O—H stretching region (3000–3800 cm^{-1}) shows that the intensity ratio of strong hydrogen bonds (tetrahedral DDAA-OH at ∼3225 cm^{-1}) to weak hydrogen bonds (incomplete tetrahedral DA-OH at ∼3420 cm^{-1}), denoted as I_{3225}/I_{3420}, increases from 0.13 for pristine PAM to 0.33 for PAM-1,2-PG. This spectral shift indicates that the original weak water–water hydrogen bonds are disrupted and replaced by more stable tetrahedral structures. MD simulations further confirm that the introduction of 1,2-PG effectively reduces the average number of water–water hydrogen bonds, directly correlating with suppressed water activity and enhanced anti-freezing properties. Differential scanning calorimetry (DSC) demonstrates the disappearance of the ice crystallization exotherm (originally at −6°C for PAM) upon 1,2-PG incorporation. X-ray absorption fine structure (XAFS) analysis indicates that upon introduction of the co-solvent, the Zn K-edge absorption edge shifts to higher energy (Figure 4g). Corresponding k-space data further show a weakened intensity of the k^3-weighted peak under the influence of 1,2-PG (Figure 4h), implying a decrease in the Zn—O coordination number within the inner solvation shell. Fourier-transform analysis of the Zn K-edge in R-space reveals a slight contraction in the Zn—O bond distance and a reduction in the coordination number from 5.81 to 5.78 (Figure 4i), confirming the effective regulation of the Zn^{2+} solvation structure. Furthermore, constructing dynamic bonding networks using functional organic ligands represents another effective strategy. Functional organic ligands can form unique coordination structures with Zn^{2+} ions, enhancing the overall performance of the hydrogel electrolyte. As depicted in Figure 4j, Chen et al. constructed a multifunctional hydrogel electrolyte through dynamic coordination bonds between Zn^{2+} and the alternating ligand 2,6-bis((E)-(allylimino)methyl)−4-chlorophenol (Al-Hbimcp) [149]. This dynamic exchange mechanism enhances the mechanical and fatigue resistance of the hydrogel, regulates Zn^{2+} solvation, guides uniform (002) Zn deposition, and suppresses dendrites. MD simulations further reveal that Al-Hbimcp breaks the hydrogen-bond network among water molecules, reducing the number of hydrogen bonds and thereby inhibiting side reactions. Leveraging these advantages, the Zn//Zn symmetric cell achieves steady cycling for over 500 h with an ionic conductivity of 38.2 mS cm^{-1}.

Collectively, through judicious component design, electrolyte additives achieve a synergistic convergence of mechanical reinforcement, deposition modulation, and interface stabilization. This integrated approach transcends the conventional limitations of single-function strategies, enabling concurrent improvements in structural integrity, electrochemical reversibility, and interfacial compatibility. By holistically addressing the interdependent challenges of Zn dendrite formation, water-induced side reactions, and mechanical fatigue in flexible configurations, additive engineering establishes a solid foundation for the development of high-performance ZIBs with extended cycling lifespans and enhanced operational safety. Moreover, this design philosophy offers valuable insights for the broader pursuit of multifunctional material systems in next-generation energy storage devices.

3.4 | Polymerization With Monomers Bearing Special Functional Groups

Functional group modification constitutes a versatile molecular engineering approach to improve the overall performance of PAM-based hydrogel electrolytes. By chemically introducing functional groups endowed with specific electronic and structural attributes into the 3D PAM network, this strategy achieves precise modulation of ion transport pathways, water molecule dynamics, and interfacial chemical properties [150]. Depending on their chemical identity, functional groups like hydroxyl, carbonyl, carboxyl, amino, or sulfonate engage in various non-covalent interactions, such as hydrogen bonding, electrostatic forces, and coordination with Zn^{2+}. These interactions collectively shape a microenvironment that accelerates Zn^{2+} migration, facilitates uniform deposition, and mitigates water-induced side reactions. Furthermore, this molecular-level design enhances the mechanical robustness and long-term stability of the hydrogel, addressing multiple challenges simultaneously. Combined with other design strategies, functional group modification offers a synergistic pathway toward next-generation flexible ZIBs featuring enhanced durability and electrochemical performance.

Polar functional groups are crucial for tuning the local dielectric properties and intermolecular interaction networks in hydrogels. By forming dense hydrogen bond networks, these groups effectively immobilize water molecules, converting highly reactive free water into stable bound water [151]. This transformation significantly mitigates inherent side reactions in aqueous electrolytes. In addition, ion–dipole interactions enabled by these polar groups regulate the solvation structure and transport pathways of Zn^{2+} ions. A representative example in Figure 5a involves grafting long-chain quaternary ammonium cations (N^+R_3) onto a PAM network via the monomer 3-acrylamidopropyl trimethylammonium chloride (APTMA) [152]. These positively charged moieties facilitate rapid Zn^{2+} migration with reduced energy barriers through electrostatic repulsion, while also immobilizing SO_4^{2-} anions on the polymer chains. This cationic channel design endows the hydrogel with both a high ionic conductivity of 28.7 mS cm^{-1} and a high Zn^{2+} transference number of 0.79. In addition, this system effectively suppresses HER, as evidenced by an H_2 concentration of only 72 ppm after 5 h, compared with 421 ppm for conventional PAM (Figure 5b). Differential scanning calorimetry (DSC) measurements further reveal a high content of unfreezable water and a low proportion of free water within the structure (Figure 5c), resulting from strengthened polymer–water interactions that help regulate interfacial water activity and contribute synergistically to Zn anode stability. Anionic functional group copolymerization has been employed to introduce strongly electronegative $—BF_3^-$ terminal groups into the PAM hydrogel, resulting in a PAME electrolyte [153]. These groups act as potent hydrogen bond acceptors, effectively trapping water molecules and converting highly active free water into stable bound water. Simultaneously, its electrostatic attraction with Zn^{2+} guides uniform ion flux distribution, promoting preferential Zn deposition on the (002) crystal plane and suppressing dendrite growth. MD simulations show that PAME chains can enter the Zn^{2+} solvation shell, partially displacing coordinated water (on average 0.23 chain segments per Zn^{2+}) and forming a stable Zn—F coordination environment (Figure 5d,e). DFT calculations further confirm that the binding energies of PAME with both Zn^{2+} and H_2O are lower than those of PAM, indicating that $—BF_3^-$ can preferentially capture Zn^{2+} and enhance water confinement, synergistically regulating deposition behavior and interfacial stability. Integrating the advantages of both anionic and cationic groups within a single molecular unit can create internally separated dual-ion transport channels. Building on the strategies of cationic and anionic functional group modification, a zwitterionic approach has been employed to combine both functionalities synergistically. Specifically, a poly(AM-co-SBMA) hydrogel electrolyte (PASHE) was developed, in which the $—SO_3^-$ groups serve as strong coordination sites for Zn^{2+} ions via electrostatic interactions, whereas the $—N^+(CH_3)_2$ groups promote efficient transport of OTf^- anions [154]. This separated ion channel promotes efficient Zn^{2+} migration, resulting in an ionic conductivity of 32.9 mS cm^{-1}. DFT calculations reveal that the binding energy between the sulfobetaine anion in PASHE and Zn^{2+} (−11.69 eV) is much lower than that of $Zn^{2+}—H_2O$ (−4.52 eV), indicating a preferential adsorption for Zn^{2+} (Figure 5f). Moreover, the desolvation energy of PASHE–$[Zn(H_2O)_5]^{2+}$ (−18.81 eV) is higher than that of $[Zn(H_2O)_6]^{2+}$ (−15.30 eV) (Figure 5g), confirming its effectiveness in promoting Zn^{2+} desolvation, accelerating deposition/stripping kinetics, and homogenizing the interfacial electric field and ion flux.

Incorporating functional molecules via copolymerization has emerged as an effective strategy to enhance the physicochemical and electrochemical properties of PAM-based hydrogels. Introducing custom-designed functional groups into the polymer network yields marked enhancements in mechanical strength, ionic conductivity, and interfacial compatibility. In particular, leveraging the π systems of functional molecules to interact with ions offers an efficient means of regulating ion transport behavior. In one example, 2-phenoxyethyl acrylate (PHEA), which contains a benzene ring, was copolymerized with AM to form a P(AM-co-PHEA) (PAP) hydrogel [155]. The benzene ring in PHEA anchors OTf^- anions through π-anion interactions, resulting in an increased Zn^{2+} transference number of 0.70 (Figure 5h). Concurrently, the introduction of the aromatic ring optimizes ion transport pathways. MD simulations demonstrate that Zn^{2+} forms more ordered and faster conduction channels in the PAP gel, leading to an enhanced diffusion coefficient (Figure 5i).

Within the strategy of functional group modification for PAM hydrogels, the incorporation of natural macromolecules offers a novel design paradigm for constructing dynamic crosslinked networks and achieving synergistic regulation through multiple functional groups. In this context, Xu et al. introduced chondroitin sulfate (CS), rich in —OH, $—SO_3^-$, and $—COO^-$ groups, into a PAM matrix [80]. Leveraging the dynamic hydrogen-bonding interactions between CS and PAM chains, they successfully constructed a PAM-CS composite hydrogel electrolyte featuring a "dynamic coordination network." FTIR spectroscopy confirms the successful incorporation of CS, and the hydrogen-bonding interactions with PAM cause the characteristic C═O peak to red-shift to 1657 cm^{-1}, verifying the formation of a dynamic coordination network. This multi-hydrogen-bond architecture significantly enhances the crosslinking density of the system, increasing the tensile strength of the hydrogel from 12.5 kPa (pure PAM) to 60 kPa, with an elongation at break of 760%. Regarding ion transport, the $—SO_3^-$ and $—COO^-$ groups

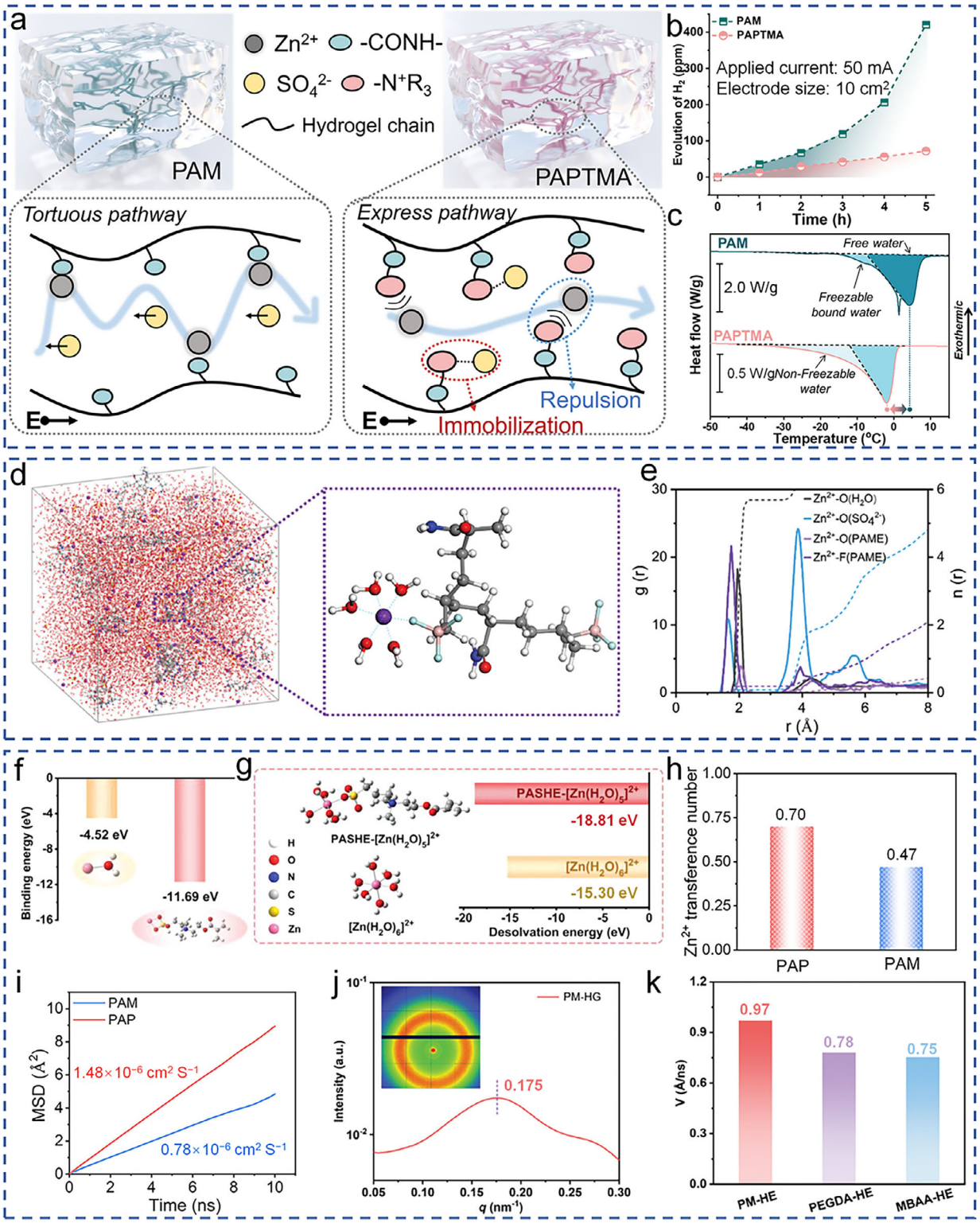

FIGURE 5 | (a) Schematic diagrams illustrating ion migration in PAM and PAPTMA hydrogels. (b) Time-dependent H_2 generation using various hydrogels. (c) DSC curves of PAPTMA and PAM hydrogel recorded at 5°C min^{-1}. Reproduced with permission [152]. Copyright 2025, Springer Nature. (d) Snapshot from MD simulations showing the representative solvation structure of Zn^{2+} in the PAME electrolyte. (e) RDF for Zn^{2+}—O (H_2O), Zn^{2+}—O (SO_4^{2-}), Zn^{2+}—O (PAME), and Zn^{2+}—F (PAME) pairs from the MD simulation, and the corresponding coordination numbers. Reproduced with permission [153]. Copyright 2024, Wiley-VCH. (f) Calculated binding energies of Zn^{2+}—H_2O and Zn^{2+}–PASHE. (g) Calculated desolvation energies of PASHE–$[Zn(H_2O)_5]^{2+}$ and $[Zn(H_2O)_6]^{2+}$. Reproduced with permission [154]. Copyright 2022, Wiley-VCH. (h) Comparison of Zn^{2+} transference number. (i) The function of mean-squared displacement vs time in PAP and PAM. Reproduced with permission [155]. Copyright 2025, Wiley-VCH. (j) SAXS curves of polymeric micelles. (k) The average rate of Zn^{2+} transport of various hydrogel electrolytes. Reproduced with permission [79]. Copyright 2024, Wiley-VCH.

TABLE 2 | Comparison of the reported ionic conductivity and Zn^{2+} transference number of ZIBs employing different PAM-based hydrogel systems.

Nos.	Hydrogel system	Modifying strategy	Ionic conductivity (mS cm^{-1})	Zn^{2+} transference number	Refs.
1	CD-PEO/PAM	Construction of multifunctional networks	22.4	0.923	[78]
2	TCOF-S-Gel	Functional filler	27.2	0.89	[161]
3	HTHEs	Functional filler	3.5	0.9	[162]
4	6m-PAM	**Functional group copolymerization**	52	0.51	[163]
5	APHE	Construction of multifunctional networks	17.8	0.71	[164]

establish fast migration channels for Zn^{2+} ions via strong electrostatic interactions, achieving a high ionic conductivity of 38.3 mS cm^{-1} and elevating the Zn^{2+} transference number from 0.26 to 0.52. MD simulations and RDF reveal that —SO_3^- and —COO^- can enter the solvation sheath of Zn^{2+} through strong electrostatic interactions, forming a stable Zn^{2+}—O (PAM-CS) coordination structure that provides a structural basis for rapid Zn^{2+} migration and uniform deposition. Beyond endowing the network with multiple functional groups through the introduction of functionalized macromolecular segments, another effective route for achieving integrated functional network design lies in constructing functional sites directly within the crosslinking nodes themselves, thereby enabling the crosslinker to play a dual role in both structural support and ion regulation. A hydrogel electrolyte with a sprocket-like competitive transport mechanism was developed using amphiphilic F127DA micelles as macro crosslinkers [79]. The ether oxygen-rich poly(ethylene oxide) (PEO) segments within the micelles compete with the immobilized —SO_3^- groups for Zn^{2+} coordination. Such competition suppresses tight ion pair formation, decouples ion association, and thereby creates efficient pathways for rapid cation transport. This design allows the electrolyte to achieve a high ionic conductivity of 60.6 mS cm^{-1} and a Zn^{2+} transference number of 0.88. Small-angle x-ray scattering (SAXS) analysis confirms a random distribution of the micelles with an average spacing of 35.89 nm (Figure 5j). Concurrently, the micelles enhance mechanical properties through physical entanglement and energy dissipation, resulting in a tensile strength of 0.23 MPa and a toughness of 0.86 MJ m^{-3}. MD simulations further reveal the fastest Zn^{2+} migration rate within this system (Figure 5k), corroborating the promoting effect of its topological structure on ion transport.

Functional group modification represents a versatile molecular engineering paradigm that enables precise regulation of ion transport, interfacial chemistry, and mechanical properties in PAM-based hydrogel electrolytes through the strategic incorporation of chemically diverse functional moieties. This approach systematically addresses the intrinsic trade-offs among ionic conductivity, Zn^{2+} transference number, electrochemical stability window, and mechanical robustness that have historically hindered the application of hydrogel electrolytes in ZIBs. The specific choice of functional groups dictates the dominant regulatory mechanism: quaternary ammonium groups establish electrostatic repulsion-based cation highways while immobilizing anions; sulfonate and carboxylate groups coordinate with Zn^{2+} ions to restructure solvation sheaths and suppress free water activity; zwitterionic systems integrate complementary functionalities to achieve decoupled ion transport; and aromatic π systems engage in π-anion interactions to refine ion selectivity and transport kinetics. Beyond ion transport modulation, these functional groups collectively enhance interfacial stability by promoting the formation of stable adsorption layers, regulating water activity, and mitigating parasitic reactions. Looking forward, further exploration of synergistic multi-component functional systems, bioinspired functional motifs, and advanced characterization techniques will be crucial for unlocking the full potential of this molecular engineering approach.

4 | Enhancement of Battery Performance via Modification of PAM-Based Hydrogel Electrolytes

4.1 | Promoted Ion Transport Behavior

Ion transport efficiency in the electrolyte is considered a key parameter that essentially governs rate capability, cycling stability, and the overall device electrochemical performance [156]. Conventional PAM hydrogels typically suffer from inherent drawbacks, including slow interfacial charge-transfer kinetics and inadequate suppression of side reactions [157]. To address these key shortcomings, a variety of rational design strategies have been recently proposed and explored to engineer the microenvironment of hydrogel electrolytes. These approaches include constructing interconnected porous networks, introducing functional groups to stabilize Zn^{2+} solvation structures, optimizing polymer chain mobility, regulating water molecular state, and building continuous ion-conducting pathways. With these sophisticated modifications, the migration barrier for Zn^{2+} is substantially lowered, the desolvation process is accelerated, and the overall ion transport kinetics are greatly improved. As a result, PAM-based hydrogel electrolytes exhibit significantly enhanced ionic conductivity, interfacial compatibility, and electrochemical stability, thereby offering an efficient pathway to superior rate capability and extended cycle life in advanced aqueous ZIBs. As a quantitative reference, the representative ion transport properties of selected modified PAM hydrogels are summarized in Table 2.

The interconnected polymer chains in PAM hydrogels are incapable of transporting ions [158]. Instead, the migration of

ions is mainly controlled by the confined liquid electrolyte present inside the network. When water content decreases, the ion transfer process becomes impeded [159]. When the water content is low, raising the Zn^{2+} concentration within the hydrogel electrolyte represents the most direct means of improving its ionic conductivity. Nevertheless, typical Zn salts like Zn sulfate ($ZnSO_4$) and Zn trifluoromethanesulfonate ($Zn(OTf)_2$) have poor solubility in hydrogel media [160]. A promising strategy to enhance the Zn^{2+} transference number under low water-content conditions involves functional modification of the hydrogel network to restrict anion migration and increase the number of free Zn^{2+} ions. This significantly increases the cation transference number, transforming the system into a single-ion conducting electrolyte (SICE) with a transference number approaching 1. For example, Xia et al. developed a single Zn^{2+}-conducting hydrogel electrolyte (SIHE) by combining a PAM network with a pseudopolyrotaxane (PPR) structure, based on a molecular spatial confinement strategy [78]. The PPR structure consists of linear polymers (PEOs) and cyclic molecules (α-cyclodextrins, CDs). Diffusion-ordered spectroscopy (DOSY) and NMR analyses confirm that the cyclodextrins are threaded onto the PEO chains, forming a mechanically interlocked architecture (Figure 6a). In this design, α-cyclodextrins act as anion traps, confining OTf^- anions between two rings via steric hindrance, while Zn^{2+} ions migrate directionally along the hydroxyl sites on the exterior of the rings. This SIHE exhibits a high Zn^{2+} transference number of 0.923 and an ionic conductivity of 22.4 mS cm^{-1}. Furthermore, MD simulations and radial distribution function analysis indicate that Zn^{2+} forms a stable hexa-aqua coordination cluster $[Zn(H_2O)_6]^{2+}$ in water, with the nearest neighbor distance to oxygen atoms being approximately 0.2 nm (Figure 6b). When an electric field of 0.6 V nm^{-1} is applied along the PEO chain direction, this hydrated species migrates directionally along the chain. The migration trajectory clearly shows that Zn^{2+} preferentially adsorbs at the hydroxyl sites on the cyclodextrins and is transported along the chain driven by the electric field, achieving ordered migration (Figure 6c). Similarly, a single-ion conducting gel electrolyte (denoted as TCOF-S-Gel) has been constructed by incorporating a sulfonic acid group ($-SO_3^-$) functionalized covalent organic framework (TCOF-S) into a PAM matrix [161]. The introduced $-SO_3^-$ moieties act as anchored anion-accepting sites, which synergistically interact with the PAM polymer chains to construct a continuous Zn^{2+} transport "ladder" structure. This unique architecture facilitates fast and selective Zn^{2+} migration while effectively restricting the movement of free anions. Benefiting from this structural design, the Zn^{2+} transference number is notably elevated to 0.89, accompanied by a substantial enhancement in ionic conductivity (Figure 6d). Work function analysis based on DFT calculations reveals that the TCOF-S skeleton possesses high conjugation, and its delocalized electrons can form an electron-shielding buffer layer on the Zn anode surface, slowing down the cation deposition rate (Figure 6e). Concurrently, the uniformly distributed $-SO_3^-$ groups on the framework act as zincophilic sites, effectively promoting homogeneous Zn deposition, significantly reducing the nucleation overpotential, and thereby inhibiting Zn dendrite formation. Bioinspired multifunctional network designs can also be employed to construct continuous Zn^{2+} transport channels. Inspired by the structure of the American lobster's flexible membrane, Zhu et al. developed a hierarchically twisted hydrogel electrolyte (HTHEs) (Figure 6f) [162]. This electrolyte utilizes layer-by-layer twisted stacks of cellulose nanofiber (CNF) membranes, with each layer twisted by 36°, forming a well-defined hierarchically twisted structure conducive to creating ordered, twisted channels. This architecture effectively traps ClO_4^- anions, reduces the anion concentration around Zn^{2+}, lowers the desolvation energy barrier for Zn^{2+}, and facilitates its rapid transport, achieving a transference number as high as 0.9. X-ray diffraction (XRD) pole figure analysis reveals that the Zn (002) orientation peak intensity in the HTHE system reaches as high as 7.2, which is significantly stronger than that in random composite hydrogel electrolyte (RCHE) and liquid electrolyte (LE) systems. This indicates that HTHE effectively guides preferential Zn deposition along the (002) crystal plane, serving as a key contributing factor to its superior cycling stability.

Inside the hydrogel network, hydrophilic polymer side chains tightly bind water molecules, greatly restricting both the amount and movement of free water. Zn^{2+} ions are tightly confined within their solvation shells, severely hindering their migration through the electrolyte and resulting in an ionic conductivity approximately one order of magnitude lower than that of conventional aqueous electrolytes. Fortunately, introducing specifically designed functional groups enables effective modulation of the Zn^{2+} solvation environment and ion-transport routes via various noncovalent interactions. As a representative example, a morpholine-crosslinked PAM hydrogel electrolyte (marked as 6m-PAM) has been developed and verified [163]. In this system, nitrogen and oxygen atoms in morpholine groups can form strong coordination bonds with Zn^{2+} ions, thereby reconstructing the original Zn^{2+} solvation sheath and reducing the number of coordinated water molecules attached to Zn^{2+} ions. As presented in Figure 6g, this modified hydrogel electrolyte delivers a high ionic conductivity of 52 mS cm^{-1}, a relatively low activation energy of 28.2 kJ mol^{-1}, as well as an elevated Zn^{2+} transference number of 0.51. Reduced density gradient (RDG) isosurface analysis indicates that the 6m-PAM system is stabilized by O—O hydrogen bonds and van der Waals interactions (Figure 6h,i). By introducing polymer backbones with weak cation adsorption capability but strong anion affinity, the ion transport behavior of the electrolyte can be precisely regulated. Zhu et al. developed an anion-philic polymer hydrogel electrolyte (APHE) based on PAM and aramid nanofibers (ANF) [164]. The polymer backbone in this electrolyte possesses both electrophilic and nucleophilic characteristics, enabling the formation of "strong anion-polymer" and "weak Zn^{2+}-polymer" interactions. This design restricts anion migration while promoting the dynamic transport of Zn^{2+}. ESP analysis further elucidates the charge distribution and interactions among the polymer, solvent, and salt (Figure 6j). NMR reveals that the $-CONH_2$ interacts with OTf^- anions, thereby reducing the free water content. The APHE demonstrates an ionic conductivity of 17.8 mS cm^{-1} and a Zn^{2+} transference number of 0.71, highlighting its effectiveness in guiding selective ion transport.

Functional modification strategies for PAM hydrogel electrolytes focus on reconstructing and optimizing the ion transport system, with the core objective of overcoming the inherent coupling between anion and cation migration. This persistent limitation severely restricts the electrochemical behavior of ZIBs. In traditional hydrogel electrolytes, free anions and Zn^{2+} migrate in a coupled manner, which not only hinders the overall ion

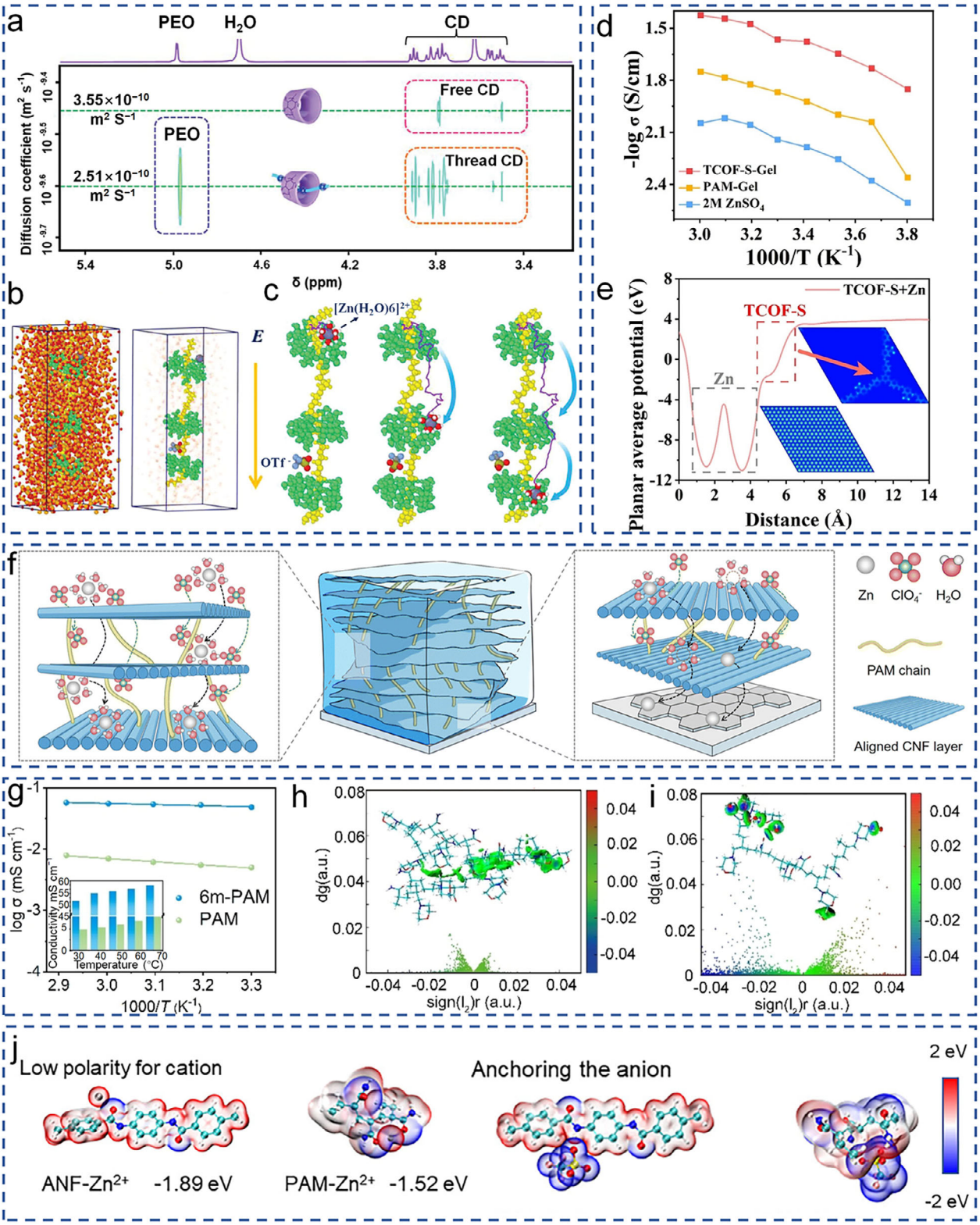

FIGURE 6 | (a) DOSY spectra of the PPR. (b) PPR MD model. (c) Zn^{2+} transport within PPR under an applied electric field. Reproduced with permission [78]. Copyright 2023, Wiley-VCH. (d) Ion conductivity of TCOF-S-Gel, PAM-Gel, and 2 M $ZnSO_4$ as a function of temperature. (e) Plane-averaged electrostatic potential profile from the Zn surface to the TCOF-S interface. Reproduced with permission [161]. Copyright 2023, Wiley-VCH. (f) Schematic of the multi-stage synergistic design in hierarchical twisted hydrogel electrolytes. Reproduced with permission [162]. Copyright 2025, Royal Society of Chemistry. (g) Arrhenius plots of different electrolytes. RDG-sign(l_2)r scatter plot of (h) 6m-PAM-6m-PAM and (i) 6m-PAM-H_2O. Reproduced with permission [163]. Copyright 2025, Elsevier. (j) Cation–dipole interactions and binding energies of Zn^{2+} with carbonyl moieties in ANF and PAM, along with the strong anchoring of OTf^- anions by amine groups. Reproduced with permission [164]. Copyright 2026, Wiley-VCH.

TABLE 3 | Comparison of the reported mechanical properties of different PAM-based hydrogel systems for ZIBs.

Nos.	Hydrogel system	Modifying strategy	Tensile strength (kPa)	Elongation (%)	Refs.
1	PAM-ZnK4Ac	Organic molecular additives	37.5	250	[166]
2	PAM-PAMPS-10PD	Organic molecular additives	7.1	520	[116]
3	PZD	Organic molecular additives	82	690	[117]
4	PCZ-gel	Construction of multifunctional networks	200	990	[139]
5	PAAm/SA	Construction of multifunctional networks	757.5	1000	[138]
6	CT-PAM	Functional filler	60.3	1328	[167]
7	P-MC	Functional filler	489	3500	[168]

transport speed but also triggers severe side reactions and electrode degradation. By breaking this restrictive migration pattern, it is possible to build continuous, selective, and highly efficient ion transport channels that prioritize fast and stable Zn^{2+} conduction, minimizing the interference of inactive anion movement. Adopting synergistic modification strategies covering molecular-scale chemical functionalization, intermolecular interaction regulation, microscopic pore structure tuning, and polymer network optimization, the core performance metrics of hydrogel electrolytes can be elevated in an all-round way. These key indicators include room-temperature ionic conductivity, ion migration kinetics, interfacial charge transfer efficiency, and long-term operational stability. Such a targeted and systematic optimization scheme effectively solves the inherent defects of pure PAM hydrogel electrolytes, supplying a high-performance, stable, and practical electrolyte platform. In turn, this lays a solid foundation for the fabrication and large-scale application of advanced aqueous ZIBs with outstanding high-rate discharge capability, ultralong cycling stability, and excellent mechanical adaptability for flexible energy storage devices.

4.2 | Targeted Enhancement of Mechanical Properties

Mechanical strength stands as one of the most indispensable performance indicators for hydrogel electrolytes, exerting a pivotal influence on both the practical application of flexible and wearable electronic devices and the long-term durability and electrochemical stability of aqueous ZIBs [45]. Pure PAM hydrogels normally suffer from inferior mechanical robustness, insufficient tensile strength, and poor structural toughness, making them prone to fracture, deformation, and mechanical failure under repeated bending, stretching, or external pressure during cycling [165]. In contrast, a hydrogel electrolyte with outstanding mechanical robustness can effectively withstand external mechanical stress and maintain structural integrity, which is vital for stable long-term operation. More importantly, a tough and rigid hydrogel matrix can physically impede the uneven Zn deposition and efficiently restrain the uncontrolled growth and penetration of Zn dendrites, a major threat that causes internal short circuits and sudden battery failure. By blocking dendrite propagation and maintaining a stable electrode/electrolyte interface, this mechanically strengthened electrolyte establishes a safer, more uniform, and controllable ion transport microenvironment. As a quantitative summary, the representative mechanical properties of selected modified PAM hydrogel systems are compiled in Table 3.

By introducing strong hydrogen bond donors or acceptors, dense hydrogen bond networks can be formed, thereby enhancing the rigidity and toughness of hydrogels. For example, Lin et al. developed a PAM-$Zn(Ac)_2$-4KAc (PAM-ZnK4Ac) hydrogel electrolyte [166]. In this system, acetate (Ac^-) anions synergize with the $-CONH_2$ on the PAM chains to disrupt the inherent hydrogen bond network of water molecules through the formation of N—H•••O hydrogen bonds. This reduces free water content while strengthening intermolecular interactions between polymer chains. However, the resulting mechanical strength varies with the concentration of Ac^-. Tensile strength initially increases with KAc concentration to a maximum value and subsequently decreases. This trend is attributed to the influence of KAc concentration on both the water content and the polymer network structure of the hydrogel electrolyte. At low KAc concentrations, higher water content leads to a weaker network structure, reducing tensile strength. An optimal balance between water content and network stiffness is achieved at a $Zn(Ac)_2$/KAc mass ratio of 1:3, yielding a peak tensile strength of approximately 30 kPa (Figure 7a). Exceeding this ratio disrupts the polymer network due to excessive salt screening of intermolecular interactions, ultimately lowering tensile strength. Furthermore, this regulation mechanism endows the hydrogel with excellent adhesive properties (shear strength reaching 10–15 kPa) (Figure 7b). The densified hydrogen bond network enables effective stress distribution during deformation, preventing local fracture and enhancing overall mechanical stability. Besides employing salt anions to regulate intermolecular interactions, directly incorporating hydroxyl-rich small organic molecules represents another feasible and effective strategy. This approach is widely adopted to fabricate dense and stable hydrogen bond networks inside the hydrogel matrix, thereby significantly boosting the mechanical strength, toughness, and structural stability of the electrolyte. As a typical example, a hydrogel electrolyte has been successfully fabricated using AM, 2-acrylamido-2-methylpropane sulfonic acid (AMPS), and 1,5-pentanediol (PD) as raw materials, which is coded as PAM-PAMPS-10PD for concise description [116]. PD, rich in hydroxyl groups, not only forms multiple hydrogen-bond cross-links with the PAM chains but also constructs a more

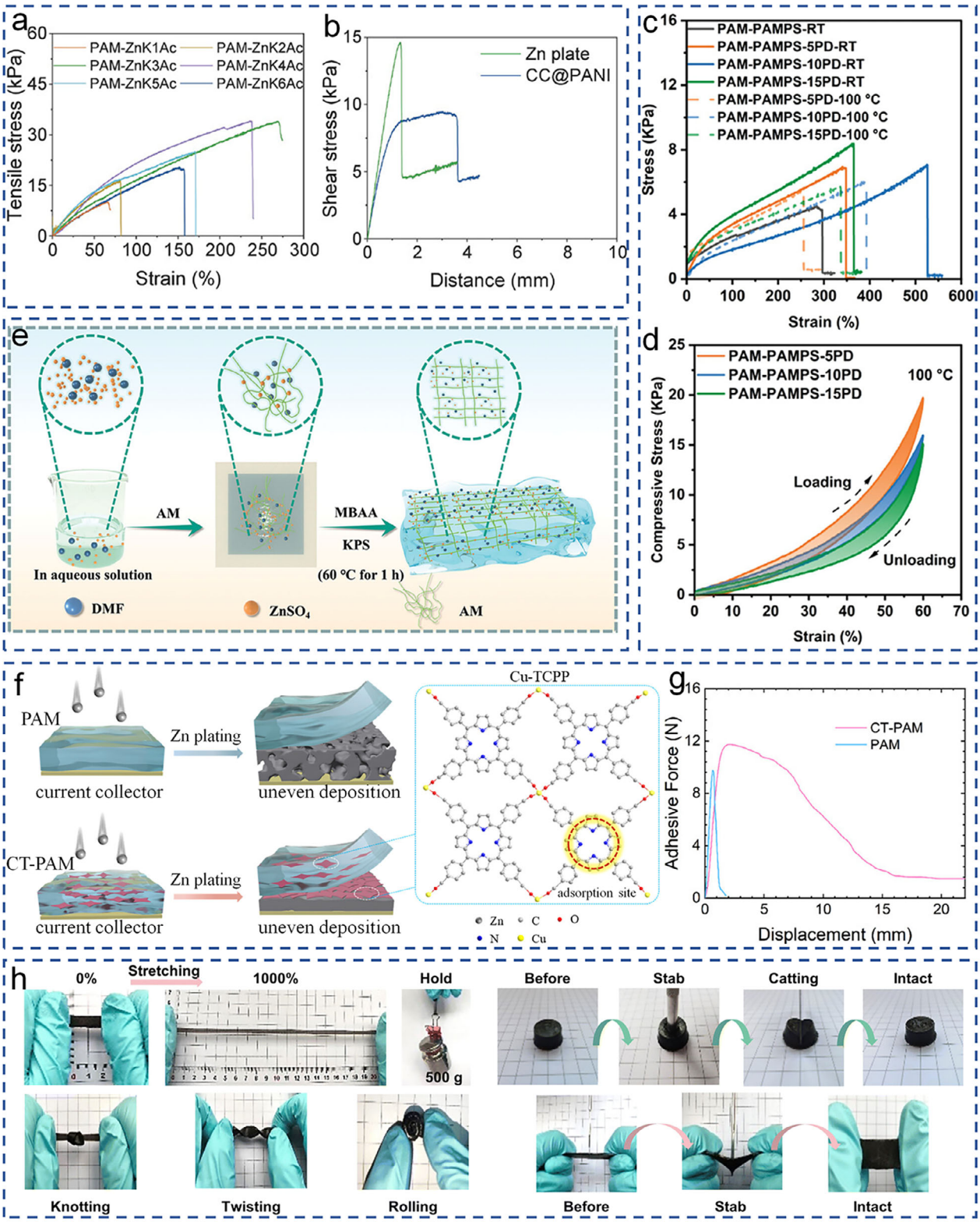

FIGURE 7 | (a) Stress–strain curves of PAM-ZnKnAc. (b) Shear strength of PAM-ZnK4Ac on Zn and CC@PANI substrates. Reproduced with permission [166]. Copyright 2025, Wiley-VCH. (c) Tensile stress–strain curves at room temperature and 100°C. (d) Compressive curves under 100°C. Reproduced with permission [116]. Copyright 2024, Wiley-VCH. (e) Schematic diagram of hydrogel synthesis. Reproduced with permission [117]. Copyright 2024, Wiley-VCH. (f) Schematic depicting the role of CT-PAM HE in achieving uniform Zn deposition. (g) Adhesive force–displacement curves of CT-PAM and PAM HEs. Reproduced with permission [167]. Copyright 2025, Wiley-VCH. (h) Optical images of the P-MC during mechanical property testing. Reproduced with permission [168]. Copyright 2024, Royal Society of Chemistry.

stable hydrogen-bond network with water molecules through its strong hydration capability. Simultaneously, the PAM-PAMPS network provides abundant anionic groups (—SO_3^-), while PD further optimizes the network structure, significantly enhancing both mechanical properties and high-temperature stability. At room temperature, the hydrogel displays a fracture elongation of approximately 520% and a tensile strength of 7.07 kPa. Even at 100°C, it retains an elongation of 390% and a strength of 5.96 kPa (Figure 7c), alongside remarkable compressive recovery capability and exceptional fatigue resistance (Figure 7d). This hydrogen-bond modulation strategy demonstrates broad temperature adaptability and can be extended to low-temperature applications by selecting appropriate polar solvent molecules. For instance, Zhang et al. introduced the polar aprotic solvent N, N-dimethylformamide (DMF) (Figure 7e) [117]. The carbonyl group in DMF serves as a strong hydrogen-bond acceptor, creating hydrogen bonds with both water molecules and the —$CONH_2$ on PAM chains, thereby reinforcing the polymer network. This hydrogel remains transparent, stretchable (with a fracture elongation of 690%), and exhibits good shape-recovery capability even at −20°C. SEM reveals a uniform 3D porous structure, which facilitates Zn^{2+} transport. Furthermore, the hydrogel demonstrates excellent moldability, twistability, and stretchability, highlighting its outstanding mechanical performance.

The construction of multifunctional dual-network structures has become an effective design strategy for concurrently improving mechanical strength and inhibiting Zn dendrite growth in hydrogel electrolytes. Its key lies in achieving synergistic reinforcement by combining different crosslinking mechanisms, such as covalent, physical, and ionic crosslinking. In the aforementioned dual-network PCZ-gel, polar groups generate physical crosslinking sites through hydrogen bonding interactions [139]. This unique crosslinking structure endows the hydrogel with outstanding mechanical performance, including a tensile stress of 200 kPa, a fracture elongation of 990%, a toughness of 1111 kJ m^{-3} and an elastic modulus of 31.0 kPa. These values are significantly higher than those of PAM gel (toughness: 184.4 kJ m^{-3}, modulus: 18.7 kPa). The gel can be elongated to ten times its initial length and endure high compression without fracturing. Similarly, Wang et al. constructed a PAM/SA dual-network hydrogel [138]. Within this architecture, Zn^{2+} ions penetrate the zigzag G-block regions of the SA chains and become trapped in the chelation pockets formed between two neighboring alginate chains. This architecture increases the fracture strength significantly to 757.5 kPa, achieves an interfacial adhesion strength of approximately 164.47 kPa, and enables complete recovery after being subjected to a 1 kg load.

The introduction of functional nanofillers enables the creation of reinforced composite structures within the hydrogel matrix, markedly improving both the mechanical strength and fracture toughness of the bulk material. Meanwhile, the plentiful active functional groups, such as hydroxyl and carboxyl moieties, are capable of forming stable interactions with Zn^{2+} ions. These interactions effectively suppress ion aggregation and boost the concentration of freely mobile ions, making it possible to optimize the mechanical properties of the electrolyte. As a typical illustration, two-dimensional porphyrin-based metal–organic framework nanosheets, namely Cu-TCPP, were adopted as versatile multifunctional fillers and incorporated into a PAM matrix to prepare a CT-PAM composite hydrogel electrolyte, as presented in Figure 7f [167]. The Cu-TCPP nanosheets exhibit a planar two-dimensional lamellar structure and an abundance of surface functional groups. Their porous framework and high specific surface area provide numerous physical crosslinking sites, significantly enhancing the interfacial interaction between the filler and polymer chains. Tensile tests demonstrate that the CT-PAM hydrogel achieves a tensile strength of 60.3 kPa and an elongation at break of up to 1328%, far exceeding that of pure PAM hydrogel. This enhancement is attributed to the composite structure formed by the rigid MOF nanosheets and flexible PAM chains, as well as the abundant hydrogen-bonding interactions at their interface, enabling effective stress dispersion and energy dissipation during deformation. Moreover, the strong interfacial bonding between filler and matrix also improves the adhesive properties of the hydrogel (Figure 7g), with its shear strength significantly higher than that of pure PAM, which is beneficial for reducing electrode/electrolyte interfacial resistance and promoting ion transport. In contrast to two-dimensional MOF fillers, one-dimensional carbon nanotubes exhibit unique advantages in enhancing the mechanical performance of hydrogels due to their distinctive tubular structure and excellent mechanical properties. Luo et al. introduced carboxylated multiwalled carbon nanotubes (MWCNTs) into a PAM network to construct a P-MC composite hydrogel electrolyte [168]. The abundant carboxyl groups on the MWCNT surface form strong hydrogen-bonding interactions with the amide groups of PAM chains, while the rigid tubular structure of MWCNTs provides physical entanglement points for the polymer chains. These synergistic effects collectively construct multiple energy dissipation structures. Thus, as demonstrated in Figure 7h, the P-MC hydrogel possesses remarkable mechanical flexibility, enduring twisting, stretching, rolling, and knotting without fracture. Even after puncture or cutting, its structure remains intact, and a thin sheet can suspend a 500 g weight without breaking, demonstrating excellent tensile strength. Mechanical tests reveal that with increasing MWCNT content, the tensile strength of the hydrogel increased from 91 to 489 kPa, elongation at break rose from 1130% to 3500%, and fracture toughness is significantly enhanced. This enhancement stems from the formation of multiple energy-dissipating networks via hydrogen bonding and physical entanglement between MWCNTs and PAM chains, which imparts both high strength and high toughness to the hydrogel.

Through various rational and targeted functional modification strategies, the comprehensive mechanical properties of PAM-based hydrogel electrolytes can be significantly enhanced across multiple dimensions, including mechanical strength, fracture toughness, elastic recovery capability, and interfacial adhesion with electrode materials. These multidimensional improvements in mechanical performance are not only essential for ensuring the structural integrity and dimensional stability of hydrogel electrolytes under complex mechanical stresses, such as repeated bending, stretching, compression, and torsion encountered in flexible device applications, but also serve a critical function in maintaining a stable and intimate electrode/electrolyte interface during long-term battery cycling. By effectively reducing interfacial detachment, minimizing contact resistance, and suppressing the formation of interfacial defects caused by mechanical deformation, the modified hydrogels can sustain efficient ion transport

at the electrode/electrolyte interface. This thus offers a solid and reliable foundation for advancing and practically implementing high-performance, long-lasting FZIBs that can meet the rigorous requirements of flexible, wearable, and portable energy storage devices.

While the preceding discussion has highlighted individual enhancements in mechanical strength and ionic conductivity, it is critical to acknowledge that these two performance metrics are often inherently conflicting in hydrogel electrolyte design. High ionic conductivity requires continuous liquid-phase pathways with low tortuosity and high polymer chain mobility, typically achieved through low crosslinking density and high water content. Conversely, high mechanical strength demands a dense, highly crosslinked network with strong inter-chain interactions, which inevitably restricts chain segmental motion, reduces pore connectivity, and increases the tortuosity of ion transport pathways, all of which lower ionic conductivity [47]. Three key parameters govern this trade-off. First is crosslinking density, where higher density enhances mechanical strength at the expense of free volume and chain mobility, leading to an increased activation energy for ion hopping. Second is water content, as higher water content promotes ionic conductivity by providing continuous liquid-phase channels but simultaneously softens the polymer network and compromises its puncture resistance. Third is functional group density, where polar groups can improve both ion selectivity and mechanical interactions, yet excessive functionalization risks over-crosslinking or electrostatic screening and ultimately degrades both properties [69].

4.3 | Modulation of Interfacial Desolvation and Deposition Behaviors

The stability of the electrode/electrolyte interface is a critical determinant of long-term battery cyclability, operational safety, and overall electrochemical performance [169]. For PAM-based hydrogel electrolytes paired with Zn anodes, the interface poses multiple inherent challenges that severely restrict battery performance. On the one hand, the intrinsic structural characteristics of PAM hydrogels often lead to incomplete physical contact between the electrolyte and the Zn anode surface, which tends to cause elevated interfacial resistance, nonuniform current distribution, and hindered ion transport [170]. This nonuniformity further aggravates the uneven deposition on the anode surface, laying the foundation for Zn dendrite formation. On the other hand, the sluggish desolvation of Zn^{2+} ions occurs at the hydrogel/anode interface, where Zn^{2+} ions fail to completely shed their solvation shells, primarily composed of coordinated water molecules, prior to their deposition onto the Zn anode surface [76]. This disordered deposition not only reduces the Coulombic efficiency but also promotes the growth of Zn dendrites [171]. Meanwhile, the side reaction-derived by-products further block the ion transport channels at the interface, impairing the charge transfer efficiency and exacerbating the instability of the electrode/electrolyte interface [172]. Collectively, these interfacial issues significantly compromise key battery performance metrics, including cycling life, Coulombic efficiency, and rate capability, becoming a major bottleneck for the practical deployment of PAM hydrogel-based ZIBs.

The strength and density of hydrogen bonds between polymer chains and water molecules determine the fraction of free water versus bound water. A higher proportion of bound water increases the viscosity of the confined liquid phase and raises the energy barrier for ion hopping, while an optimized hydrogen bond network (e.g., through cryoprotective additives or functional groups) lowers the desolvation energy barrier by providing alternative low-energy pathways for ion migration [173]. Water molecules in the primary solvation sheath of Zn^{2+} are in dynamic exchange with the surrounding hydrogen bond network. When strong hydrogen bond acceptors (e.g., carbonyl, sulfonate, or ether groups) are introduced into the PAM network, they compete with water molecules for hydrogen bonding, effectively weakening the water–water hydrogen bond network and reducing the residence time of water molecules in the Zn^{2+} solvation sheath. This accelerates the desolvation kinetics and enhances the Zn^{2+} diffusion coefficient. In addition, the 3D hydrogen bond network within the hydrogel creates a percolation pathway for ion transport [22]. A well-designed network with optimal crosslinking density and functional group distribution minimizes tortuosity and maximizes continuous liquid-phase channels. Conversely, excessive hydrogen bonding restricts polymer chain mobility and reduces pore connectivity, leading to decreased ionic conductivity.

Polar molecules can effectively reconstruct the hydrogen-bond network within the PAM hydrogel structure, thereby reducing the activity of free water molecules, suppressing their evaporation and electrolysis, and simultaneously enhancing the hydrogel's water retention capability. Based on this hydrogen-bond reconstruction strategy, a PAM-based organohydrogel electrolyte has been developed using a dimethyl sulfoxide (DMSO)/water binary solvent system (Figure 8a) [174]. DMSO, as a polar aprotic solvent with strong hydrogen-bond-accepting capability, directionally reconstructs the hydrogen-bond network by forming competitive DMSO—H_2O hydrogen bonds. FTIR spectroscopy of the O—H stretching region (2800–4000 cm^{-1}) reveals that the introduction of DMSO leads to a noticeable increase in medium and weak hydrogen bonds at higher wavenumbers, accompanied by a reduction in the proportion of strong hydrogen bonds at lower wavenumbers (Figure 8b). Quantitative analysis through MD simulations further confirms that the total number of hydrogen bonds increases from approximately 8.2×10^3 in the pure PAM hydrogel to 10.5×10^3 in the DMSO-containing organohydrogel. This seemingly paradoxical increase reflects the immobilization of free water molecules through DMSO—H_2O hydrogen bonding, which reduces free water activity and effectively suppresses water evaporation and decomposition. DFT calculations reveal that DMSO exhibits a stronger binding affinity with Zn^{2+} (−1.2 eV) compared to H_2O (−0.6 eV), enabling DMSO to preferentially participate in the Zn^{2+} solvation sheath and replace coordinated water molecules. Consequently, this modified organohydrogel electrolyte achieves significant enhancements in water retention capability and the stability of both cathode and anode interfaces, enabling the Zn//Zn symmetric cell to achieve ultralong cycling stability exceeding 5000 h. HER frequently raises the interfacial pH, resulting in the generation of by-products such as Zn hydroxide sulfate. The electronically insulating and electrochemically inactive nature of these by-products further exacerbates the inhomogeneity of the electric field distribution on the anode surface. Constructing a macroscopically spatially heterogeneous

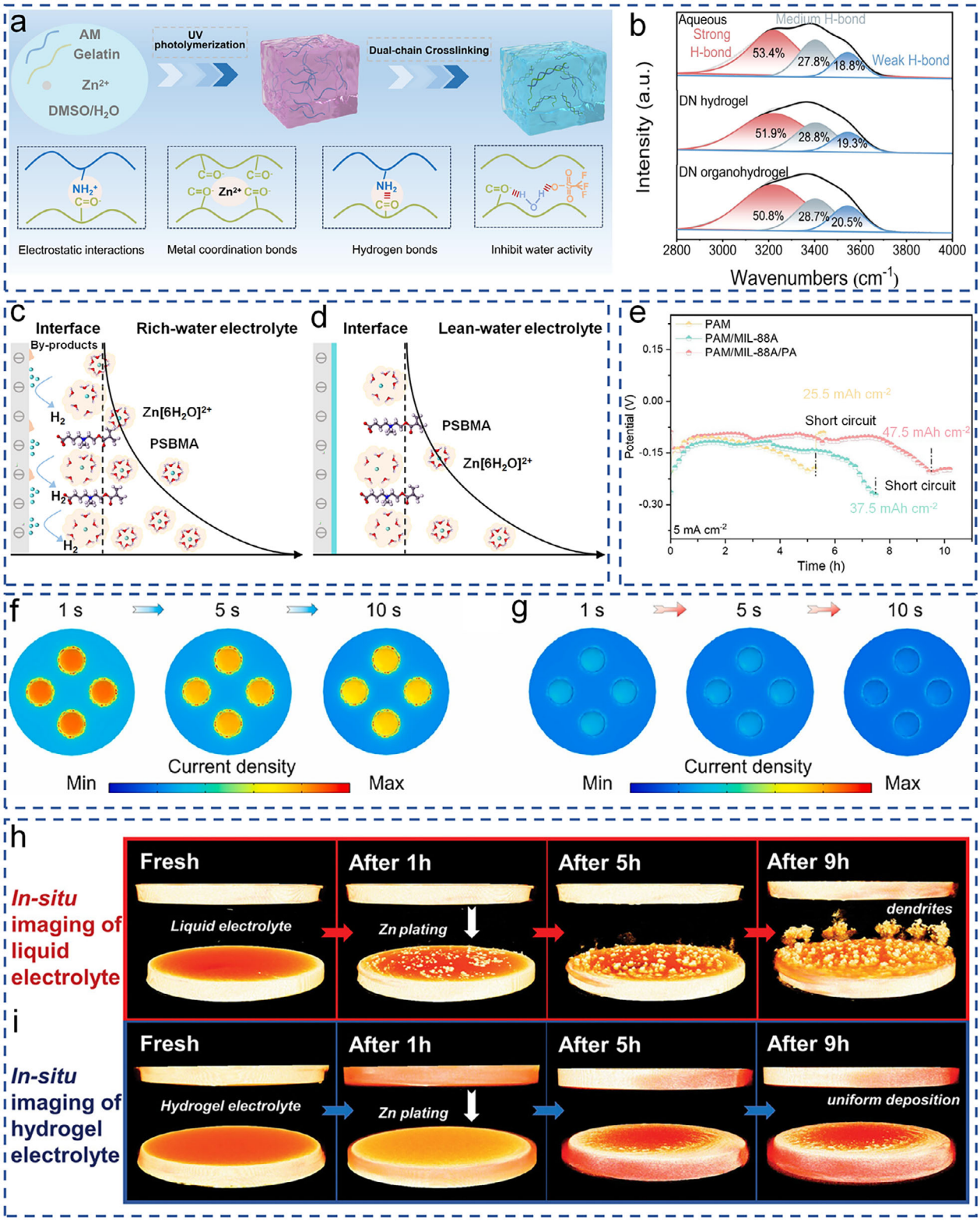

FIGURE 8 | (a) Synthesis diagram of the dual-network organohydrogel. (b) FTIR spectra of organohydrogel electrolytes. Reproduced with permission [174]. Copyright 2024, Elsevier. Schematic depicting the electrochemical behavior of (c) water-rich and (d) water-lean hydrogels. Reproduced with permission [175]. Copyright 2025, Wiley-VCH. (e) Overcharge cycling tests of Zn symmetric cells employing various gel electrolytes at a current density of 5.0 mA cm^{-2}. Reproduced with permission [176]. Copyright 2025, Wiley-VCH. Spatial distribution of local current density at the Zn anode interface for (f) ZSO and (g) PAM@ZIF-8. Reproduced with permission [131]. Copyright 2026, Elsevier. In situ synchrotron tomography (ST) was employed to examine the morphology of Zn dendrites formed in Zn symmetric cells after galvanostatic plating at 6 mA cm^{-2} with (h) liquid and (i) hydrogel electrolytes. Reproduced with permission [178]. Copyright 2023, Wiley-VCH.

structure within the hydrogel matrix to regulate the local aqueous environment and suppress interfacial side reactions represents a promising and effective approach. As a typical implementation, a spatially heterogeneous functional network has been successfully constructed by integrating water-rich PAM hydrogel regions with water-deficient poly(sulfobetaine methacrylate) (PSBMA) hydrogel zones [175]. This heterogeneous structure enables precise regulation of the local water content and distribution across the hydrogel, creating distinct microenvironments that work synergistically to inhibit side reactions and optimize ion transport behavior. XRD patterns analysis further confirms that high-water-content PSBMA hydrogel electrolytes generate minor by-products that alter Zn deposition behavior, while the water-deficient zwitterionic hydrogel not only optimizes the Zn deposition process through enhanced desolvation but also guides a uniform deposition morphology via its anchoring effect on the Zn surface. Therefore, under water-deficient conditions, the lower water content more efficiently inhibits proton corrosion and the HER, while also decreasing the overpotential for Zn deposition (Figure 8c,d). Based on this design, a Zn//Zn symmetric cell employing this electrolyte achieves stable cycling for up to 1200 h under an 80% depth of discharge. To prevent disordered nucleation and growth of passivation layers, one effective approach is to mitigate local pH elevation, a key factor governing interfacial chemistry. Recent advances have demonstrated effective strategies in this direction. Chen et al. incorporated sodium citrate (SC) into a PAM/sodium carboxymethyl cellulose (CMC) dual network hydrogel (denoted as PAM/SC/CMC-Na) [37], where the three carboxylate groups of each citrate ion establish reversible protonation and deprotonation equilibria that stabilize interfacial pH. Citrate species capture excess H^+ during acidification and release protons when OH^- accumulates, acting as a multisite buffering reservoir. This buffering action suppresses the formation of basic Zn sulfates by preventing local OH^- from reaching the precipitation threshold, while also mitigating HER kinetics by reducing the driving force for proton reduction. Consequently, the combined suppression of passivation layers and HER promotes uniform Zn deposition, as evidenced by the ultralong cycling stability (over 11430 h) achieved with the PAM/SC/CMC-Na system.

MOFs, featuring highly ordered porous networks, tunable pore sizes, and programmable ion-sieving capabilities, offer a promising route to overcoming the intrinsic challenges of gel electrolytes in ZIBs. As a typical illustration, a phytic acid (PA)-phosphorylated MIL-88A MOF has been incorporated into a PAM gel electrolyte, constructing a synergistic ion rectification and charge redistribution strategy that enables the achievement of a highly reversible Zn anode [176]. This integration leverages the unique structural and functional advantages of MOFs to optimize ion transport, suppress side reactions, and boost the overall electrochemical stability of the gel electrolyte system. In this strategy, the phosphate groups of PA act as zincophilic sites to promote rapid ion migration, while the porous MIL-88A framework dissipates local charge accumulation, thereby synergistically suppressing dendrite growth. In an over-charge test at 5.0 mA cm^{-2} (Figure 8e), the Zn//Zn symmetric cell using this electrolyte delivers a cumulative deposition capacity of up to 47.5 mAh cm^{-2} without short-circuiting, significantly outperforming pure PAM (25.5 mAh cm^{-2}) and PAM/MIL-88A systems (37.5 mAh cm^{-2}). Confocal laser scanning microscopy (CLSM) analysis presents a dense and flat Zn deposition layer with a surface roughness of only 1.05 μm, representing a 76.9% improvement in smoothness compared to PAM. SEM images also manifest effective suppression of dendrite growth. Leveraging these advantages, the battery exhibits long-term cycling stability exceeding 3600 h and a high Zn utilization rate of 56.9%. Beyond regulating interfacial charge through ion rectification, MOFs can also reconstruct the solvation environment of Zn^{2+} ions and guide preferential crystal growth via their unique pore chemistry and surface functional groups. ZIF-8 nanoparticles have been incorporated into a PAM hydrogel matrix to fabricate a PAM@ZIF-8 composite electrolyte [131]. The C═N functional groups within the ZIF-8 framework can confine SO_4^{2-} anions and water molecules, which not only suppresses interfacial side reactions but also accelerates the Zn^{2+} desolvation process. Meanwhile, its selective adsorption stabilizes the Zn (002) crystal plane, modulates crystal growth kinetics, and encourages oriented Zn growth on the (002) plane. XRD analysis further confirms that no by-product peaks are detected on the cycled Zn anode, and the Zn (002)/Zn (101) peak intensity ratio reaches 1.40, significantly higher than that of the PAM hydrogel (0.41) and the liquid $ZnSO_4$ (ZSO) system (0.33). Electrochemical tests show that the Zn//Cu cell maintains an average Coulombic efficiency of 99.6% over 1800 cycles at 5 mA cm^{-2} and 1 mAh cm^{-2}, while the Zn//Zn symmetric cell achieves an ultralong cycle life of 6500 h at 1 mA cm^{-2} and 1 mAh cm^{-2}. Finite element simulations further present that PAM@ZIF-8 homogenizes Zn^{2+} flux and electric field distribution (Figure 8f,g), avoiding the dendrite growth caused by ion gradients in conventional electrolytes.

Functional groups can be introduced onto the polymer backbone of hydrogels through chemical modification. These introduced groups can optimize ion transport pathways and lower the desolvation barrier of Zn^{2+} ions through non-covalent interactions. For instance, a bifunctional zwitterionic hydrogel electrolyte (BZHE) has been designed, which ingeniously separates anionic (—BF_3^-) and cationic (—C—N^+) groups [177]. The cationic moieties help regulate Zn^{2+} transport and enable uniform Zn deposition. Meanwhile, the —BF_3^- groups reconfigure the Zn^{2+} solvation sheath through water coordination to inhibit side reactions. The Zn deposition process at 10 mA cm^{-2} was monitored by in situ optical microscopy, which revealed markedly different behaviors between the two electrolytes. In the PAM electrolyte system, loose deposits appear within 10 min, and after 60 min these evolve into pronounced Zn dendrites accompanied by significant surface roughening. In comparison, BZHE forms a uniform Zn deposit devoid of dendrites after 60 min, demonstrating its enhanced capacity to inhibit side reactions and regulate nucleation kinetics. Consequently, BZHE allows Zn//Zn symmetric cells to achieve ultralong cycling stability exceeding 6300 h at a current density of 1 mA cm^{-2}/0.25 mAh cm^{-2}. Aside from designs that enhance solvation structures via group separation, creating oriented internal ion migration pathways offers another proven route to control ion migration and curb dendrite growth. Consider an in situ prepared glass-fiber-reinforced dual-ion zwitterionic hydrogel electrolyte, as it takes advantage of the electrostatic interactions inherent to zwitterionic segments [178]. This electrolyte generates oriented ion transport channels within the gel, enabling efficient cation movement while immobilizing anions. This strategy optimizes ion migration behavior while preserving a high ionic conductivity

TABLE 4 | Comparison of wide-temperature full-cell cycling performance for different PAM-based hydrogel systems in ZIBs.

Nos.	Hydrogel system	Modifying strategy	Test conditions	Wide-temperature cycling performance	Refs.
1	PAM-T-S	Functional group copolymerization	Zn//VO_2 1 C/0.5 C	5000 cycles at −20°C 1000 cycles at 60°C	[184]
2	GE	Organic molecular additives	Zn//$Zn_{0.58}V_2O_5{\cdot}H_2O$ 0.1 A g^{-1}	100 cycles at −40°C	[185]
3	CSAM-C	Construction of multifunctional networks	Zn//PANI 5 A g^{-1}	2500 cycles at −30°C	[186]
4	Glu/ZC/PAM	Organic molecular additives	Zn//$NH_4V_4O_{10}$ 0.5 A g^{-1}	300 cycles at −30°C 50 cycles at 70°C	[110]
5	PAP	Functional group copolymerization	Zn//$Zn_2V_2O_7$ 2 A g^{-1}	400 cycles at −20°C 400 cycles at 50°C	[155]

of 24.32 mS cm^{-1}. The deposition process was examined using in situ scanning transmission electron microscopy (STEM). Given the susceptibility of the hydrogel to electron-beam degradation, static imaging was conducted at four time points (fresh state, 1, 5, and 9 h) following galvanostatic discharge at 6 mA cm^{-2}. Electrochemical measurements indicate that the hydrogel electrolyte achieves a stable voltage plateau within just 1 h, whereas the liquid electrolyte suffers from repeated voltage fluctuations and inferior stability. STEM imaging results further reveal that in the liquid electrolyte, extensive Zn dendrite growth occurs after 5 h, causing a sharp voltage drop, and by 9 h, the dendritic structure extends over half the distance to the counter electrode (Figure 8h). By contrast, in the hydrogel electrolyte, even after 9 h of deposition, no appreciable dendrite formation is observed on the electrode surface, and the deposited layer remains uniform and compact (Figure 8i). Collectively, these electrochemical and morphological findings confirm that this zwitterionic hydrogel promotes uniform Zn deposition, markedly suppresses dendrite formation, and consequently improves the cycling durability of the battery.

The electrode/electrolyte interface in ZIBs faces a set of interrelated issues, such as severe free-water-induced side reactions, dendrite formation, parasitic byproduct generation, and a restricted electrochemical stability window. To confront these issues, a series of effective interfacial regulation strategies has been developed by integrating molecular engineering and structural design into hydrogel electrolytes. At the molecular level, functional groups such as hydroxyl, carboxyl, sulfonate, and zwitterionic moieties are introduced to modulate water activity, restrict free water mobility via hydrogen bonding or electrostatic interactions, and facilitate desolvation of Zn^{2+} ions. Through synergistic effects between chemical functionalities and architectural features, a stable, efficient, and deformation-tolerant solid–liquid interface is constructed. This engineered interface not only withstands repeated volume changes during cycling but also maintains ionic conductivity under mechanical stress. As a result, it provides a critical material foundation for significantly extending the cycling life (e.g., over thousands of hours), improving Coulombic efficiency (often above 99.5%), and enhancing the overall safety of ZIBs by minimizing gas evolution and thermal runaway risks.

4.4 | Boosting Wide-Temperature Adaptability

In conventional PAM hydrogel electrolytes, free water molecules tend to form ice crystals at sub-zero temperatures, while at elevated temperatures, accelerated water activity exacerbates parasitic side reactions and interfacial degradation [179]. These issues drastically reduce ionic conductivity, increase interfacial charge-transfer resistance, and trigger uncontrolled dendritic Zn growth alongside parasitic side reactions [180]. To address these drawbacks, recent studies have concentrated on designing various functional modification strategies that regulate the internal hydrogen-bond network and the state of water molecules within hydrogels. These strategies include introducing cryoprotective additives (e.g., glycerol, ethylene glycol, or DMSO), incorporating functional groups that strongly bind water (such as hydroxyl or zwitterionic moieties), and constructing partially crosslinked or anti-freezing polymer matrices [77, 181]. These approaches not only suppress ice crystallization at low temperatures but also mitigate water-induced side reactions at high temperatures, thereby maintaining efficient ion transport pathways and preserving electrode/electrolyte interfacial stability across a broad thermal range. Consequently, the wide-temperature tolerance of hydrogel electrolytes has been significantly enhanced. Nevertheless, achieving stable operation of ZIBs across a wide temperature window, especially under both freezing and high-temperature conditions, remains a key challenge for practical applications [182]. Addressing this challenge requires simultaneous optimization of ionic conductivity, interfacial kinetics, and mechanical flexibility under extreme thermal conditions. For quantitative comparison, the wide-temperature full-cell cycling performance of representative functionalized PAM hydrogel systems is listed in Table 4.

The freezing of water involves the transformation of randomly arranged water molecules into an ordered ice lattice through intermolecular hydrogen bonds. Thus, reducing the freezing point of hydrogel electrolytes hinges on breaking the hydrogen bonds among water molecules [183]. At high temperatures, the same disrupted network and reduced free-water activity suppress water evaporation and inhibit side reactions such as HER and anode corrosion. Guan et al. copolymerized AM with [2-(methacryloyloxy)ethyl]dimethyl(3-

sulfopropyl)ammonium betaine (SPE) and thymine (Thy) to form a ternary copolymer gel electrolyte (PAM-T-S) [184]. In this gel electrolyte, Thy establishes hydrogen bonds with free water, thereby markedly lowering water activity through the entrapment of water molecules inside the hydrogel network. This strong hydrogen-bonding not only suppresses water crystallization (no ice-crystal peak observed in DSC curves) but also modulates the solvation structure of Zn^{2+}, transforming it from $[Zn(H_2O)_6]^{2+}$ to $[Zn(H_2O)_4(Thy)(SPE)]^{2+}$ (Figure 9a). This change lowers the desolvation energy barrier of Zn^{2+} from 14.66 to 10.56 kJ·mol^{-1}, thereby maintaining a relatively high ionic conductivity of 23.5 mS cm^{-1} even at low temperatures. Thus, the synergistic effects of Thy and SPE enable outstanding wide-temperature performance, with symmetric cells lasting >3000 h at −20°C and >820 h at 60°C (Figure 9b). Beyond immobilizing water molecules via strong hydrogen bonds to suppress ice formation, an alternative effective approach involves directly lowering the water content within the system, thus fundamentally reducing the population of freezable water molecules. One demonstration of this strategy is the construction of a water-in-polymer system achieved through in situ polymerization of weakly solvating 1,3-dioxolane (DOL), initiated by natural proton sources in the electrolyte, which produces a water-deficient gel electrolyte [185]. In contrast to conventional gels with 80% water content, this electrolyte contains only 20% water. This substantial decrease in hydrogen-bond networks (Figure 9c) broadens the electrochemical window to 2.59 V. Moreover, under low-temperature conditions (−20°C), the Zn anode surface in a liquid electrolyte (LE) displays rough and disordered deposition morphology, indicating poor low-temperature adaptability. In contrast, at an even lower temperature of −40°C, the Zn anode using the gel electrolyte (GE) maintains a smooth surface. White-light interferometry characterization of the 3D topography of cycled electrodes further corroborates these findings (Figure 9d). Collectively, these findings confirm that GE markedly improves the deposition stability and cycling reversibility of Zn anodes at both ambient and low temperatures.

As a typical chaotropic agent, the perchlorate ion (ClO_4^-) demonstrates unique advantages in regulating the wide-temperature performance of hydrogels. Its key mechanism lies in the ability of ClO_4^- to effectively disrupt the inherent strong hydrogen-bond network among water molecules, thereby significantly lowering the electrolyte freezing point while also reducing water activity at high temperatures. For instance, a hydrogen-bond hydrogel denoted as CSAM, consisting of modified polysaccharide carboxymethyl chitosan (CMCS) and PAM, has been designed based on the Hofmeister effect [186]. By selecting $Zn(ClO_4)_2$ as the electrolyte salt, ClO_4^- can markedly disrupt the hydrogen bonds between water molecules, resulting in an aqueous electrolyte with a low freezing point. Simultaneously, ClO_4^- can establish weak hydrogen bonds with the hydrogel and water molecules, reducing the free-water content. This gel retains a high ionic conductivity of 7.8 mS cm^{-1} at −30°C (Figure 9e) and enables a flexible Zn//PANI battery to cycle steadily for 2500 cycles at −30°C and 5 A g^{-1} (Figure 9f). Building on the disruption of the hydrogen-bond network by ClO_4^-, the introduction of additional functional molecules can further synergistically optimize electrolyte performance, achieving multiple goals such as freeze resistance, high ionic conductivity, and interfacial stability across a wide temperature range. For example, Wang et al. incorporated ClO_4^- and glucose (Glu) into a PAM matrix to form a Glu/ZC/PAM hydrogel electrolyte [110]. The —NH_2 groups of PAM immobilize water molecules, thereby regulating the hydrogen-bond network among them and reducing the proportion of strong hydrogen bonds. The contact ion pairs between ClO_4^- anions and water molecules further suppress water activity. To further investigate the interfacial water activity in Glu/ZC/PAM, the Gibbs free energy for H^+ adsorption (ΔG_H) was calculated (Figure 9g). In the Glu/ZC/PAM gel, influenced by the PAM chains and Glu molecules, the decomposition of water on the Zn anode becomes more difficult, reducing proton supply and thereby hindering H_2 evolution. Moreover, the O atoms on Glu molecules can substitute for active water molecules within the Zn^{2+} solvation sheath, decreasing desolvation-water-induced parasitic reactions at the anode/electrolyte interface. Radial distribution function analysis confirms that in the Glu/ZC/PAM system, the hydration number of Zn^{2+} decreased from 5.60 in pure ZC to 5.24, with Glu molecules partially displacing coordinated water to assemble a $[Zn(Glu)(H_2O)_5]^{2+}$ coordination complex. Concurrently, the introduction of Glu reduced the coordination number of Zn^{2+} around ClO_4^- anions from 0.40 to 0.35. Glu restructures the Zn^{2+} solvation sheath via competitive coordination and frees additional ClO_4^- to immobilize water. Owing to these effects, the Glu/ZC/PAM gel possesses a superior ionic conductivity of 36.21 mS cm^{-1} and good water-retention capability. The fabricated Zn//NVO cell retains a substantial capacity of 254 mAh g^{-1} after 300 cycles at −30°C and delivers a high specific capacity of 488 mAh g^{-1} at 70°C, exhibiting stable cycling and thus demonstrating remarkable wide-temperature performance (Figure 9h,i).

Copolymerization of hydrogels with functional molecules enables precise tuning of the water hydrogen-bond network through the synergistic action of integrated chain segments and functional groups, thereby suppressing water activity over a broad thermal range [187]. The aforementioned ether- and ester-enriched PAP hydrogel contains abundant oxygen-containing functional groups, which can act as competitive hydrogen-bond acceptors [155]. These groups form sufficiently strong interactions with water molecules, thereby disrupting the inherent hydrogen-bond network of water. Raman spectroscopy analysis reveals that the proportion of "bound water" decreases in the PAP hydrogel (Figure 9j), while the fractions of "intermediate water" and "free water" increase, indicating that water molecules are more effectively anchored to the polymer backbone, resulting in reduced mobility and a significantly delayed freezing point. The absence of a distinct crystallization peak in the DSC curve further confirms its excellent anti-freezing performance. At −20°C, this system allows Zn//Zn symmetric cells to cycle stably for 1200 h. Importantly, the same hydrogen-bond reconfiguration also curbs water reactivity at elevated temperatures; the PAP electrolyte enables symmetric cells to operate for 2400 h at 50°C (Figure 9k) and full cells to retain 95.6% of initial capacity after 400 cycles at 50°C (Figure 9l), underscoring its genuine wide-temperature adaptability.

Regulating the hydrogen-bond network within hydrogel electrolytes via molecular design has become an effective approach to overcome the critical challenge of low-temperature operation in ZIBs. By incorporating functional monomers such as those bearing hydroxyl, ether, ester, or zwitterionic groups into the polymer,

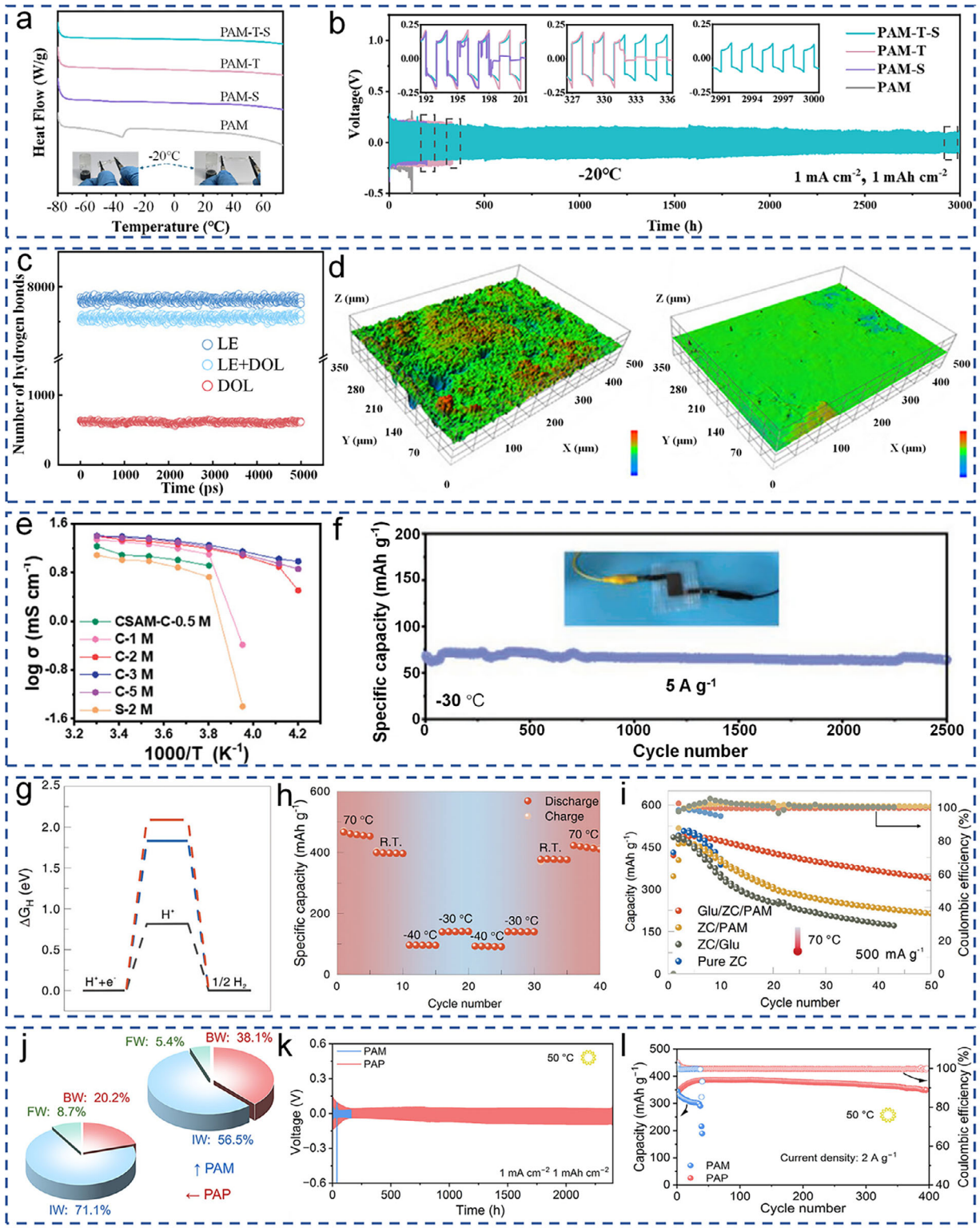

FIGURE 9 | (a) DSC tests from −80°C to 70°C. (b) Cycling performance at −20°C under 1 mA cm^{-2} and 1 mAh cm^{-2}. Reproduced with permission [184]. Copyright 2025, Wiley-VCH. (c) MD simulation of the hydrogen bond number in the different electrolytes. (d) White-light interferometer photographs of Zn anode after cycling using LE and GE, respectively, at −20°C. Reproduced with permission [185]. Copyright 2025, Wiley-VCH. (e) The ionic conductivities of the CSAM-C and CSAM-S-2 M hydrogel from −35°C to 30°C. (f) Cycling performance of the flexible battery with CSAM-C at 5 A g^{-1} under −30°C. Reproduced with permission [186]. Copyright 2022, Wiley-VCH. (g) The ΔG_H values of bare Zn, Glu/Zn, and PAM/Zn. (h) Rate capability of the Zn//NVO pouch battery with Glu/ZC/PAM electrolyte measured at various temperatures: −40°C, −30°C, room temperature, and 70°C, under a current density of 500 mA g^{-1}. (i) Long-term cycling performance of Zn//NVO pouch batteries at 70°C. Reproduced with permission [110]. Copyright 2024, Wiley-VCH. (j) Proportions of water in different states derived from Raman spectroscopy. (k) Cycling performances of Zn//Zn cells at 50°C. (l) Cycling performance of Zn//ZVO at 50°C. Reproduced with permission [155]. Copyright 2025, Wiley-VCH.

it is possible to introduce competitive hydrogen-bonding sites that interact with water molecules more strongly than water–water interactions. This effectively breaks the inherent hydrogen-bond network, suppresses free water activity, and inhibits ice crystal formation even at sub-zero temperatures. Beyond cryoprotection, these molecular engineering strategies concurrently modulate the solvation structure of Zn^{2+} ions by altering the local coordination environment, reducing the desolvation energy barrier, and facilitating faster ion transport kinetics. As a result, the optimized hydrogel electrolytes maintain high ionic conductivity (often exceeding 10 mS cm^{-1} at −20°C), ensure uniform and dendrite-free Zn deposition, and enable stable cycling for hundreds to thousands of hours under low-temperature conditions. Moreover, the same hydrogen-bond regulation strategy also addresses high-temperature challenges. By anchoring water molecules through strong hydrogen-bonding interactions and incorporating high-boiling-point co-solvents or molecular crowding agents, water evaporation is effectively suppressed, the 3D network remains structurally intact, and side reactions such as hydrogen evolution are mitigated. This ensures sustained ionic conductivity, mechanical integrity, and interfacial stability even at elevated temperatures. The integration of such molecular-level regulation with structural design, including crosslinked networks, reinforced frameworks, or porous architectures, yields hydrogel electrolytes that combine thermal robustness with mechanical flexibility. Collectively, these advances provide a critical material foundation for the development of flexible, all-climate Zn-based energy storage devices capable of meeting stringent safety requirements. By enabling reliable operation across a wide temperature range, from sub-zero to elevated temperatures, these hydrogel systems represent a significant step forward in the practical deployment of safe and durable energy storage technologies for applications in cold climates, outdoor electronics, and emerging wearable devices.

4.5 | Expanding the Flexible and Wearable Functionality of Batteries

Serving as a vital power source for wearable electronics, ZIBs require electrolyte materials that seamlessly integrate mechanical flexibility, interfacial stability, and robust electrochemical performance [188]. The conventional PAM network, typically formed by free-radical polymerization of AM monomers, exhibits a homogeneous crosslinked structure with limited capacity for energy dissipation [189]. This structural characteristic results in low tensile strength (often below 100 kPa), poor fracture toughness, and inadequate resistance to cyclic mechanical loading. When subjected to repeated deformation, a common operational scenario in wearable applications, these hydrogels undergo progressive network degradation, including chain scission, crosslink rupture, and permanent plastic deformation [190]. Simultaneously, the hydrogel/electrode interface, which relies primarily on weak physical interactions such as hydrogen bonding and van der Waals forces, is prone to delamination under dynamic stress [191]. This interfacial failure leads to increased charge-transfer resistance, uneven current distribution, and exacerbated Zn dendrite formation. These combined mechanical and interfacial deficiencies constrain the long-term reliability of PAM-based hydrogels in flexible ZIBs, underscoring the need for advanced material designs that enhance mechanical robustness without compromising electrochemical functionality.

By introducing polymers or functional groups rich in hydrogen-bonding sites, a dynamic and reversible hydrogen-bond crosslinked network can be constructed within the PAM framework. This approach effectively enhances the mechanical toughness and fatigue resistance of the hydrogel while achieving synergy between interfacial stability and flexible applications. For instance, chitosan (CS) has been incorporated into a PAM network to form a C-PAMCS hydrogel [121]. The amino groups in CS form strong hydrogen bonds with PAM chains, significantly increasing the tensile strength of the hydrogel from 19 to 50 kPa and achieving a fracture strain of up to 1200%. This dynamic network dissipates mechanical energy through chain slippage and conformational adjustments during cyclic deformation, thereby improving its long-term stability in flexible devices (Figure 10a). As shown in Figure 10b, the practical potential of this hydrogel in flexible energy storage systems was further demonstrated by powering an electronic wristwatch using two C-PAMCS batteries connected in series. Furthermore, by introducing biomass molecules with multiple functional groups, simultaneous enhancement of hydrogel mechanics and synergistic regulation of water activity and ion transport can be achieved. Xu et al. designed a chondroitin sulfate-functionalized polyacrylamide (PAM-CS) hydrogel electrolyte (Figure 10c) [80]. The flexible pouch cell incorporating this hydrogel delivers stable power output under extreme mechanical deformations such as bending, puncturing, and shearing (Figure 10d), demonstrating its high safety and environmental adaptability for wearable devices.

Incorporating a second polymer network into the PAM matrix enables the formation of an interconnected crosslinked architecture that simultaneously improves mechanical strength and ionic conductivity while enhancing electrode/electrolyte interfacial contact [69]. One example is a PAM-PVP dual-network hydrogel synthesized through UV-initiated polymerization [192]. Hydrogen bonding between the carbonyl groups of PVP and the amino groups of PAM increases network compactness and gives rise to a uniform microporous structure (Figure 10e), which facilitates ordered ion transport pathways. By integrating printed Zn-ion micro-batteries (PZIMBs) with pressure sensors (Figure 10f), a fully printed electronic-skin interactive system was developed (Figure 10g), along with integrated pressure-sensor arrays and LED-array interactive systems, effectively validating the practical applicability of PZIMBs in flexible electronic devices (Figure 10h). Designing interpenetrating networks that combine continuous skeletons and multiple interactions is an effective approach to further enhance the overall performance and practical viability of hydrogel electrolytes. For instance, Dai et al. incorporated an ethylene glycol-based deep eutectic solvent (DES) and sodium carboxymethyl cellulose (CMC-Na) to construct an interpenetrating network hydrogel electrolyte (PZEC) (Figure 10i) [193]. The 3D network of CMC-Na interpenetrates with the flexible PAM chains to form a continuous skeleton, while the —OH groups in DES establish strong hydrogen bonds with amide and carboxyl groups. Meanwhile, the $—COO^-$ groups of CMC-Na anchor free water through electrostatic and hydrogen-bonding interactions, guiding the ordered migration of Zn^{2+}. This design maintains high ionic conductivity while

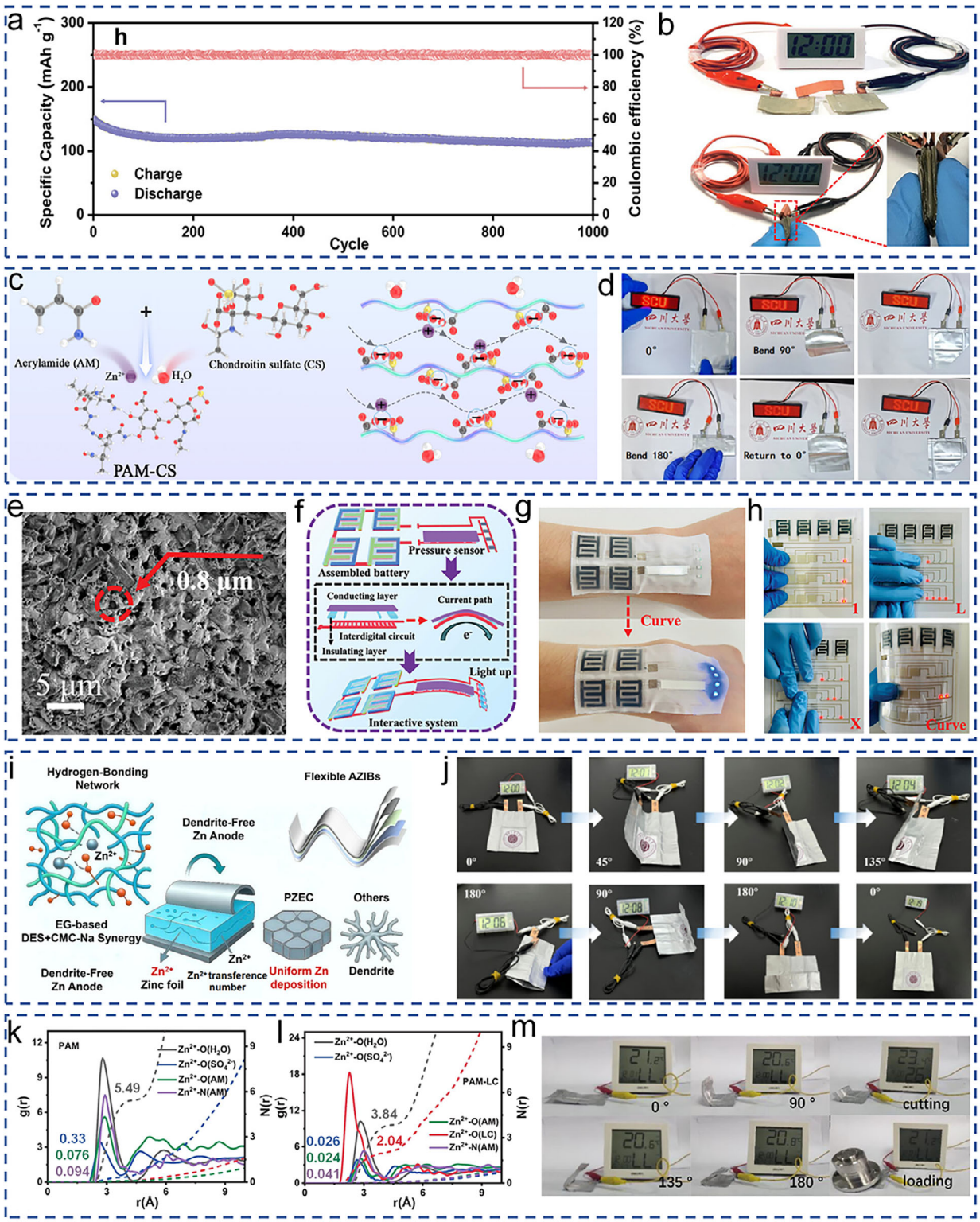

FIGURE 10 | (a) Cyclic performance at 10 A g^{-1}. (b) Photographs of an electronic watch powered by two cells connected in series. Reproduced with permission [121]. Copyright 2023, Wiley-VCH. (c) Schematic illustration of the fabricated PAM-CS. (d) Photographs of the "SCU" LED display powered under various conditions. Reproduced with permission [80]. Copyright 2025, Wiley-VCH. (e) SEM image of PAM-PVP. (f) Schematic diagram depicting the working principle of an interactive integrated system that mimics electronic skin. (g) Optical image of the interactive integrated system resembling electronic skin. (h) Integrated interactive system comprising a pressure-sensing array and an LED array. Reproduced with permission [192]. Copyright 2023, Wiley-VCH. (i) Synergistic engineering of DES/CMC-Na hydrogen-bond networks enabling dendrite-free Zn anodes and ultra-stable FZIBs. (j) Flexible Zn//VO_2 pouch cells incorporating the PZEC powering a timer under various bending angles. Reproduced with permission [193]. Copyright 2025, Elsevier. RDF and coordination number in (k) PAM and (l) PAM-LC. (m) Photographs of the pouch cell operating stably under various conditions. Reproduced with permission [194]. Copyright 2026, Elsevier.

significantly enhancing the material's mechanical strength and chemical stability. The pouch cell assembled based on PZEC operates stably under repeated deformation, further validating its practical potential for FZIBs (Figure 10j). Constructing dynamic networks with specific functions can achieve similar effects. For instance, a PAM–LC dynamic network has been constructed by introducing L-carrageenan (LC) [194]. The three $-SO_3^-$ groups in LC strongly coordinate with Zn^{2+}, reconstructing its primary solvation sheath and reducing the hydration number from 5.63 to 3.84, thereby effectively lowering the desolvation energy barrier of Zn^{2+} (Figure 10k,l). Simultaneously, this coordination creates unique ion-migration channels within the gel, promoting rapid Zn^{2+} transport and guiding Zn growth along specific orientations, leading to optimized deposition morphology. Moreover, ZIBs based on the PAM-LC hydrogel exhibit significantly improved electrochemical performance. This dynamic network also demonstrates excellent resistance to compressive fatigue, effectively dissipating mechanical stress, thereby ensuring stable power-supply capability of the assembled flexible battery under complex mechanical conditions such as bending, squeezing, and even local cutting, highlighting its application potential in real-world wearable scenarios (Figure 10m).

Functional modification serves as a key route to enhancing the overall performance of PAM-based hydrogel electrolytes, and it is significant for promoting their application in high-performance ZIBs. Synergistic modifications endow hydrogels with outstanding mechanical flexibility, allowing them to retain structural integrity under complex deformations. Additionally, they tune the solvation structure and ion transport pathways, enabling uniform Zn deposition and suppressing side reactions, thus greatly prolonging battery cycle life. Consequently, functional modification transforms PAM-based hydrogels from mere ionic conductors into intelligent electrolyte platforms that integrate mechanical flexibility, electrochemical stability, and favorable interfacial compatibility.

5 | Summary and Perspectives

In summary, PAM hydrogel electrolytes exhibit broad application prospects owing to their 3D crosslinked network structure, excellent hydrophilicity, and tunable mechanical properties. However, conventional PAM hydrogels generally face challenges such as poor mechanical strength, hydrogen evolution side reactions induced by high free-water activity, and uncontrolled Zn dendrite growth, which severely limit their practical application under high-rate conditions, extended cycle life, and extreme environments. A range of systematic functional modification strategies has been developed, including polymer network design, regulation of water activity, optimization of Zn salt-water–polymer ratios, and construction of multiphase systems. Through these approaches, the functionalization of PAM hydrogels has emerged as a key strategy to overcome these bottlenecks and achieve high-performance aqueous ZIBs.

At the level of modification strategies, despite the distinct mechanisms underlying various approaches, their design philosophies converge on the precise regulation of the three core components of the hydrogel system: the polymer network, water molecules, and Zn salts [195]. Functional fillers, leveraging their high specific surface area and abundant surface functional groups, establish physical crosslinking sites and multiple energy dissipation networks within the polymer matrix [196]. While significantly enhancing mechanical properties, certain fillers can also dynamically migrate to the electrode interface, forming an in situ protective layer that induces uniform nucleation. Organic additives, through molecular-level hydrogen bond reconstruction, solvation structure regulation, and diverse π-interactions, achieve effective suppression of water activity, optimization of ion transport pathways, and remodeling of the interfacial electric field [197]. Copolymerizable functional group modification, by covalently integrating cationic, anionic, or zwitterionic moieties into the polymer backbone, fundamentally endows the network with intrinsic functional characteristics, enabling the construction of selective ion channels and inducing preferential Zn deposition along the (002) crystal plane [198]. Furthermore, topological structural designs such as dynamic crosslinked networks or "sprocket-like" micellar crosslinking demonstrate a viable pathway for achieving synergistic optimization of mechanical reinforcement and ion transport through structural complexity [199].

The ultimate efficacy of the aforementioned functionalization strategies is collectively reflected in the comprehensive enhancement of the key properties of PAM hydrogels. In terms of mechanical properties, the hydrogel evolves from a fragile single-network structure into a composite material possessing high strength, high toughness, and excellent fatigue resistance. This not only enables it to act as a physical barrier to effectively suppress dendrite penetration but also allows it to accommodate the complex deformations encountered in flexible devices. Regarding ion transport, through the construction of continuous Zn^{2+} hopping sites, electrostatic repulsion channels, or separated anion–cation pathways, both the ionic conductivity and the Zn^{2+} transference number are significantly improved, thereby effectively reducing concentration polarization and overpotential. In terms of interfacial stability, side reactions such as hydrogen evolution, corrosion, and dendrite growth are effectively suppressed through the regulation of the Zn^{2+} solvation structure, reduction of free water activity, construction of a gradient SEI layer, and induction of preferential (002) plane deposition. The synergistic optimization of these properties ultimately culminates in breakthrough electrochemical performance at the device level.

It is worth emphasizing that an in-depth analysis of existing research reveals that the most significant performance breakthroughs arise not from the optimization of a single parameter, but from the synergistic enhancement of multiple key factors. Solely pursuing mechanical reinforcement may come at the expense of ionic conductivity, while focusing exclusively on ion selectivity may overlook interfacial stability. The most successful design strategies consistently embody a holistic consideration of ion transport, water molecule states, mechanical properties, and interfacial chemistry, achieving the unification of ion selectivity, rapid transport, effective water confinement, and structural robustness. Despite significant progress in the research of functionalized PAM hydrogels, numerous challenges remain for their practical application in scalable energy storage and flexible electronic devices. Future research directions may include the following aspects (Scheme 3).

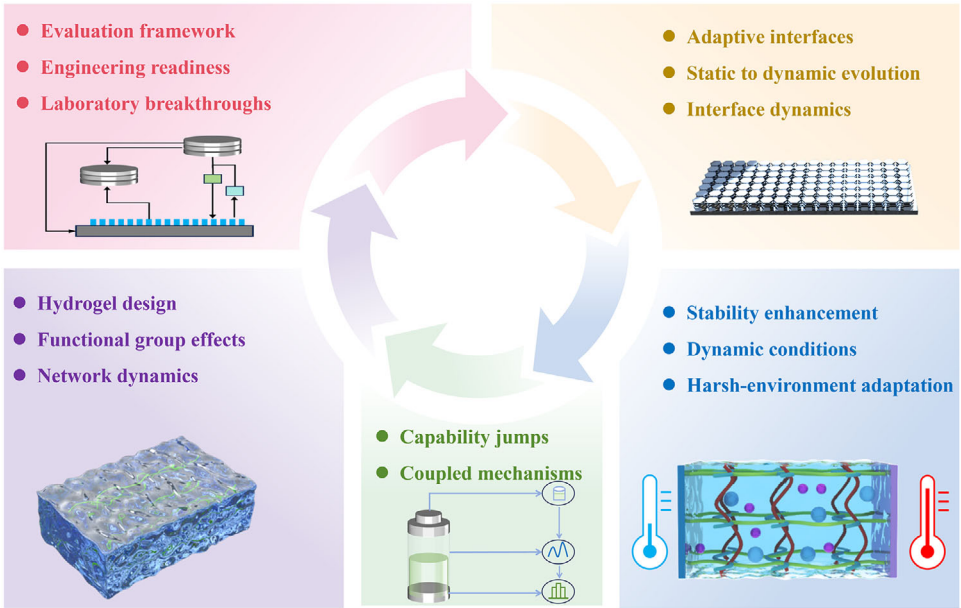

SCHEME 3 | Future opportunities and directions of functionally modified hydrogels for ZIBs.

5.1 | Rethinking Hydrogel Design From Functional Group Effects to Network Dynamics

Most existing studies ascribe performance improvements to particular interactions of functional groups with Zn^{2+} or water molecules, yet the contribution of the intrinsic dynamic evolution of the PAM network itself to ion transport is often overlooked. In reality, the segmental mobility of PAM chains under swollen conditions, the dynamic reorganization of hydrogen-bond networks, and the reversible breaking and recombination of crosslinking points may profoundly influence the entire hopping-migration-desolvation process of ions. Future investigations should aim to establish a direct correlation between network dynamics and ion transport efficiency, rather than simplistically attributing all phenomena to static functional group effects. For instance, distinguishing the contributions of "functional group affinity for Zn^{2+}" versus "chain segment mobility in facilitating ion migration" across different timescales warrants in-depth exploration.

5.2 | Deepening Mechanistic Understanding and Achieving Synergistic Performance Breakthroughs

Current understanding of ion transport in hydrogel electrolytes remains largely macroscopic, lacking clear theoretical and experimental insights into the microscopic ion transport process under varying charge environments. This gap leads to inherent trade-offs among ionic conductivity, mechanical strength, water activity, and interfacial stability. Future breakthroughs will hinge on establishing a unified structure-dynamics-performance framework that bridges fundamental understanding with practical design. This framework should leverage in situ characterization and multiscale simulations to derive quantifiable principles connecting chain dynamics, confined water states, and transport barriers, while also advancing synergistic strategies that reconcile fast ion transport with mechanical robustness and water confinement, for instance, through the integration of dynamic sacrificial bonds or the preservation of intrinsic Zn^{2+} migration pathways alongside effective free water suppression.

5.3 | Enhancing Stability Under Dynamic and Extreme Conditions

While most studies have employed static coin-type cells, ZIBs operate under repeated bending and folding that cause interfacial slippage, stress concentration, and dynamic redistribution of the electric field and ion flux. These conditions can induce dendrite growth behavior fundamentally different from that in static cells. Accordingly, establishing dynamic testing standards and theoretical models is urgently needed to elucidate the structural evolution, interfacial stability, and dendrite-suppression mechanisms of hydrogel electrolytes under mechanical stress. Systematic evaluation of their long-term stability under extreme temperatures and high humidity is equally critical.

5.4 | Unveiling the Evolution From Static to Dynamic Adaptive Interfaces

Interfacial engineering has largely focused on constructing perfect static protective layers, aiming to permanently suppress side reactions. The intrinsically dynamic behaviors of the Zn anode, including volume expansion, surface reconstruction, and dendrite initiation, cannot be sustainably accommodated by a static interface. In contrast, the inherent flexibility and dynamic crosslinking of PAM hydrogels enable the construction of adaptive interfaces that achieve real-time reconstruction, in situ repair, and conformal contact on the Zn surface. Future efforts should therefore exploit the dynamic nature of PAM networks to realize adaptive control of local electric fields and ion flux, moving beyond the concept of a passive barrier.

5.5 | Restructuring the Evaluation Framework From Laboratory Breakthroughs to Engineering Readiness

The evaluation of PAM hydrogels primarily focuses on key metrics like cycle life and ionic conductivity, while critical issues for practical application remain underexplored: how to ensure mechanical integrity after thinning, maintain interfacial contact with high-mass-loading electrodes, and control batch-to-batch stability in scalable production. Additionally, the neurotoxicity of acrylamide and its potential release during long-term operation have not been systematically assessed. Future research should incorporate manufacturability and biosafety into the evaluation framework, instead of pursuing only extreme breakthroughs in electrochemical performance.

5.6 | Critical Analysis of Current Functional Modification Strategies

While significant progress has been achieved in functionalizing PAM-based hydrogel electrolytes, a critical examination reveals inherent trade-offs and limitations associated with each strategy. Functional fillers (e.g., MOFs, COFs, CNTs) enhance mechanical strength and create ordered ion transport channels, yet they often suffer from poor dispersion stability, high cost, and potential aggregation-induced heterogeneity. Organic additives offer a facile and scalable route to modulate solvation structures and suppress water activity; however, their long-term stability and potential leaching during cycling remain underexplored. Copolymerization with functional monomers provides permanent and uniform modification of the polymer backbone but may compromise chain mobility and increase synthesis complexity. Multifunctional network designs achieve synergistic reinforcement but face challenges in balancing crosslinking density with ionic conductivity. A critical insight emerging from this analysis is that no single strategy universally outperforms others; instead, the optimal approach depends on specific application requirements.

5.7 | Scalability and Commercialization Potential

Translating functionalized PAM-based hydrogel electrolytes from laboratory breakthroughs to practical applications requires addressing several critical barriers. First, most current syntheses rely on free-radical polymerization with small batch sizes; continuous manufacturing processes such as roll-to-roll photopolymerization or inkjet printing should be explored to enable large-scale production. Second, expensive components such as COFs, CNTs, or functional monomers may limit economic viability; low-cost biomass-derived alternatives (e.g., cellulose, chitosan, or natural polysaccharides) represent promising substitutes. Third, the reversible nature of non-covalent interactions (e.g., hydrogen bonding, electrostatic interactions) introduces variability under different synthesis conditions. Establishing standardized protocols and quality control metrics is urgently needed. Fourth, acrylamide, the monomer of PAM, is neurotoxic, and its potential residual content or long-term release during battery operation has not been systematically evaluated. Future research should incorporate biocompatibility assessments and develop encapsulation strategies to mitigate health risks. Finally, end-of-life management of hydrogel electrolytes remains unexplored. Designing degradable or recyclable PAM-based systems will be essential for environmentally sustainable energy storage.

5.8 | Advanced Characterization Methods for Mechanistic Understanding

A deeper mechanistic understanding of ion transport, water dynamics, and interfacial evolution in PAM-based hydrogels requires the integration of advanced characterization techniques. In situ synchrotron-based small-angle x-ray scattering (SAXS) and wide-angle x-ray scattering (WAXS) can probe the dynamic reorganization of polymer networks and the evolution of pore structures under electrochemical cycling. Solid-state NMR spectroscopy, particularly ^{1}H and ^{17}O NMR, enables quantitative analysis of water states (free, bound, and intermediate water) and their temperature-dependent behavior. Cryogenic transmission electron microscopy (cryo-TEM) preserves the native hydrated structure of hydrogels, allowing direct visualization of polymer chain morphology, filler distribution, and interfacial contact at nanoscale resolution. In situ Raman spectroscopy and FTIR can track real-time changes in hydrogen-bonding networks and solvation structures during Zn plating/stripping. MD simulations and DFT calculations complement experimental observations by providing atomic-scale insights into ion transport pathways, desolvation energetics, and preferential crystal plane adsorption. The combined use of these advanced characterization tools will be instrumental in establishing a unified structure–dynamics–performance framework, guiding the rational design of next-generation hydrogel electrolytes.

5.9 | Sustainability and Degradability: A Forward-Looking Perspective

Beyond the technical challenges above, the environmental sustainability of PAM-based hydrogel electrolytes is a critical yet often overlooked concern. Although ZIBs are celebrated for their green attributes, conventional chemically crosslinked PAM networks resist natural degradation, raising the risk of secondary microplastic pollution, especially given the anticipated large-scale deployment of flexible ZIBs. To close this sustainability gap, future research should prioritize degradable PAM-based hydrogels via labile crosslinkers (e.g., disulfide, acetal, ester bonds) responsive to environmental triggers, photodegradable moieties for light-induced degradation, biohybrid networks incorporating natural biodegradable polymers (e.g., cellulose, chitosan, alginate), and dynamic covalent crosslinking (e.g., boronate esters, imine bonds) for controlled depolymerization. Such triggerable degradable designs would reduce the environmental footprint of spent batteries and facilitate the recovery of valuable components like Zn salts and electrode materials. We encourage the community to adopt sustainability as a design criterion from the outset, aligning high-performance PAM hydrogels with green chemistry and circular economy principles.

Overall, research on functionalized PAM-based hydrogel electrolytes is at a critical stage, transitioning from performance breakthroughs toward system integration and mechanistic under-

standing. By adhering to multi-parameter synergistic optimization, deepening the understanding of microscopic mechanisms, and tackling challenges in scalable fabrication, environmental adaptability, and sustainable development, this field is poised to realize next-generation aqueous ZIBs that combine high safety, long lifespan, high energy density, and excellent environmental adaptability. Such advances would provide strong support for grid-scale energy storage and flexible electronic technologies.

Author Contributions

Zhihao Li: validation, formal analysis, methodology. **Hongfei Wang**: conceptualization, writing – original draft, funding acquisition, validation. **Tianyu Zhang**: formal analysis, software. **Jintao Feng**: software, formal analysis. **Kaihan Xie**: conceptualization, writing – original draft, validation, methodology. **Yong Hu**: conceptualization, funding acquisition, writing – review and editing, project administration, supervision.

Acknowledgements

The authors appreciate the financial support from the National Natural Science Foundation of China (Nos. 22272150 and 22502176) and Zhejiang Provincial Natural Science Foundation of China (No. LMS26B030007).

Conflicts of Interest

The authors declare no conflicts of interest.

Data Availability Statement

Research data are not shared.

References

1. Y. Guan, J. Yan, Y. Shan, et al., "Burden of the Global Energy Price Crisis on Households," *Nature Energy* 8 (2023): 304–316, https://doi.org/10.1038/s41560-023-01209-8.

2. C. Tian, J. Wang, R. Sun, et al., "Improved Interfacial Ion Migration and Deposition through the Chain-Liquid Synergistic Effect by a Carboxylated Hydrogel Electrolyte for Stable Zinc Metal Anodes," *Angewandte Chemie International Edition* 62 (2023): 202310970, https://doi.org/10.1002/anie.202310970.

3. H. Wang, W. Ye, B. Yin, et al., "Modulating Cation Migration and Deposition with Xylitol Additive and Oriented Reconstruction of Hydrogen Bonds for Stable Zinc Anodes," *Angewandte Chemie International Edition* 135 (2023): e202218872, https://doi.org/10.1002/ange.202218872.

4. L. Xu, N. Lin, A. T. D. Perera, et al., "Cross-Sector Energy System Resilience and Interdependence in a Changing Climate," *Joule* 9 (2025): 101967, https://doi.org/10.1016/j.joule.2025.101967.

5. S. Zhou, X. Meng, Y. Chen, et al., "Zinc-Ion Anchor Induced Highly Reversible Zn Anodes for High Performance Zn-Ion Batteries," *Angewandte Chemie International Edition* 63 (2024): e202403050, https://doi.org/10.1002/anie.202403050.

6. J. Zhou, Y. Mei, F. Wu, et al., "Regulated Ion/Electron-Conducting Interphase Enables Stable Zinc-Metal Anodes for Aqueous Zinc-Ions Batteries," *Angewandte Chemie International Edition* 62 (2023): e202304454, https://doi.org/10.1002/anie.202304454.

7. Y. Shang and D. Kundu, "A Path Forward for the Translational Development of Aqueous Zinc-Ion Batteries," *Joule* 7 (2023): 244–250, https://doi.org/10.1016/j.joule.2023.01.011.

8. Y. Fang, X. Xie, B. Zhang, et al., "Regulating Zinc Deposition Behaviors by the Conditioner of PAN Separator for Zinc-Ion Batteries," *Advanced Functional Materials* 32 (2022): 2109671, https://doi.org/10.1002/adfm.202109671.

9. H. Chen, X. Li, K. Fang, H. Wang, J. Ning, and Y. Hu, "Aqueous Zinc-Iodine Batteries: from Electrochemistry to Energy Storage Mechanism," *Advanced Energy Materials* 13 (2023): 2302187, https://doi.org/10.1002/aenm.202302187.

10. X. Chen, P. Ye, H. Wang, H. Huang, Y. Zhong, and Y. Hu, "Discriminating Active B–N Sites in Coralloidal B, N Dual-Doped Carbon Nano-Bundles for Boosted Zn-Ion Storage Capability," *Advanced Functional Materials* 33 (2023): 2212915, https://doi.org/10.1002/adfm.202212915.

11. H. Dong, J. Li, J. Guo, et al., "Insights on Flexible Zinc-Ion Batteries from Lab Research to Commercialization," *Advanced Materials* 33 (2021): 2007548, https://doi.org/10.1002/adma.202007548.

12. Y. Chen, Y. Kang, Y. Zhao, et al., "A Review of Lithium-Ion Battery Safety Concerns: the Issues, Strategies, and Testing Standards," *Journal of Energy Chemistry* 59 (2021): 83–99, https://doi.org/10.1016/j.jechem.2020.10.017.

13. D. Ji and J. Kim, "Trend of Developing Aqueous Liquid and Gel Electrolytes for Sustainable, Safe, and High-Performance Li-Ion Batteries," *Nano-Micro Letters* 16 (2023): 2, https://doi.org/10.1007/s40820-023-01220-4.

14. X. Guo, H. He, S. Zhao, et al., "Unveiling Aqueous Lithium-Ion Batteries via Advanced Modelling and Characterisation: a Review," *Energy Storage Materials* 70 (2024): 103505, https://doi.org/10.1016/j.ensm.2024.103505.

15. N. Zhang, X. Chen, M. Yu, Z. Niu, F. Cheng, and J. Chen, "Materials Chemistry for Rechargeable Zinc-Ion Batteries," *Chemical Society Reviews* 49 (2020): 4203–4219, https://doi.org/10.1039/C9CS00349E.

16. C. Tian, H. Wang, L. Xie, Y. Zhong, and Y. Hu, "Arrays of Hierarchical Zincophilic Nanorods with Trapping-and-Leveling Deposition for Ultra-stable Zn Metal Anodes," *Advanced Energy Materials* 14 (2024): 2400276, https://doi.org/10.1002/aenm.202400276.

17. J. Zhu, Z. Tie, S. Bi, and Z. Niu, "Towards More Sustainable Aqueous Zinc-Ion Batteries," *Angewandte Chemie International Edition* 63 (2024): 202403712, https://doi.org/10.1002/anie.202403712.

18. Q. Zhang, J. Luan, Y. Tang, X. Ji, and H. Wang, "Interfacial Design of Dendrite-Free Zinc Anodes for Aqueous Zinc-Ion Batteries," *Angewandte Chemie International Edition* 59 (2020): 13180–13191, https://doi.org/10.1002/anie.202000162.

19. A. Innocenti, D. Bresser, J. Garche, and S. Passerini, "A Critical Discussion of the Current Availability of Lithium and Zinc for Use in Batteries," *Nature Communications* 15 (2024): 4068, https://doi.org/10.1038/s41467-024-48368-0.

20. C. Zhou, L. Shan, Z. Xing, et al., "Interface Layer Engineering of Zinc Anode for Durable Seawater-Based Zinc-Ion Batteries," *Advanced Materials* 38 (2026): 16045, https://doi.org/10.1002/adma.202516045.

21. Y. Wang, Q. Li, H. Hong, et al., "Lean-Water Hydrogel Electrolyte for Zinc Ion Batteries," *Nature Communications* 14 (2023): 3890, https://doi.org/10.1038/s41467-023-39634-8.

22. J. L. Yang, T. Xiao, T. Xiao, et al., "Cation-Conduction Dominated Hydrogels for Durable Zinc–Iodine Batteries," *Advanced Materials* 36 (2024): 2313610, https://doi.org/10.1002/adma.202313610.

23. F. Yang, L. Zhou, T. Zhang, et al., "A Zincophilic and Negatively-Charged Self-Reconstructed Stratified Interface for Regulating Zn^{2+} Conduction and Nucleation toward Conformal Dendrite-Free Deposition," *Angewandte Chemie International Edition* 65 (2026): 23653, https://doi.org/10.1002/anie.202523653.

24. Y. Wang, H. Zhang, Y. Chen, et al., "Hydrogel Electrolytes for Temperature Robust Aqueous Zinc-Ion Batteries," *Advanced Energy Materials* 15 (2025): 03226, https://doi.org/10.1002/aenm.202503226.

25. Y. Yan, S. Duan, B. Liu, et al., "Tough Hydrogel Electrolytes for Anti-Freezing Zinc-Ion Batteries," *Advanced Materials* 35 (2023): 2211673, https://doi.org/10.1002/adma.202211673.

26. T. Zhang, Y. Liu, F. Yang, et al., "Rational Design of Artificial Solid Electrolyte Interphases for Stable Zinc Metal Anodes: Mechanistic

Insights, Construction Strategies, and Practical Implementation," *Coordination Chemistry Reviews* 553 (2026): 217586, https://doi.org/10.1016/j.ccr.2026.217586.

27. Y. Geng, L. Pan, Z. Peng, et al., "Electrolyte Additive Engineering for Aqueous Zn Ion Batteries," *Energy Storage Materials* 51 (2022): 733–755, https://doi.org/10.1016/j.ensm.2022.07.017.

28. X. Zheng, T. Ahmad, and W. Chen, "Challenges and Strategies on Zn Electrodeposition for Stable Zn-Ion Batteries," *Energy Storage Materials* 39 (2021): 365–394, https://doi.org/10.1016/j.ensm.2021.04.027.

29. M. Zhu, H. Wang, H. Wang, et al., "A Fluorinated Solid-State-Electrolyte Interface Layer Guiding Fast Zinc-Ion Oriented Deposition in Aqueous Zinc-Ion Batteries," *Angewandte Chemie International Edition* 63 (2024): e202316904, https://doi.org/10.1002/anie.202316904.

30. Y. Liu, T. Zhang, Z. Li, Z. Ma, and Y. Hu, "Multiscale Interfacial Regulation for Stable Zinc Anodes: from Fundamental Mechanisms to Practical Applications," *Advanced Energy Materials* 16 (2026): 70704, https://doi.org/10.1002/aenm.70704.

31. Y. Wei, Z. Wang, J. Li, et al., "Wood-Structured Electrolyte for Ultra-Stable Zinc-Ion Batteries under High Discharge Conditions," *Advanced Materials* 38 (2026): 22128, https://doi.org/10.1002/adma.202522128.

32. Y. Chen, F. Gong, W. Deng, H. Zhang, and X. Wang, "Dual-Function Electrolyte Additive Enabling Simultaneous Electrode Interface and Coordination Environment Regulation for Zinc-Ion Batteries," *Energy Storage Materials* 58 (2023): 20–29, https://doi.org/10.1016/j.ensm.2023.03.010.

33. X. Kong, C. Feng, B. Zhang, et al., "Sodium Sulfamate-Modified Luffa Cellulose Fiber Separator for Efficient Modulation of Zn^{2+} Transport," *Chemical Engineering Journal* 528 (2026): 172150, https://doi.org/10.1016/j.cej.2025.172150.

34. L. Pan, L. Zhu, C. Han, et al., "Regulating Zinc Deposition and Desolvation of Zinc Metal Anode via Hydrophobic/Hydrophilic Functionalized Separator," *Journal of Energy Storage* 139 (2025): 118840, https://doi.org/10.1016/j.est.2025.118840.

35. Y. Wang, Y. Kong, T. Zhang, C. Chen, H. Wang, and Y. Hu, "Fluorine-Functionalized Chemistry toward Stable Zn Anode in Aqueous Zn-Ion Batteries," *Advanced Energy Materials* 15 (2025): 2502353, https://doi.org/10.1002/aenm.202502353.

36. Y. Chen, B. Yin, Y. Zeng, et al., "Ion-Dipole-Interaction-Manipulated Bilateral Interface Chemistry for Deep Rechargeability and High Redox Activity of Zn-Organic Batteries," *Chem* 11 (2025): 102411, https://doi.org/10.1016/j.chempr.2025.102411.

37. J. Chen, Y. Tao, T. Zhang, et al., "Toward Durable Wide-Temperature Zn-MnO_2 Batteries: a Polarized Dual-Crosslinked Hydrogel Electrolyte for Concurrent Anode and Cathode Stabilization," *Chemical Engineering Journal* 535 (2026): 175539, https://doi.org/10.1016/j.cej.2026.175539.

38. Y. Wang, H. Tian, S. Wu, et al., "A Co-Solvent Hydrogel Electrolyte for High-Temperature and Anti-Corrosion Zinc-Ion Batteries," *Advanced Functional Materials* 35 (2025): 27198, https://doi.org/10.1002/adfm.202527198.

39. W. Yang, J. Zeng, W. Yang, et al., "Regulating Ion Migration and Deposition through a Cellulose Hydrogel Electrolyte Enabled by Anion-Reinforced Effect for Zinc-Ion Batteries," *Advanced Functional Materials* 36 (2026): 07159, https://doi.org/10.1002/adfm.202507159.

40. J. Wang, Y. Huang, B. Liu, et al., "Flexible and Anti-Freezing Zinc-Ion Batteries Using a Guar-Gum/Sodium-Alginate/Ethylene-Glycol Hydrogel Electrolyte," *Energy Storage Materials* 41 (2021): 599–605, https://doi.org/10.1016/j.ensm.2021.06.034.

41. G. Li, B. Guo, M. Shi, et al., "Sulfonate-Mediated Cation-Switching in Hydrogel Electrolytes to Unlock Fast Ion Transport for Low-Temperature Zinc Batteries," *Advanced Materials* 38 (2026): 22750, https://doi.org/10.1002/adma.202522750.

42. Q. Wang, J. Huang, L. Qi, et al., "A Bioinspired Gradient Hydrogel Electrolyte Network with Optimized Interfacial Chemistry toward Robust Aqueous Zinc-Ion Batteries," *ACS Nano* 19 (2025): 26770–26781, https://doi.org/10.1021/acsnano.5c06914.

43. L. Sun, Y. Yao, L. Dai, et al., "Sustainable and High-Performance Zn Dual-Ion Batteries with a Hydrogel-Based Water-in-Salt Electrolyte," *Energy Storage Materials* 47 (2022): 187–194, https://doi.org/10.1016/j.ensm.2022.02.012.

44. X. Xu, S. Li, S. Yang, and B. Li, "Superelastic Hydrogel Electrolyte Incorporating Helical Protein Molecules as Zinc Ion Transport Pathways to Enhance the Cycling Stability of Zinc Metal Batteries," *Energy & Environmental Science* 17 (2024): 7919–7931, https://doi.org/10.1039/D4EE02510E.

45. Q. Zhou, F. Zhang, Z. Tan, et al., "Gradient Hydrogel Electrolyte Enables High Ionic Conductivity and Robust Mechanical Properties for Dendrite-Free Aqueous Zinc-Ion Battery," *Advanced Materials* 38 (2026): 12775, https://doi.org/10.1002/adma.202512775.

46. M. Zhu, X. Wang, H. Tang, et al., "Antifreezing Hydrogel with High Zinc Reversibility for Flexible and Durable Aqueous Batteries by Cooperative Hydrated Cations," *Advanced Functional Materials* 30 (2020): 1907218, https://doi.org/10.1002/adfm.201907218.

47. Z. Du, S. Shen, X. Su, et al., "A Robust and Tough Composite Hydrogel Electrolyte with Anion-Locked Supramolecular Network for Zinc Ion Batteries," *Advanced Materials* 37 (2025): 2502328, https://doi.org/10.1002/adma.202502328.

48. Z. Ji, Y. Zhao, X. Zhang, et al., "Multiscale Computational Insights for Hydrogel Electrolytes in Aqueous Zinc Metal Batteries," *Advanced Energy Materials* 16 (2026): 71071, https://doi.org/10.1002/aenm.71071.

49. C. Li, F. Liu, H. Yao, et al., "Dynamic pH Regulation and Interfacial Ion Redistribution via Molecular Buffering for Dendrite-Free Zn Metal Anodes," *Advanced Functional Materials* 36 (2026): 14260, https://doi.org/10.1002/adfm.202514260.

50. A. Bayaguud, Y. Fu, and C. Zhu, "Interfacial Parasitic Reactions of Zinc Anodes in Zinc Ion Batteries: Underestimated Corrosion and Hydrogen Evolution Reactions and Their Suppression Strategies," *Journal of Energy Chemistry* 64 (2022): 246–262, https://doi.org/10.1016/j.jechem.2021.04.016.

51. H. Lu, J. Hu, L. Wang, et al., "Multi-Component Crosslinked Hydrogel Electrolyte toward Dendrite-Free Aqueous Zn Ion Batteries with High Temperature Adaptability," *Advanced Functional Materials* 32 (2022): 2112540, https://doi.org/10.1002/adfm.202112540.

52. Q. Luo, X. Zeng, J. Lei, et al., "Green and in-Situ Formation Polyacrylamide Gel Electrolyte with Controllable Acceleration Polymerization Mechanism for Highly Stable Zinc Anodes," *Chemical Engineering Journal* 523 (2025): 168097, https://doi.org/10.1016/j.cej.2025.168097.

53. Z. Hu, Z. Han, H. Liu, et al., "Mechanically Strong and Tough Ionic Liquid Gel Electrolyte for Four-Electron Zinc–Iodine Batteries," *Journal of the American Chemical Society* 147 (2025): 46632–46641, https://doi.org/10.1021/jacs.5c18431.

54. W. Zeng, S. Zhang, J. Lan, et al., "Double Network Gel Electrolyte with High Ionic Conductivity and Mechanical Strength for Zinc-Ion Batteries," *ACS Nano* 18 (2024): 26391–26400, https://doi.org/10.1021/acsnano.4c09879.

55. Z. Shen, Z. Zhai, T. Zhang, et al., "Phase-Behavior-Driven Hydrogen-Bond Engineering Enables Temperature-Resilient Fibrous Zinc-Ion Batteries," *Advanced Materials* 38 (2026): 73246, https://doi.org/10.1002/adma.73246.

56. Z. Shen, Y. Liu, Z. Li, et al., "Highly-Entangled Hydrogel Electrolyte for Fast Charging/Discharging Properties in Aqueous Zinc Ion Batteries," *Advanced Functional Materials* 35 (2025): 2406620, https://doi.org/10.1002/adfm.202406620.

57. X. Ye, S. Shang, B. Zhao, et al., "Synergistic Rb^{+}-Dual-Network Polymer Gel Electrolyte Enhances Stability of Dendrite-Free Zn^{2+} Batteries," *Chemical Engineering Journal* 522 (2025): 167946, https://doi.org/10.1016/j.cej.2025.167946.

58. X. Li, Y. Zhou, Z. Wei, et al., "High-Performance Hydrogel-Based Temperature Sensor by Integrating Ion Channels and Stabilized Ion Gradients," *Advanced Functional Materials* 36 (2026): 74877, https://doi.org/10.1002/adfm.74877.

59. W. Song, L. Ye, J. Peng, et al., "Enabling High-Performance Zn Anodes through Nitrogen-Participated p–π Conjugation in Hydrogel Electrolytes," *Advanced Energy Materials* 15 (2025): 03484, https://doi.org/10.1002/aenm.202503484.

60. W. Zhao, S. Xiao, J. Xing, et al., "Bioinspired Alternating Rigid-Soft Layered Design Enhances Structural–Functional-Electrochemical Integrated Cement-Based Batteries toward Zero–carbon Buildings," *Materials Today* 95 (2026): 103288, https://doi.org/10.1016/j.mattod.2026.103288.

61. X. Zhao, J. Fu, M. Chen, et al., "A Self-Phase Separated Electrolyte toward Durable and Rollover-Stable Zinc Metal Batteries," *Journal of the American Chemical Society* 147 (2025): 2714–2725, https://doi.org/10.1021/jacs.4c15132.

62. F. Mo, G. Liang, Q. Meng, et al., "A Flexible Rechargeable Aqueous Zinc Manganese-Dioxide Battery Working at −20°C," *Energy & Environmental Science* 12 (2019): 706–715, https://doi.org/10.1039/C8EE02892C.

63. Y. Liu, A. Gao, J. Hao, et al., "Soaking-Free and Self-Healing Hydrogel for Wearable Zinc-Ion Batteries," *Chemical Engineering Journal* 452 (2023): 139605, https://doi.org/10.1016/j.cej.2022.139605.

64. Z. Shen, Z. Zhai, Y. Liu, et al., "Hydrogel Electrolytes-Based Rechargeable Zinc-Ion Batteries under Harsh Conditions," *Nano-Micro Letters* 17 (2025): 227, https://doi.org/10.1007/s40820-025-01727-y.

65. H. Peng, D. Wang, F. Zhang, et al., "Improvements and Challenges of Hydrogel Polymer Electrolytes for Advanced Zinc Anodes in Aqueous Zinc-Ion Batteries," *ACS Nano* 18 (2024): 21779–21803, https://doi.org/10.1021/acsnano.4c06502.

66. Y. Lei, F. Liu, L. Chen, et al., "Polyanionic Hydrogel Electrolytes to Regulate Ion Transport Behavior in Long Cycle Life Zinc-Ion Batteries," *Nano Energy* 143 (2025): 111284, https://doi.org/10.1016/j.nanoen.2025.111284.

67. J. Han, S. Jung, S. E. Heo, et al., "Anisotropic Ion-Guiding Hydrogel Electrolyte with High-Water Affinity for Zn Ion Battery," *Small* 21 (2025): 2500799, https://doi.org/10.1002/smll.202500799.

68. H. Xia, W. Zhang, C. Miao, et al., "Ultra-Thin Amphiphilic Hydrogel Electrolyte for Flexible Zinc-Ion Paper Batteries," *Energy & Environmental Science* 17 (2024): 6507–6520, https://doi.org/10.1039/D4EE01993H.

69. Z.-J. Chen, T.-Y. Shen, X. Xiao, et al., "An Ultrahigh-Modulus Hydrogel Electrolyte for Dendrite-Free Zinc Ion Batteries," *Advanced Materials* 36 (2024): 2413268, https://doi.org/10.1002/adma.202413268.

70. Y. Ge, L. Peng, X. Cao, and N. Wang, "Triboelectrically Active Hydrogel Drives Self-Charging Zinc-Ion Battery and Human Motion Sensing," *Nano Energy* 126 (2024): 109601, https://doi.org/10.1016/j.nanoen.2024.109601.

71. Y. Sun, L.-N. Song, X. Y. Du, et al., "In Situ Copolymerizing ZrO_2 with Hydrogel Electrolytes toward High-Rate and Long-Life Quasi-Solid-State Zn–Ion Batteries," *Advanced Energy Materials* 15 (2025): 2404944, https://doi.org/10.1002/aenm.202404944.

72. D. Luo, L. Yang, Z. Geng, et al., "Underlying Principles and Practical Design Strategies of Hydrogel Electrolytes for Long-Term Stable Zinc Batteries," *Advanced Energy Materials* 16 (2026): 04151, https://doi.org/10.1002/aenm.202504151.

73. H. Li, Z. Liu, G. Liang, et al., "Waterproof and Tailorable Elastic Rechargeable Yarn Zinc Ion Batteries by a Cross-Linked Polyacrylamide Electrolyte," *ACS Nano* 12 (2018): 3140–3148, https://doi.org/10.1021/acsnano.7b09003.

74. S. Chen, L. Ma, K. Zhang, M. Kamruzzaman, C. Zhi, and J. A. Zapien, "A Flexible Solid-State Zinc Ion Hybrid Supercapacitor Based on Co-Polymer Derived Hollow Carbon Spheres," *Journal of Materials Chemistry A* 7 (2019): 7784–7790, https://doi.org/10.1039/C9TA00733D.

75. B. Wang, J. Li, C. Hou, Q. Zhang, Y. Li, and H. Wang, "Stable Hydrogel Electrolytes for Flexible and Submarine-Use Zn-Ion Batteries," *ACS Applied Materials & Interfaces* 12 (2020): 46005–46014, https://doi.org/10.1021/acsami.0c12313.

76. C. Liu, W. Xu, C. Mei, et al., "A Chemically Self-Charging Flexible Solid-State Zinc-Ion Battery Based on VO_2 Cathode and Polyacrylamide–Chitin Nanofiber Hydrogel Electrolyte," *Advanced Energy Materials* 11 (2021): 2003902, https://doi.org/10.1002/aenm.202003902.

77. T. Wei, Y. Ren, Z. Li, X. Zhang, D. Ji, and L. Hu, "Bonding Interaction Regulation in Hydrogel Electrolyte Enable Dendrite-Free Aqueous Zinc-Ion Batteries from −20 to 60°C," *Chemical Engineering Journal* 434 (2022): 134646, https://doi.org/10.1016/j.cej.2022.134646.

78. H. Xia, G. Xu, X. Cao, et al., "Single-Ion-Conducting Hydrogel Electrolytes Based on Slide-Ring Pseudo-Polyrotaxane for Ultralong-Cycling Flexible Zinc-Ion Batteries," *Advanced Materials* 35 (2023): 2301996, https://doi.org/10.1002/adma.202301996.

79. M. Sun, G. Ji, M. Li, and J. Zheng, "A Robust Hydrogel Electrolyte with Ultrahigh Ion Transference Number Derived from Zincophilic "Chain-Gear" Network Structure for Dendrite-Free Aqueous Zinc Ion Battery," *Advanced Functional Materials* 34 (2024): 2402004, https://doi.org/10.1002/adfm.202402004.

80. D. Xu, Y. Wang, H. Tian, Y. Chen, X. Tian, and Q. Zhang, "Dynamic Cross-Linking Network Construction of Flexible Hydrogel Electrolyte Enabling Dendrite-Free Zinc Anode," *Advanced Energy Materials* 15 (2025): 2502217, https://doi.org/10.1002/aenm.202502217.

81. P. Sun, S. Zhang, C. Fang, Q. Lin, L. Feng, and J. Chen, "Reconstructing Solvation and Interface Dynamics for High-Performance Hydrogel Polymer Zn-S Batteries," *Small Methods* 10 (2026): 02253, https://doi.org/10.1002/smtd.202502253.

82. W. Zhuang, Z. Wang, C. Li, et al., "Acidic Hydrogel Enables Full-Period Mn^{2+}/MnO_2 Conversion in High-Energy Quasi-Solid-State Zn-MnO_2 Batteries," *Advanced Materials* 38 (2026): 22827, https://doi.org/10.1002/adma.202522827.

83. Q. Zhao, S. Ye, S. Wang, X. Wang, and X. Rao, "Toward High-Performance Hydrogel Electrolytes for Zn-Ion Batteries: Electrolyte Mechanisms, Interfacial Engineering, and Performance Breakthroughs," *Chemical Engineering Journal* 530 (2026): 173634, https://doi.org/10.1016/j.cej.2026.173634.

84. B. Zhang, X. Cai, S. Tian, et al., "Zwitterionic Hydrogels Endow Zinc-Ion Micro-Batteries with Superior Durability for Electrophysiological Monitoring," *Advanced Energy Materials* 15 (2025): 03986, https://doi.org/10.1002/aenm.202503986.

85. Z. Wang, R. Xue, H. Zhang, et al., "A Hydrogel Electrolyte toward a Flexible Zinc-Ion Battery and Multifunctional Health Monitoring Electronics," *ACS Nano* 18 (2024): 7596–7609, https://doi.org/10.1021/acsnano.4c00085.

86. X. He, L. Zhao, Y. Zhang, X. Zhang, J. Yi, and Q. Xu, "Cathode-Hydrogel Electrolyte Interaction in Aqueous Zinc-Ion Batteries: Degradation Mechanism and Optimization Strategies," *Advanced Functional Materials* 35 (2025): 10796, https://doi.org/10.1002/adfm.202510796.

87. H. Xia, T. Shui, X. Wan, et al., "Microphase-Separated Hydrogel Electrolytes with Selective Ion Transportation Pathways for Flexible Zinc-Ion Batteries," *Advanced Materials* 38 (2026): 18881, https://doi.org/10.1002/adma.202518881.

88. X. Li, D. Wang, and F. Ran, "Key Approaches and Challenges in Fabricating Advanced Flexible Zinc-Ion Batteries with Functional Hydrogel Electrolytes," *Energy Storage Materials* 56 (2023): 351–393, https://doi.org/10.1016/j.ensm.2023.01.034.

89. C.-Y. Li, J.-L. Wang, D.-T. Zhang, et al., "Situ Physical/Chemical Cross-Linked Hydrogel Electrolyte Achieving Ultra-Stable Zinc Anode-Electrolyte Interface towards Dendrite-Free Zinc Ion Battery," *Journal of Energy Chemistry* 97 (2024): 342–351, https://doi.org/10.1016/j.jechem.2024.05.049.

90. M. Yang, S. Bi, X. Wang, et al., "Intrinsic Ion Concentration Difference Induced Antipolyelectrolyte Effect for Promoting Stability of Zn Anodes," *Journal of the American Chemical Society* 147 (2025): 9294–9303, https://doi.org/10.1021/jacs.4c15126.

91. J. Cong, Y. Wang, X. Lin, et al., "Kinetics Compensation Mechanism in Cosolvent Electrolyte Strategy for Aqueous Zinc Batteries," *Journal of the American Chemical Society* 147 (2025): 8607–8617, https://doi.org/10.1021/jacs.4c16880.

92. S. Duan, M. Hua, C. W. Zhang, et al., "Noncovalent Aggregation for Diverse Properties in Hydrogels: a Comprehensive Review," *Chemical Reviews* 125 (2025): 7918–7964, https://doi.org/10.1021/acs.chemrev.5c00069.

93. Z. Song, S. Yuan, X. Zhang, X. Zhao, and Q. Zou, "High-Performance MnO_2 Hydrogel Composite Electrodes Constructed via In Situ Hofmeister Effect for Zinc–Ion Batteries," *Advanced Energy Materials* 15 (2025): 02994, https://doi.org/10.1002/aenm.202502994.

94. S. Gong, Y. Chao, F. Yang, et al., "Bifunctional Potential Structure Design Breaks Electrolyte Limitations of Zinc Ion Battery," *Angewandte Chemie International Edition* 63 (2024): 202401629, https://doi.org/10.1002/anie.202401629.

95. D. Han, C. Cui, K. Zhang, et al., "A Non-Flammable Hydrous Organic Electrolyte for Sustainable Zinc Batteries," *Nature Sustainability* 5 (2022): 205–213, https://doi.org/10.1038/s41893-021-00800-9.

96. P. Chen, X. Sun, T. Pietsch, B. Plietker, E. Brunner, and M. Ruck, "Electrolyte for High-Energy- and Power-Density Zinc Batteries and Ion Capacitors," *Advanced Materials* 35 (2023): 2207131, https://doi.org/10.1002/adma.202207131.

97. L. Li, S. Liu, W. Liu, et al., "Electrolyte Concentration Regulation Boosting Zinc Storage Stability of High-Capacity $K_{0.486}V_2O_5$ Cathode for Bendable Quasi-Solid-State Zinc Ion Batteries," *Nano-Micro Letters* 13 (2021): 34, https://doi.org/10.1007/s40820-020-00554-7.

98. Q. Zhao, Z. Sun, H. Liu, H. Ying, and S. Dou, "A Systematic Understanding of Zinc Salts in Electrolyte Design for Aqueous Zinc-Ion Batteries," *ACS Nano* 19 (2025): 35237–35275, https://doi.org/10.1021/acsnano.5c10278.

99. J. X. Li, H. F. Wang, D.-H. Guan, X. X. Wang, C. L. Miao, and J.-J. Xu, "Crystal Transformation Strategy in Hydrogen-Bonded Organic Framework Solid-State Electrolyte for Stable Zinc-Ion Batteries," *Advanced Materials* 37 (2025): 2500721, https://doi.org/10.1002/adma.202500721.

100. M. Chen, J. Chen, W. Zhou, X. Han, Y. Yao, and C. P. Wong, "Realizing an All-Round Hydrogel Electrolyte toward Environmentally Adaptive Dendrite-Free Aqueous Zn–MnO_2 Batteries," *Advanced Materials* 33 (2021): 2007559, https://doi.org/10.1002/adma.202007559.

101. S. Qin, R. Qi, Y. Wang, et al., "A Jointly Triggered H_2 Evolution Model Modulated Polyanionic Hydrogel Electrolyte for Reversible Zn Chemistry," *Advanced Functional Materials* 35 (2025): 2505946, https://doi.org/10.1002/adfm.202505946.

102. Y. Wang, B. Liang, D. Li, et al., "Hydrogel Electrolyte Design for Long-Lifespan Aqueous Zinc Batteries to Realize a 99% Coulombic Efficiency at 90°C," *Joule* 9 (2025): 101944, https://doi.org/10.1016/j.joule.2025.101944.

103. Q. He, Y. Zhong, J. Li, et al., "Constructing Kosmotropic Salt-Compatible PVA Hydrogels for Stable Zinc Anodes via Strong Hydrogen Bonds Preshielding Effect," *Advanced Energy Materials* 14 (2024): 2400170, https://doi.org/10.1002/aenm.202400170.

104. Y. Liu, F. Li, J. Hao, et al., "A Polyanionic Hydrogel Electrolyte with Ion Selective Permeability for Building Ultra-Stable Zn/I_2 Batteries with 100°C Wide Temperature Range," *Advanced Functional Materials* 34 (2024): 2400517, https://doi.org/10.1002/adfm.202400517.

105. X. Yan, J. Zhang, Y. Sheng, et al., "Decoupling the Trade-Off between Mechanical Properties and Ionic Conductivity in Hydrogel Polymer Electrolytes by Anomalous Water-Induced Microphase Separation," *ACS Nano* 19 (2025): 40579–40593, https://doi.org/10.1021/acsnano.5c16323.

106. H. Lu, B. Yin, T. Zhang, et al., "Dual-Additive Synergistic Complementation Electrolyte Engineering with "Job-Sharing" Modulation Mechanism for Long-Lifespan Zn-Iodine Batteries," *ACS Applied Materials & Interfaces* 17 (2025): 21234–21245, https://doi.org/10.1021/acsami.5c00459.

107. Y. Ding, L. Yin, T. Du, et al., "A Trifunctional Electrolyte Enables Aqueous Zinc Ion Batteries with Long Cycling Performance," *Advanced Functional Materials* 34 (2024): 2314388, https://doi.org/10.1002/adfm.202314388.

108. T. Su, W. Ren, M. Xu, et al., "A Reusable Biomass Electrolyte with Dual-Interface Regulation towards Flexible and Durable Zinc-Iodine Batteries," *Energy Storage Materials* 78 (2025): 104279, https://doi.org/10.1016/j.ensm.2025.104279.

109. M. Qiu, P. Sun, Y. Wang, et al., "Anion-Trap Engineering toward Remarkable Crystallographic Reorientation and Efficient Cation Migration of Zn Ion Batteries," *Angewandte Chemie International Edition* 61 (2022): 202210979, https://doi.org/10.1002/anie.202210979.

110. Y. Wang, L. Mo, X. Zhang, et al., "Regulating Water Activity for all-Climate Aqueous Zinc-Ion Batteries," *Advanced Energy Materials* 14 (2024): 2402041, https://doi.org/10.1002/aenm.202402041.

111. Y. Gao, Y. Liu, Y. Jia, B. Feng, L. Ma, and M. Zhu, "Hydrogen-Bond Acceptor and Anion Receptor-Mediated Regulation of Interfacial Proton Mobility for Long-Lifespan Aqueous Zinc Batteries," *Advanced Functional Materials* 36 (2026): 14985, https://doi.org/10.1002/adfm.202514985.

112. K. Yan, Y. Fan, X. Yang, et al., "A Single Ion Conductive "Plasticine-Like" Solid Electrolyte Combined with a Modulated D-Band Center of Interfacial Zinc Atoms for Highly Reversible Zinc Metal Anodes," *Energy & Environmental Science* 18 (2025): 5333–5346, https://doi.org/10.1039/D5EE00737B.

113. C. Li, Y. Liu, J. Liu, et al., "Well-Aligned Liquid Crystal Interface and Expanded Solvation Sheath Accelerate Zn^{2+} Desolvation Kinetics for Stable Zinc Batteries," *Journal of the American Chemical Society* 147 (2025): 27640–27650, https://doi.org/10.1021/jacs.5c06049.

114. S. Zhang, M. Ye, Y. Zhang, Y. Tang, X. Liu, and C. C. Li, "Regulation of Ionic Distribution and Desolvation Activation Energy Enabled by in Situ Zinc Phosphate Protective Layer toward Highly Reversible Zinc Metal Anodes," *Advanced Functional Materials* 33 (2023): 2208230, https://doi.org/10.1002/adfm.202208230.

115. P. Yang, C. Feng, Y. Liu, et al., "Thermal Self-Protection of Zinc-Ion Batteries Enabled by Smart Hygroscopic Hydrogel Electrolytes," *Advanced Energy Materials* 10 (2020): 2002898, https://doi.org/10.1002/aenm.202002898.

116. S. Huang, S. He, S. Huang, et al., "Molecular Crowding Agent Modified Polyanionic Gel Electrolyte for Zinc Ion Batteries Operating at 100°C," *Advanced Functional Materials* 35 (2025): 2419153, https://doi.org/10.1002/adfm.202419153.

117. J. Zhang, C. Lin, L. Zeng, et al., "A Hydrogel Electrolyte with High Adaptability over a Wide Temperature Range and Mechanical Stress for Long-Life Flexible Zinc-Ion Batteries," *Small* 20 (2024): 2312116, https://doi.org/10.1002/smll.202312116.

118. Y. Tan, R. Liao, Y. Mu, et al., "Hierarchically-Structured and Mechanically-Robust Hydrogel Electrolytes for Flexible Zinc-Iodine Batteries," *Advanced Functional Materials* 34 (2024): 2407050, https://doi.org/10.1002/adfm.202407050.

119. J. Li, J. Ren, C. Li, et al., "High-Adhesion Anionic Copolymer as Solid-State Electrolyte for Dendrite-Free Zn-Ion Battery," *Nano Research* 15 (2022): 7190–7198, https://doi.org/10.1007/s12274-022-4370-y.

120. W. Wang, C. Li, W. Zhuang, et al., "Rational Constructions of High-Performance Flexible Aqueous Gel-State Zinc Ionic Batteries," *Advanced Functional Materials* 35 (2025): 2423311, https://doi.org/10.1002/adfm.202423311.

121. Q. Liu, Z. Yu, Q. Zhuang, J. K. Kim, F. Kang, and B. Zhang, "Anti-Fatigue Hydrogel Electrolyte for All-Flexible Zn-Ion Batteries," *Advanced Materials* 35 (2023): 2300498, https://doi.org/10.1002/adma.202300498.

122. K. Hectors and W. De Waele, "Cumulative Damage and Life Prediction Models for High-Cycle Fatigue of Metals: A Review," *Metals* 11 (2021): 204, https://doi.org/10.3390/met11020204.

123. J. Xu, Y. Zhu, Q. Gui, et al., "High-Performance Fatigue-Resistant Dual- Polyrotaxane Hydrogel Electrolytes for Flexible Aqueous Zinc-Ion Batteries," *Small* 21 (2025): 2500124, https://doi.org/10.1002/smll.202500124.

124. R. Wu, R. Wang, S. Yang, et al., "Bio-Inspired Hyaluronic Acid Enhanced Dual-Network Hydrogel Electrolyte Unlocks Dendrite-Free Zn Deposition and Exceptional Cycling Stability in Flexible Zinc Ion Batteries," *Chemical Engineering Journal* 530 (2026): 173528, https://doi.org/10.1016/j.cej.2026.173528.

125. C. Y. Chan, Z. Wang, Y. Li, H. Yu, B. Fei, and J. H. Xin, "Single-Ion Conducting Double-Network Hydrogel Electrolytes for Long Cycling Zinc-Ion Batteries," *ACS Applied Materials & Interfaces* 13 (2021): 30594–30602, https://doi.org/10.1021/acsami.1c05941.

126. Q. Zheng, L. Liu, Z. Hu, et al., "Altering the Zn^{2+} Migration Mechanism Enables the Composite Hydrogel Electrolytes with High Zn^{2+} Conduction and Superior Anti-Dehydration," *Advanced Functional Materials* 35 (2025): 2504782, https://doi.org/10.1002/adfm.202504782.

127. B. Sun, Y. Zong, K. Bao, et al., "Activating Gel Polymer Electrolyte Based Zinc-Ion Conduction with Filler-Integration for Advanced Zinc Batteries," *ACS Applied Materials & Interfaces* 15 (2023): 37916–37924, https://doi.org/10.1021/acsami.3c06702.

128. S. Ji, J. Qin, S. Yang, et al., "A Mechanically Durable Hybrid Hydrogel Electrolyte Developed by Controllable Accelerated Polymerization Mechanism towards Reliable Aqueous Zinc-Ion Battery," *Energy Storage Materials* 55 (2023): 236–243, https://doi.org/10.1016/j.ensm.2022.11.050.

129. D. Lin, J. Li, M. Wang, et al., "Nanofluidic-Engineered Carbon Nanotube Ion Highways in Hydrogels Enable High-Power Aqueous Zinc-Ion Batteries," *Science Advances* 11 (2025): adx9812, https://doi.org/10.1126/sciadv.adx9812.

130. G. Ji, M. Sun, M. Li, and J. Zheng, "Sulfonate-Modified Covalent Organic Framework Integrated Hydrogel Electrolyte: Enhancing AZIBs Performances by Tailoring Microstructures and Functional Groups," *Advanced Functional Materials* 35 (2025): 2500110, https://doi.org/10.1002/adfm.202500110.

131. C. Chen, M. Zhao, T. Zhang, K. Xie, H. Wang, and Y. Hu, "Lewis Acid-Base Mediated MOF-Polymer Hydrogel Electrolyte for Oriented Ion Conduction and Textured Zn (002) Deposition," *Composites Part B: Engineering* 309 (2026): 113053, https://doi.org/10.1016/j.compositesb.2025.113053.

132. D. Rong, S. Zou, Y. Wu, S. He, and Q. Rong, "Electric Field-Induced Gradient Polyanionic Hydrogel Electrolytes with Zinc-Ion Selective Transport for Stable Zinc-Ion Batteries," *Chemical Engineering Journal* 524 (2025): 169746, https://doi.org/10.1016/j.cej.2025.169746.

133. X. Ou, Q. Liu, J. Pan, et al., "CO_2-Sourced Anti-Freezing Hydrogel Electrolyte for Sustainable Zn-Ion Batteries," *Chemical Engineering Journal* 435 (2022): 135051, https://doi.org/10.1016/j.cej.2022.135051.

134. J. Liu and O. A. Scherman, "Cucurbit[n]uril Supramolecular Hydrogel Networks as Tough and Healable Adhesives," *Advanced Functional Materials* 28 (2018): 1800848, https://doi.org/10.1002/adfm.201800848.

135. S. Yang, Q. Wu, Y. Li, et al., "A Bio-Inspired Multifunctional Hydrogel Network with Toughly Interfacial Chemistry for Dendrite-Free Flexible Zinc Ion Battery," *Angewandte Chemie International Edition* 63 (2024): 202409160, https://doi.org/10.1002/anie.202409160.

136. W. L. Cheng, Z.-Q. Cheng, Z.-Z. Hu, et al., "A Fish-Gelatin-Modified Multifunctional Hydrogel with "Salt-in-Water" for Dendrite-Free Flexible Zinc-Ion Batteries," *Chemical Engineering Journal* 521 (2025): 166945, https://doi.org/10.1016/j.cej.2025.166945.

137. H. Lu, J. Hu, X. Wei, et al., "A Recyclable Biomass Electrolyte towards Green Zinc-Ion Batteries," *Nature Communications* 14 (2023): 4435, https://doi.org/10.1038/s41467-023-40178-0.

138. X. Wang, P. Lei, C. Zheng, et al., "Flexible and Durable Meter-Long Fiber-Shaped Zn-Ion Battery Enabled by Zincophilic, Tough Double-Network Hydrogel Electrolytes," *Advanced Functional Materials* 35 (2025): 2500916, https://doi.org/10.1002/adfm.202500916.

139. H. Zhang, X. Gan, Z. Song, and J. Zhou, "Amphoteric Cellulose-Based Double-Network Hydrogel Electrolyte Toward Ultra-Stable Zn Anode," *Angewandte Chemie International Edition* 135 (2023): e202217833, https://doi.org/10.1002/ange.202217833.

140. P. Lin, J. Cong, J. Li, et al., "Achieving Ultra-Long Lifespan Zn Metal Anodes by Manipulating Desolvation Effect and Zn Deposition Orientation in a Multiple Cross-Linked Hydrogel Electrolyte," *Energy Storage Materials* 49 (2022): 172–180, https://doi.org/10.1016/j.ensm.2022.04.010.

141. M. Sun, G. Ji, and J. Zheng, "A Hydrogel Electrolyte with Ultra-high Ionic Conductivity and Transference Number Benefit from Zn^{2+} "Highways" for Dendrite-Free Zn-MnO_2 Battery," *Chemical Engineering Journal* 463 (2023): 142535, https://doi.org/10.1016/j.cej.2023.142535.

142. K. Zhu, X. Niu, W. Xie, et al., "An Integrated Janus Hydrogel with Different Hydrophilicities and Gradient Pore Structures for High-Performance Zinc-Ion Batteries," *Energy & Environmental Science* 17 (2024): 4126–4136, https://doi.org/10.1039/D4EE01018C.

143. Y. An, C. Shu, Y. Liu, et al., "Modulating the Hydrogen Bond for a Stable Zinc Anode with a Wide Temperature Range via the Sucrose and Polyacrylamide Synergistic Effect," *ACS Nano* 19 (2025): 11146–11163, https://doi.org/10.1021/acsnano.4c18178.

144. L. Wang, H. Wang, J. Cao, et al., "Restructuring Hydrogen Bond Networks in Polyacrylamide Hydrogels via Trehalose Additives for Wide-Temperature-Range Zn-Ion Batteries," *ACS Nano* 19 (2025): 28397–28409, https://doi.org/10.1021/acsnano.5c06805.

145. P. Shen, S. Xu, D. Li, et al., "A Bioinspired Flexible Hydrogel Electrolyte with β-Sheet–Directed Interphase for Dendrite-Free Zn Metal Batteries," *Energy Storage Materials* 81 (2025): 104464, https://doi.org/10.1016/j.ensm.2025.104464.

146. S. Chen, Y. Wang, A. Sun, et al., "Biomass Hydrogel Electrolyte with High Interfacial Compatibility Enables Stable Aqueous Zinc-Ion Batteries," *Chemical Engineering Journal* 525 (2025): 169845, https://doi.org/10.1016/j.cej.2025.169845.

147. K. Zhu, J. Luo, D. Zhang, et al., "Molecular Engineering Enables Hydrogel Electrolyte with Ionic Hopping Migration and Self-Healability toward Dendrite-Free Zinc-Metal Anodes," *Advanced Materials* 36 (2024): 2311082, https://doi.org/10.1002/adma.202311082.

148. S. J. Guo, M.-Y. Yan, D. M. Xu, et al., "Anti-Freezing Hydrogel Electrolyte with a Regulated Hydrogen Bond Network Enables High-Rate and Long Cycling Zinc Batteries," *Energy & Environmental Science* 18 (2025): 418–429, https://doi.org/10.1039/D4EE02772H.

149. Z.-J. Chen, T.-Y. Shen, M.-H. Zhang, et al., "Tough, Anti-Fatigue, Self-Adhesive, and Anti-Freezing Hydrogel Electrolytes for Dendrite-Free Flexible Zinc Ion Batteries and Strain Sensors," *Advanced Functional Materials* 34 (2024): 2314864, https://doi.org/10.1002/adfm.202314864.

150. J. Pu, Y. Gao, Z. Geng, et al., "Grafted MXene Assisted Bifunctional Hydrogel for Stable and Highly Sensitive Self-Powered Fibrous System," *Advanced Functional Materials* 34 (2024): 2304453, https://doi.org/10.1002/adfm.202304453.

151. Z. Liu, H. Wan, J. Li, et al., "Coupling Polar Terminal Designation and Double-Network Structural Construction of Hydrogel Electrolyte for Boosting Dendrite-Free Aqueous Zinc-Ion Batteries," *Advanced Functional Materials* 36 (2026): e20721, https://doi.org/10.1002/adfm.202520721.

152. D. Lin, Y. Lin, R. Pan, et al., "Water-Restrained Hydrogel Electrolytes with Repulsion-Driven Cationic Express Pathways for Durable Zinc-Ion Batteries," *Nano-Micro Letters* 17 (2025): 193, https://doi.org/10.1007/s40820-025-01704-5.

153. J. Li, H. Zhang, Z. Liu, et al., "Boosting Dendrite-Free Zinc Anode with Strongly Polar Functional Group Terminated Hydrogel Electrolyte

for High-Safe Aqueous Zinc-Ion Batteries," *Advanced Functional Materials* 35 (2025): 2412865, https://doi.org/10.1002/adfm.202412865.

154. W. Zhang, F. Guo, H. Mi, et al., "Kinetics-Boosted Effect Enabled by Zwitterionic Hydrogel Electrolyte for Highly Reversible Zinc Anode in Zinc-Ion Hybrid Micro-Supercapacitors," *Advanced Energy Materials* 12 (2022): 2202219, https://doi.org/10.1002/aenm.202202219.

155. J. Zhong, C. Xia, T. Zhang, et al., "Non-Covalent Molecular Engineering of Hydrogel Electrolytes via π-Anion Confinement and Hydrogen-Bond Reconfiguration for Wide-Temperature and Ultra-Stable Zn-Ion Batteries," *Advanced Functional Materials* 36 (2026): 27894, https://doi.org/10.1002/adfm.202527894.

156. B. Luo, B. Jiang, F. Chang, et al., "In-Situ Detection of pH and Dissolved Oxygen in Electrolyte of Aqueous Zinc-Ion Batteries," *Nature Communications* 16 (2025): 8462, https://doi.org/10.1038/s41467-025-63260-1.

157. J. Yuan, Y. Li, P. Xu, et al., "Sodium Dodecyl Sulfonate-Mediated Gel Electrolyte for Horizontal Zinc Deposition in Robust Zinc-Ion Batteries," *Journal of Materials Science & Technology* 230 (2025): 311–318, https://doi.org/10.1016/j.jmst.2025.01.025.

158. K. Zhang, P. Kong, C. Wu, C. Ma, J. Ye, and Y. Wu, "Polyacrylamide Soft Colloidal Electrode for Long-Lasting Aqueous Zn-I Batteries," *Chemical Engineering Journal* 512 (2025): 162685, https://doi.org/10.1016/j.cej.2025.162685.

159. S. Guo, L. Qin, T. Zhang, et al., "Fundamentals and Perspectives of Electrolyte Additives for Aqueous Zinc-Ion Batteries," *Energy Storage Materials* 34 (2021): 545–562, https://doi.org/10.1016/j.ensm.2020.10.019.

160. Z. Chen, J. Zhang, F. Gong, et al., "Hofmeister Effect Enabled Anti-Freezing Dual-Network Hydrogel Electrolyte for Dendrite-Free Zinc-Ion Batteries," *Chemical Engineering Journal* 533 (2026): 174369, https://doi.org/10.1016/j.cej.2026.174369.

161. T. Qiu, T. Wang, W. Tang, et al., "Rapidly Synthesized Single-Ion Conductive Hydrogel Electrolyte for High-Performance Quasi-Solid-State Zinc-Ion Batteries," *Angewandte Chemie International Edition* 62 (2023): e202312020, https://doi.org/10.1002/anie.202312020.

162. W. Zhu, Z. Lei, and P. Wu, "Multi-Stage Collaborative Design of Hierarchical Twisted Hydrogel Electrolytes for Aqueous Zinc-Ion Batteries with High Capacity, Ultralong Stability, and Mechanical Robustness," *Energy & Environmental Science* 18 (2025): 3647–3658, https://doi.org/10.1039/D5EE00001G.

163. W. Wei, M. Zhang, H. Yan, et al., "Simultaneous Regulation of Solvation Shell and Ion Migration in Morpholine-Crosslinked Polyacrylamide Hydrogel Electrolytes for Durable Zinc Metal Batteries," *Journal of Energy Chemistry* 102 (2025): 703–711, https://doi.org/10.1016/j.jechem.2024.11.025.

164. X. Zhu, T. Zhang, J. Zhang, et al., "Customizing Ion Transport by Anionphilic Nanofiber-Polymer Electrolyte for Stable Zinc Metal Batteries," *Advanced Materials* 38 (2026): e19057, https://doi.org/10.1002/adma.202519057.

165. G. Cao, L. Zhao, X. Ji, et al., ""Salting out" in Hofmeister Effect Enhancing Mechanical and Electrochemical Performance of Amide-Based Hydrogel Electrolytes for Flexible Zinc-Ion Battery," *Small* 19 (2023): 2207610, https://doi.org/10.1002/smll.202207610.

166. Y. Lin, J. Huang, S. Wang, et al., "Stretchable, Adhesive, Anti-Freezing Hydrogel Electrolytes with Dual-Functional Water Regulation Enabled by Amide Group–Salt–Water Interactions for all-Climate Zinc-Ion Batteries," *Advanced Materials* 37 (2025): 09975, https://doi.org/10.1002/adma.202509975.

167. S. Shao, Y. Lin, X. Lin, et al., "Regulating Reversible Zn Deposition via a 2D Metal–Organic Framework-Laden Hydrogel Electrolyte," *Small* 21 (2025): 06390, https://doi.org/10.1002/smll.202506390.

168. F. Luo, S. Yang, Q. Wu, et al., "Hydrogel Electrolytes with an Electron/Ion Dual Regulation Mechanism for Highly Reversible Flexible Zinc Batteries," *Energy & Environmental Science* 17 (2024): 8570–8581, https://doi.org/10.1039/D4EE03067B.

169. Y. Dai, C. Zhang, X. Zhang, et al., "Interfacial Energy Storage in Aqueous Zinc-Ion Batteries," *Energy & Environmental Science* 18 (2025): 9018–9030, https://doi.org/10.1039/D5EE03741G.

170. J. Long, T. Han, X. Lin, et al., "An Integrated Flexible Self-Healing Zn-Ion Battery Using Dendrite-Suppressible Hydrogel Electrolyte and Free-Standing Electrodes for Wearable Electronics," *Nano Research* 16 (2023): 11000–11011, https://doi.org/10.1007/s12274-023-5882-9.

171. C. Chen, Z. Long, X. Du, et al., "Interfacial Ionic Effects in Aqueous Zinc Metal Batteries," *Energy Storage Materials* 71 (2024): 103571, https://doi.org/10.1016/j.ensm.2024.103571.

172. Y. Ai, C. Yang, Z. Yin, et al., "Biomimetic Superstructured Interphase for Aqueous Zinc-Ion Batteries," *Journal of the American Chemical Society* 146 (2024): 15496–15505, https://doi.org/10.1021/jacs.4c03943.

173. S. Cui, W. Miao, X. Wang, K. Sun, H. Peng, and G. Ma, "Multifunctional Zincophilic Hydrogel Electrolyte with Abundant Hydrogen Bonds for Zinc-Ion Capacitors and Supercapacitors," *ACS Nano* 18 (2024): 12355–12366, https://doi.org/10.1021/acsnano.4c01304.

174. X. Zhang, Q. Yu, G. Qu, et al., "Synergistic Enhancement of Cathode/Anode Interfaces with High Water-Retentive Organohydrogel Enabling Highly Stable Zinc Ion Batteries," *Journal of Energy Chemistry* 98 (2024): 670–679, https://doi.org/10.1016/j.jechem.2024.07.023.

175. G. Liu, S. Zhang, R. Wang, et al., "Inhibiting Proton Corrosion and Hydrogen Evolution Reaction on the Surface of Zinc Anodes by Hierarchical Structure Hydrogel to Realize Long-Life Aqueous Zinc Metal Batteries," *Advanced Energy Materials* 16 (2026): 03823, https://doi.org/10.1002/aenm.202503823.

176. Z. Yan, F. Luo, S. Yang, et al., "Polydentate Ligand-Induced Surface Reconstruction of MIL-88A Reinforced Gel Electrolytes for Highly Reversible Zinc Batteries via Ion Rectification and Charge Redistribution," *Advanced Functional Materials* 36 (2026): 14679, https://doi.org/10.1002/adfm.202514679.

177. Y. Wang, K. Zhong, J. Zhang, et al., "Concomitant Zinc Dendrite Mitigation and Iodide Shuttle Confinement: A Bifunctional Zwitterionic Hydrogel Electrolyte Unlocking Ultralong-Cycling Aqueous Zinc-Iodine Batteries," Advanced Functional Materials 36 (2026): 26937, https://doi.org/10.1002/adfm.202526937.

178. O. Zhanadilov, H. J. Kim, H. J. Lai, et al., "Exploiting High-Voltage Stability of Dual-Ion Aqueous Electrolyte Reinforced by Incorporation of Fiberglass into Zwitterionic Hydrogel Electrolyte," *Small* 19 (2023): 2302973, https://doi.org/10.1002/smll.202302973.

179. S. Cui, L. Meng, W. Miao, X. Xie, H. Peng, and G. Ma, "Hydrogen Bonding-Reinforced Zwitterionic Hydrogel Electrolytes for Wide-Temperature Tolerant Zinc-Ion Capacitors," *Chemical Engineering Journal* 521 (2025): 166818, https://doi.org/10.1016/j.cej.2025.166818.

180. F. Bu, Y. Gao, W. Zhao, et al., "Bio-Inspired Trace Hydroxyl-Rich Electrolyte Additives for High-Rate and Stable Zn-Ion Batteries at Low Temperatures," *Angewandte Chemie International Edition* 63 (2024): 202318496, https://doi.org/10.1002/anie.202318496.

181. X. Wei, J. Guan, Y. Mu, et al., "Decoding Hydrogen-Bond Network of Electrolyte for Cryogenic Durable Aqueous Zinc-Ion Batteries," *Nano-Micro Letters* 18 (2026): 127, https://doi.org/10.1007/s40820-025-01970-3.

182. J. Xu, Y. Yang, Q. Dai, et al., "Towards Ultra-Stable Wide-Temperature Zinc-Ion Batteries by Using Ion-Sieving Organic Framework Membrane," *Angewandte Chemie International Edition* 64 (2025): 202423118, https://doi.org/10.1002/anie.202423118.

183. Y. Quan, M. Yang, M. Chen, et al., "Electrolyte Additive of Sorbitol Rendering Aqueous Zinc-Ion Batteries with Dendrite-Free Behavior and Good Anti-Freezing Ability," *Chemical Engineering Journal* 458 (2023): 141392, https://doi.org/10.1016/j.cej.2023.141392.

184. J. Guan, Y. Mu, X. Wei, et al., "Ternary Gel Electrolyte Enabling Wide-Temperature and High-Rate Performance in Aqueous Zinc-Ion Batteries," *Advanced Functional Materials* 35 (2025): 2508306, https://doi.org/10.1002/adfm.202508306.

185. Z. Liu, Y. Zhang, M. Li, et al., "Lean-Water Gel Electrolyte Enables Zinc Ion Battery at −70°C," *Angewandte Chemie International Edition* 64 (2025): 202511520, https://doi.org/10.1002/anie.202511520.

186. S. Huang, L. Hou, T. Li, Y. Jiao, and P. Wu, "Antifreezing Hydrogel Electrolyte with Ternary Hydrogen Bonding for High-Performance Zinc-Ion Batteries," *Advanced Materials* 34 (2022): 2110140, https://doi.org/10.1002/adma.202110140.

187. S. Ji, H. Luo, S. Qin, et al., "Component Fluctuation Modulated Gelation Effect Enable Temperature Adaptability in Zinc-Ion Batteries," *Advanced Energy Materials* 14 (2024): 2400063, https://doi.org/10.1002/aenm.202400063.

188. B. Song, J. Zhang, S. Hao, et al., "Multifunctional Hydrogel Interfaces: Reshaping the Future of Flexible Electronics," *Advanced Materials* 38 (2026): e20644, https://doi.org/10.1002/adma.202520644.

189. T.-Y. Yang, T. T. Su, H. L. Wang, K. Li, W. F. Ren, and R. C. Sun, ""Tennis Racket" Hydrogel Electrolytes to Synchronously Regulate Cathode and Anode of Zinc-Iodine Batteries," *Journal of Energy Chemistry* 102 (2025): 454–462, https://doi.org/10.1016/j.jechem.2024.11.004.

190. Q. He, G. Fang, Z. Chang, et al., "Building Ultra-Stable and Low-Polarization Composite Zn Anode Interface via Hydrated Polyzwitterionic Electrolyte Construction," *Nano-Micro Letters* 14 (2022): 93, https://doi.org/10.1007/s40820-022-00835-3.

191. G. Ji, M. Sun, M. Li, and J. Zheng, "A Lean-Water Hydrogel Electrolyte with Engineered Water-Lubricated Pathways Constructed by Unique Water-Inter-Micelle Structure," *Advanced Materials* 38 (2026): 15706, https://doi.org/10.1002/adma.202515706.

192. Y. Lu, Z. Wang, M. Li, et al., "3D Printed Flexible Zinc Ion Micro-Batteries with High Areal Capacity toward Practical Application," *Advanced Functional Materials* 34 (2024): 2310966, https://doi.org/10.1002/adfm.202310966.

193. G. Dai, Y. Zhou, Z. Liu, et al., "Hydrogen-Bonding Network Tailoring via EG-Based DES/CMC-Na Synergy Enables Longevous and Dendrite-Free Flexible Aqueous Zinc-Ion Batteries," *Chemical Engineering Journal* 525 (2025): 170644, https://doi.org/10.1016/j.cej.2025.170644.

194. Y. Liu, M. Tian, Y. Chen, et al., "Dynamic Cross-Linked and Sulfonic-Functionalized Hydrogel Electrolyte for High-Performance Zinc-Ion Batteries," *Chemical Engineering Journal* 527 (2026): 171563, https://doi.org/10.1016/j.cej.2025.171563.

195. C. Yan, Y. Wang, X. Deng, and Y. Xu, "Cooperative Chloride Hydrogel Electrolytes Enabling Ultralow-Temperature Aqueous Zinc Ion Batteries by the Hofmeister Effect," *Nano-Micro Letters* 14 (2022): 98, https://doi.org/10.1007/s40820-022-00836-2.

196. Y. Dou, S. Li, X. Zhu, et al., "The Role of Lignin-Molybdenum Disulfide as a Nano-Filler in Enhancing the Performance of Crosslinked Hydrogel Nanofibers Membrane for Lithium-Ion Battery Separators," *Chemical Engineering Journal* 507 (2025): 160432, https://doi.org/10.1016/j.cej.2025.160432.

197. C. Jin, C. Yang, L. Xie, et al., "Regulating Water Activity and Solvation Structure via Zwitterion-Enhanced Polymer Electrolyte for Long-Life Zn-Ion Hybrid Capacitors with Low-Temperature Applicability," *Advanced Energy Materials* 15 (2025): 2402843, https://doi.org/10.1002/aenm.202402843.

198. M. Du, Q. Kang, Z. Guo, et al., "Acrylamide-Based Hydrogels for Rechargeable Zinc-Based Batteries: Properties, Synthesis and Applications," *Journal of Materials Chemistry A* 14 (2026): 3155–3184, https://doi.org/10.1039/D5TA08176A.

199. K. Huang, J. Zhou, A. Xiao, B. Lin, Z. Huang, and T. Wu, "A Versatile Hydrogel for Sensing-Energy Storage Integrated Wearable Electronics," *Chemical Engineering Journal* 526 (2025): 171315, https://doi.org/10.1016/j.cej.2025.171315.